Monolithic Microwave Transformers

Couplers, Inductors, Transformers, Spiral, GaAs, Coupling, Simulation,

This document is the cumulation of work done from 1986 to 1991 at Carleton University and Bell-Northern Research (now Nortel Network) in Ottawa, Ontario, Canada, in the fulfillment of the requirements for the degree of Masters in Engineering. This work was supervised by Dr. Barry Syrett at Carleton. It is one of the earliest analytical treatments of monolithic microwave transformers, and since then much more work has been done by many in this field. I had intended to publish parts of this work more widely, but life got in the way so it was never done. The work was distributed informally. John Long based some of his analyses on this work and, unlike me, he did publish, referencing this thesis. As a result, I have had more requests for this document, so I decided it was time to make it available.

The document was written on a MAC in an early version of FrameMaker, with some graphics cut and pasted in (that is, using real scissors and real glue). I discovered that updating this document to a more modern version of FrameMaker introduced some problems with some graphics. I scanned in the pasted-in graphs. The final result is not beautiful, but it contains all the information. If you have any problems with it, please contact me.

In the mean time, I continue to use the GEMCAP program with the latest version producing Spice files (that I import into ADS) running on a PC. It has served me well. There are products on the market that use these transformers. One note I should mention, the equivalent circuit used in the thesis results in errors when used in noise calculations. I now use the circuit below:

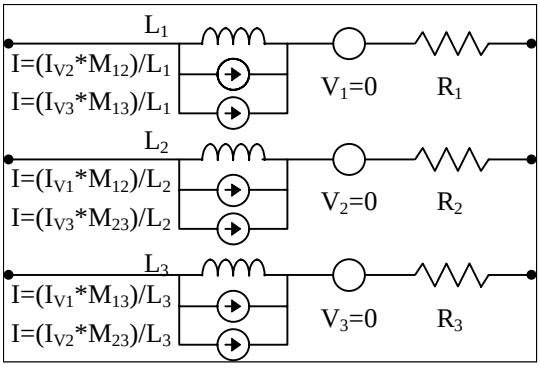

Good luck!

Gord Rabjohn
Sirenza Microdevices, Ottawa Design Centre,
350 Palladium Drive, Suite 130,
Kanata (Ottawa), Ontario, Canada, K2V 1A8.
613-271-4305
rabjohn@ieee.org

March, 2002

MONOLITHIC MICROWAVE TRANSFORMERS

by

Gordon G. Rabjohn B.A.Sc.

A thesis submitted to the Faculty of Graduate Studies and Research

in partial fulfilment of the requirements for the degree of

Master of Engineering

Department of Electronics

Carleton University

Ottawa, Ontario.

April 1991

CARLETON UNIVERSITY

FACULTY OF GRADUATE STUDIES AND RESEARCH

The undersigned recommend to the Faculty of Graduate Studies and Research acceptance of this thesis entitled,

"MONOLITHIC MICROWAVE TRANSFORMERS"

submitted by Gordon G. Rabjohn

in partial fulfilment of the requirements for

the degree of Master of Engineering.

.....(Barry Syrett).....
Thesis Supervisor

.....(Jim Wight).....
Chairman, Department of Electronics

Carleton University

April 1991

ABSTRACT

This thesis discusses the design and characteristics of monolithic spiral transformers for use at microwave frequencies. Monolithic transformers can be fabricated on GaAs Monolithic Microwave Integrated Circuits (MMICs) to perform matching, coupling and balun functions. A computer based program for the analysis of complex coupled microstrip structures on MMICs is described and evaluated. This program is used to evaluate coupled microstrip lines, spiral inductors, transformers, and Lange couplers. Stray coupling between adjacent inductors is also evaluated. Measured results are presented to validate the program. A procedure is presented to aid in the design of monolithic transformers. Various types of monolithic baluns are also described and compared.

ACKNOWLEDGEMENTS

This thesis would have been impossible without the help and generosity of individuals too numerous to mention. I thank my thesis supervisor, Barry Syrett, for his support and encouragement. BNR, and especially the people in the Advanced Technology Laboratory, and the Radio Group must also be acknowledged for their help. All of the measurements were done using BNR equipment, and many of the devices were processed on GaAs processing runs procured by them. I wish to thank, in particular, John Sitch, Bob Surridge, and Mark Suthers for some fruitful discussions that added immeasurably to this thesis. Finally, I wish to thank my wife, Kelley, for her understanding, and support, and for checking much of the mathematical detail.

TABLE OF CONTENTS

LIST OF FIGURES

LIST OF NOMENCLATURE

AMD	Arithmetic Mean Distance.
B	Magnetic flux.
C	Capacitance.
C_{mn}	Mutual capacitance as defined by the capacitance matrix.
C_{cmn}	Capacitive element representing a capacitance between the mth and nth conductor (or to ground if m=n) in an electrical model.
d	Distance between filamentary conductors.
E	Electric field.
F	Frequency.
GMD	Geometric Mean Distance.
h	Substrate thickness.
H	Magnetic field strength.
I_n	Current flowing in the nth conductor.
I'_n	First derivative with respect to time of current flowing in the nth conductor.
k	Inductive coupling coefficient.
K_1, K_2, K_3	Fitting parameters.
l	Length.
L	Inductance.
L_n	Self inductance of the nth winding of a transformer.
M	Mutual inductance.
M_{mn}	Mutual inductance between the mth and nth winding of a transformer.
n	Turns ratio.
N	Number of turns, or integer number in general.
Q_n	Charge on the nth conductor.
R	Resistance.
R_{RF}	Effective RF resistance.
R_0	Characteristic impedance, when the impedance is assumed to be real.
S_{mn}	Scattering parameters with the nth port excited and the mth port monitored.
t	Metalization thickness.
V_n	Voltage across the nth winding.

w	Width.
x	Normalized frequency, or simply an x coordinate.
Z_{in}	Impedance seen at the input (primary) of a transformer.
Z_{out}	Impedance seen at the output (secondary) of a transformer.
Z_0	Characteristic impedance.
ε	Permittivity of free space.
ε_{eff}	Effective dielectric constant.
ε_r	Relative dielectric constant.
Φ	Flux linkage.
σ	Conductivity.
μ	Permeability of free space.
ν	Velocity of light, c.
ω	Angular frequency, $2\pi F$.

LIST OF NOMENCLATURE

AMD	Arithmetic Mean Distance.
B	Magnetic flux.
C	Capacitance.
C_{mn}	Mutual capacitance as defined by the capacitance matrix.
C_{cmn}	Capacitive element representing a capacitance between the mth and nth conductor (or to ground if m=n) in an electrical model.
d	Distance between filamentary conductors.
E	Electric field.
F	Frequency.
GMD	Geometric Mean Distance.
h	Substrate thickness.
H	Magnetic field strength.
I_n	Current flowing in the nth conductor.
I'_n	First derivative with respect to time of current flowing in the nth conductor.
k	Inductive coupling coefficient.
K_1, K_2, K_3	Fitting parameters.
l	Length.
L	Inductance.
L_n	Self inductance of the nth winding of a transformer.
M	Mutual inductance.
M_{mn}	Mutual inductance between the mth and nth winding of a transformer.
n	Turns ratio.
N	Number of turns, or integer number in general.
Q_n	Charge on the nth conductor.
R	Resistance.
R_{RF}	Effective RF resistance.
R_0	Characteristic impedance, when the impedance is assumed to be real.
S_{mn}	Scattering parameters with the nth port excited and the mth port monitored.
t	Metalization thickness.
V_n	Voltage across the nth winding.

w	Width.
x	Normalized frequency, or simply an x coordinate.
Z_{in}	Impedance seen at the input (primary) of a transformer.
Z_{out}	Impedance seen at the output (secondary) of a transformer.
Z_0	Characteristic impedance.
ε	Permittivity of free space.
ε_{eff}	Effective dielectric constant.
ε_r	Relative dielectric constant.
Φ	Flux linkage.
σ	Conductivity.
μ	Permeability of free space.
ν	Velocity of light, c.
ω	Angular frequency, $2\pi F$.

CHAPTER 1
INTRODUCTION

1.1. Transformers in Microwave Circuits

Transformers have been in use since the first application of alternating current energy. All applications of transformers centre around one of two characteristics of transformers: the ability to easily transform impedance levels (changing the ratio of current to voltage without losing a significant amount of power) and the ability to transfer energy between two electrical meshes without having the meshes at the same potential. For example, transformers can be used: to generate a high AC voltage when only a low voltage is available; to match a low impedance load to a high impedance source; to isolate loads from ground; to provide 180 degree phase shifts; to shape pulses; and, by tuning, to provide bandpass filter characteristics.

Below the microwave frequencies, transformers consist of two inductors mounted so that they share flux linkages. In the audio range, this is done by winding the inductors on a high permeability common core, such as laminated iron, which serves to confine the magnetic flux. At radio frequencies, the iron core material is usually replaced with powdered iron or ferrite, which has more suitable high frequency loss characteristics. If the ferrite is made moveable, the transformer self- and mutual inductances can be adjusted, making them useful in tuned resonant circuits. Air core transformers can also be used in situations where the power or frequency limitations of the ferrite materials can not be tolerated. At low frequencies, the stray capacitance is usually minimized and avoided, but transformers designed for radio frequency use can take advantage of the stray capacitance. Such transformers are known as transmission line transformers, and have wider bandwidths and lower losses than simple inductive transformers. At microwave frequencies, the traditional transformer configurations are unacceptable because core losses become intolerable, and the self resonant frequency tends to be too low. If the self inductance of the windings is reduced to increase the resonant frequency, the windings become small and awkward to assemble, and the mutual inductance decreases, yielding a transformer with poor coupling factor.

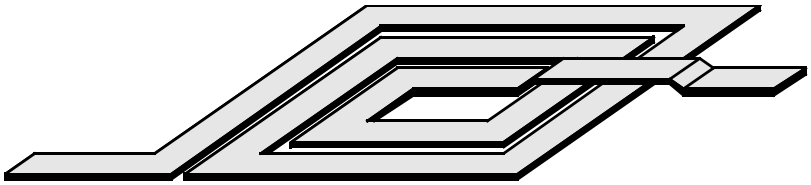

Figure 1.1. Basic monolithic square spiral inductor.

At microwave frequencies, different structures are used to implement transformer functions. An impedance transformation can be made with a quarter wavelength transmission line. Balun structures can be made with “Magic Tees”, “Rat race” structures, coupled transmission line structures, or various structures involving finline, slotline, and coplanar waveguide. Although these structures are satisfactory for thin and thick film integrated circuits, they are too large for efficient use in MMIC (Monolithic Microwave Integrated Circuit) designs. Furthermore, their bandwidth is usually limited to an octave or less.

Microwave circuit designers frequently use high impedance transmission lines when an inductance is required. By wrapping a high impedance microstrip line into a spiral, as shown in Figure 1.1, the physical dimensions of the inductor can be reduced, and the inductance (and therefore Q) can be increased. This form of inductor, known as either a square spiral inductor, or a circular spiral inductor, has been widely used in MMICs, and there are numerous techniques for their design. A logical extension of this concept is the spiral transformer. A spiral transformer consists of two spiral inductors interwound so that their mutual inductance is optimized. The first example of such a concept actually being used was in 1982 when Podel et al. [1] described a monolithic balanced amplifier that used interwound spiral inductors similar to those shown in Figure 1.2 for interstage coupling and biasing. Very little information that could be used for design was given, and it appears that little was available. Some experimental work, backed up with a computer-aided design program based on electromagnetic field theory, was performed by Jansen et al [2][3]. In this paper,

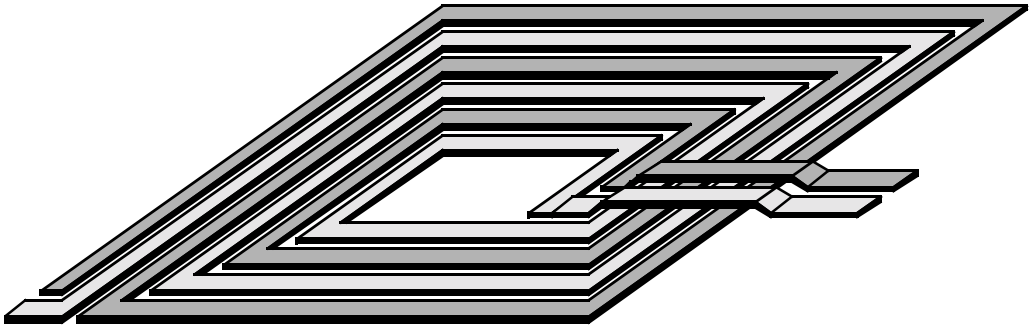

Figure 1.2. Basic monolithic square spiral transformer.

they simulated and built a monolithic spiral transformer, and measured its characteristics. Here, the first indication of one of the principal limitations of planar transformers is given: the inter-winding capacitance leads to asymmetrical operation when used as a balun. These two papers, and several Gallium Arsenide (GaAs) monolithic integrated circuits that use transformers marketed by Pacific Monolithics have encouraged more detailed research work. One paper, [4][5], describes an implementation of a Ruthroff [6] transformer using fairly long coupled line sections. Another paper [7] describes a program for modelling certain types of monolithic transformers. A full wave electromagnetic analysis of similar transformers has also been performed [8], however little work was done in analysing different topologies of transformers.

Most of the impetus for the research into planar transformers has been spurred by the widespread development of high frequency GaAs integrated circuits. GaAs is a useful material for the fabrication of microwave monolithic integrated circuits (MMICs) because it can be made semi-insulating (as opposed to silicon which is a semiconductor), yielding well isolated circuits and low-loss transmission lines. Metal-Semiconductor Field Effect Transistors (MESFETs) with cutoff frequencies above 30 GHz can be made on GaAs with straightforward processing steps. Although transistors fabricated on silicon can have cutoff frequencies almost as high as GaAs FETs, transmission lines fabricated on silicon tend to be lossy. The high cost of processing GaAs MMICs, and the need for compact, dense circuitry

has increased interest in “almost lumped” devices such as Metal Insulator Metal (MIM) capacitors, inductors, and transformers. These functions would have been implemented with distributed elements if more conventional thin or thick film technologies were to be used. GaAs FETs require high precision lithography and well polished substrates, and these qualities are also required for the aforementioned “almost lumped” devices.

1.2. Objectives of the Thesis

The purpose of this research is to determine a procedure that can be used to analyse a broad range of monolithic transformers, including those with centre taps, and coupled elements in general, without the need to resort to full-wave analysis techniques. This thesis describes the design, execution, and verification of a computer program for the analysis of monolithic spiral transformers, and similar coupled structures. The procedures to be developed are intended for use on microstrip line circuitry, and will be particularly useful for MMIC designs. This procedure is then used to analyse a variety of transformer structures, so that advantages and disadvantages of monolithic transformers can be assessed. New designs for balanced transformers are suggested. The computer-aided design procedure is verified with numerous measurements of experimental structures.

1.3. Thesis Outline

The second chapter deals with the theories behind the analysis of planar monolithic coupled structures. Techniques used for calculating the capacitance and inductance matrices of coupled lines, and the manner in which they are implemented in the developed computer program are described. Chapter 3 deals with the application of the program for the analysis of simple, two terminal devices such as transmission lines and inductors. It forms the basis for the transformers analysed in the fourth chapter. In both chapters, simulated data is compared with other published data, other CAD programs, and measured data. Chapter 4 also deals with the simulation of the balun, which is a special class of transformer used for phase splitting. Baluns have special requirements which are not easily met on small MMIC chips. Finally, some general observations and recommendations for further research are presented in Chapter 5.

CHAPTER 2
TECHNIQUES FOR THE ANALYSIS OF MICROSTRIP COUPLED LINES

2.1. Introduction

Monolithic microwave transformers are complex devices that are not described by any simple models. In order to predict their performance, it is necessary to devise a computer algorithm to model the physical processes that are occurring therein. A completely general electromagnetic simulator is far beyond the scope of this thesis. Instead, the simulator described in this work is based on circuit concepts; rather than working with fields directly, we work with circuit elements such as capacitance, inductance and resistance. This thesis will deal only with microstrip transmission line, which is the most common form of transmission medium on MMICs. In a microstrip circuit, all conductors are formed on a planar dielectric substrate. The backside of the substrate has a conducting layer which forms the circuit's ground.

This chapter introduces transformer modelling by describing the physical processes occurring in a transformer. A circuit model can be derived for a transformer by looking at these processes. In other words, the first part of this chapter describes how one generates an electrical model from the physical layout. The second part of the chapter is devoted to the algorithms required to determine the values of the elements in the electrical model, based on the physical dimensions of the transformer. In particular, the capacitance matrix, the inductance matrix, and the loss matrix must be derived. Finally, the last part of the chapter describes how the various algorithms are integrated into a flexible and practical computer program.

2.2. Transformer Modelling

The electrical equivalent circuit model of a microwave spiral transformer, such as the one shown in Figure 1.2, can be complicated, so the first model considered will be that of an ideal transformer. In an ideal transformer, perfect flux linkage is assumed. In other words, it is assumed that all of the flux from the primary inductor links the secondary inductor as well. If the inductance of both windings approaches infinity, then the frequency response will not have a low frequency limit. If the stray capacitance is assumed to be negligible, then the frequency response will not have an upper limit either. With these assumptions, the transformer can be modelled as a simple voltage or current transformation, with the voltage or current ratio given by n where:

$$n = \text{Turns Ratio} = \frac{\text{Secondary Windings}}{\text{Primary Windings}} \tag{2.1}$$

$$n = \frac{I_1}{I_2} = \frac{V_2}{V_1} = \sqrt{\frac{Zout}{Zin}} \tag{2.2}$$

Z_{in} is the impedance seen into the primary when an impedance of Z_{out} is imposed on the secondary. This model can be implemented exactly in most simulators using the current source and voltage source connected as shown in Figure 2.1. Note that this circuit implementation also isolates the primary mesh from the secondary mesh, which is important in applications such as baluns. This model is accurate for iron core transformers at power line

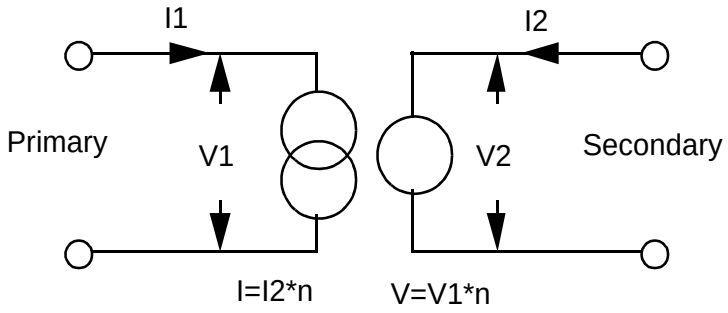

Figure 2.3. Basic transformer model

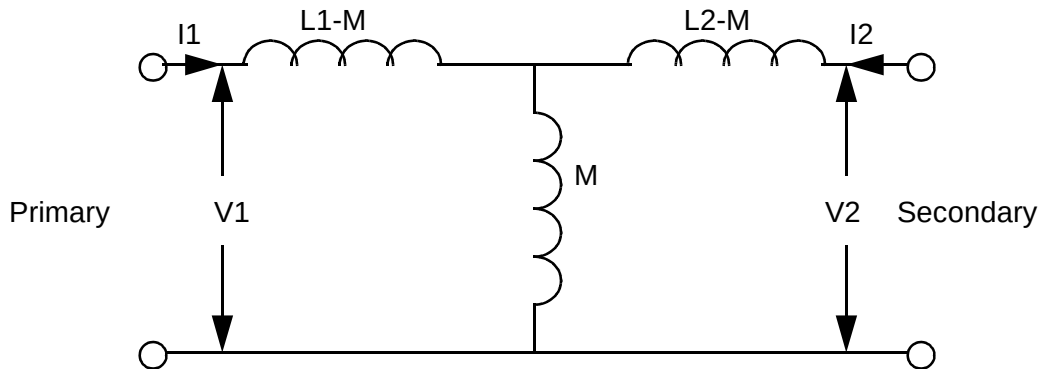

Figure 2.4. T section model of a transformer.

frequencies, and sometimes audio frequencies, if the effect of magnetic saturation in the iron core is not important. If the effects of the self inductance must be included, then this inductance can be included in parallel with either the primary or secondary winding of the transformer.

In transformers where inductive coupling is not complete, such as in air core transformers, a more complex model is required. At this point, it is necessary to define several terms. The primary self inductance (L_1) is the inductance of the primary winding of the transformer with the secondary winding open circuited. The secondary self inductance (L_2) is defined in a similar fashion. The mutual inductance (M) can be defined as the flux linking the secondary winding divided by the current in the primary winding (or vice-versa), or the voltage induced in the secondary winding as a result of a current in the primary winding changing at a rate of 1 A/s. More useful is the following pair of simultaneous equations that describe this simple transformer model:

$$\begin{aligned} V_1 &= L_1 I_1' + M_{12} I_2' \\ V_2 &= L_2 I_2' + M_{12} I_1' \end{aligned} \tag{2.3}$$

The variables marked with a prime (I') are the first time derivatives if the variable. These simultaneous equations can be implemented in circuit form in a circuit simulator by using the topology shown in Figure 2.2. Note that this model does not isolate the primary mesh

from the secondary mesh as the model shown in Figure 2.1 does. It can be seen that the ideal 1:1 transformer (n=1) is just a special case of this model where L_1=L_2=M and L_1 and L_2 are allowed to approach infinity. A factor has been defined to describe how closely a transformer comes to being ideal. This factor, termed the coupling coefficient, represents the fraction of flux linkage from the primary winding that links the secondary winding, or vice-versa. (Note that the primary-to-secondary coupling coefficient is the same as the secondary-to-primary coupling coefficient because of reciprocity.) The coupling coefficient, *k*, is given by:

$$k = \frac{M}{\sqrt{L_1 L_2}} \tag{2.4}$$

It is easy to prove that the value of *k* must always be less than 1 for any real transformer. A value greater than 1 implies that the secondary winding is linking more of the flux from the primary winding than the primary winding is, which is clearly impossible.

The model illustrated in Figure 2.2 indicates that any non-ideal transformer will have a limited bandwidth, even if parasitic capacitance is neglected. The usefulness of a transformer drops off at low frequencies because the inductive reactance of the windings becomes too low. At high frequencies, the reactance of the series inductors will limit energy transfer. The value of *k* determines the size of these inductors, and, with the self inductance, the upper frequency of operation. Therefore, it is important to keep the value of *k* high to maintain bandwidth.

In transformers where *k* is significantly less than 1, (2.1) and (2.2) no longer apply, so the turns ratio becomes meaningless. Rather, the self and mutual inductance must be specified.

In transformers used at RF frequencies, the eddy current losses occurring in the core material and the conductor losses can no longer be ignored. These losses can be accounted for by resistances in series with each winding.

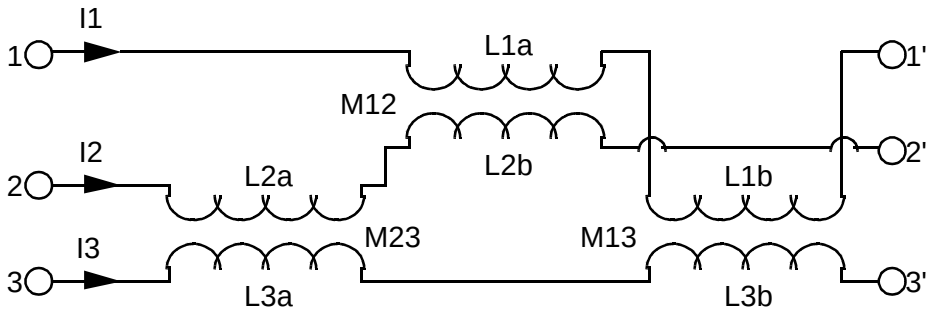

L1a+L1b=L1=Winding 1 self inductance.
L2a+L2b=L2=Winding 2 self inductance.
L3a+L3b=L3=Winding 3 self inductance.

Figure 2.5. A three winding transformer model.

So far, only transformers with two windings have been considered. In many real applications, such as baluns, transformers with several windings must be considered. Equation (2.4) can easily be extended to cover multiple winding transformers, as shown in (2.5).

$$\begin{aligned} V_1 &= L_1 I_1' + M_{12} I_2' + M_{13} I_3' \\ V_2 &= M_{12} I_1' + L_2 I_2' + M_{23} I_3' \\ V_3 &= M_{13} I_1' + M_{23} I_2' + L_3 I_3' \end{aligned} \tag{2.5}$$

The most straight-forward way to implement a multiple winding transformer in a circuit simulator is by using simple two-winding transformers. The circuit shown in Figure 2.3 illustrates this concept for a three winding transformer. Each winding is between nodes *N* and *N'*. V_N is the voltage between these nodes. Each coupled inductor pair in this circuit can be replaced by any of the models described earlier (Figures 2.1 and 2.2), and such models are available in most simulators. However, there are several disadvantages in using this model for a multi-line transformer. The number of nodes used in the coupled line model increases with the square of the number of coupled inductors. The number of nodes required to simulate *N* coupled inductors using this model equals N^2. In the topology described later, the number of nodes required is a linear function of the number of coupled

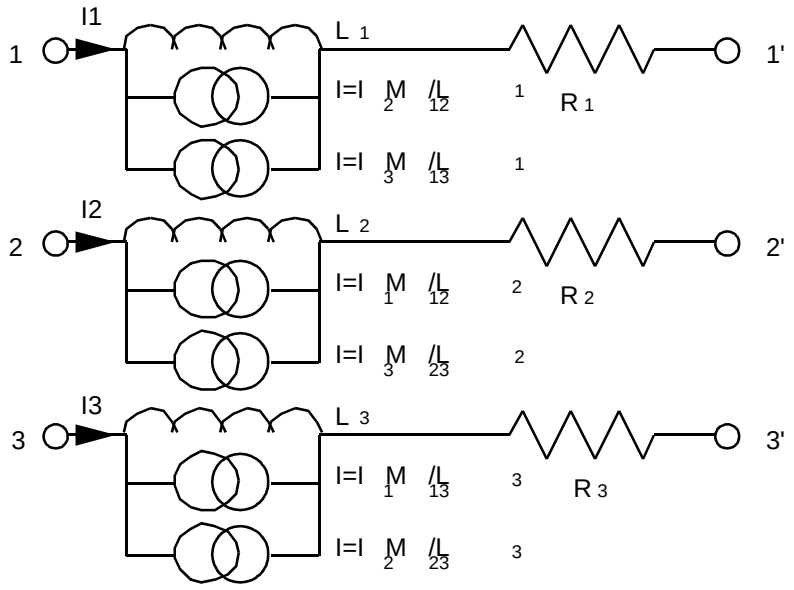

Figure 2.6. Three winding transformer that uses controlled sources.

inductors. A numerical difficulty also arises because each coupled inductor pair is modelling only a part of the transformer. When calculations are done to determine values for M_{xy} and L_x for real triple (or more) coupled inductors, calculated values of k for the individual coupled inductor pairs can legitimately exceed 1. Some simulators do not allow the value of k to exceed 1.

The multiple-coupled inductor model that will form the basis of most of the simulations is shown in Figure 2.4. It is a straightforward implementation of (2.5) with series resistors to simulate loss, but requires only $3N$ nodes for implementation. An added advantage is that loss can be implemented with series resistors without using any additional nodes. This model is based on elements that are available in all general purpose simulators, viz inductances, resistances, and controlled current sources. Circuits constructed from these elements can be solved both in the time domain and the frequency domain.

The $L_{\mathrm{M}}\, I_{\mathrm{M}}$ terms in (2.5) are represented by the inductors in Figure 2.4. The $M_{\mathrm{MN}}\, I'_{\mathrm{N}}$ terms are simulated by controlled sources that force current through the inductor L_{M}, thereby

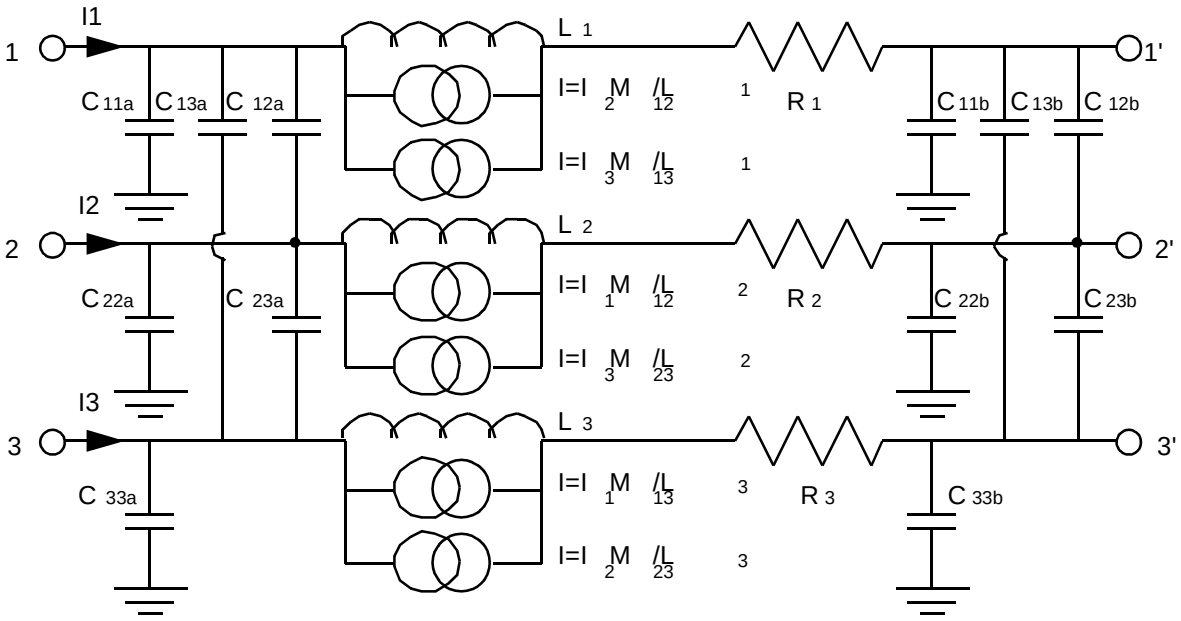

Figure 2.7. Three winding transformer model with parasitics.

adding to the voltage V_M with the appropriate time derivative. The coefficients for the current sources are proportional to the mutual inductance and inversely proportional to the inductance that the current source must drive (L_M).

The final effect that must be included in a high frequency transformer model is the effect of interwinding capacitance. There exists capacitance between any pair of windings. If the transformer is to be fabricated in monolithic form over a ground plane, the capacitance from each element to this ground plane must also be considered. The final model that is used in all work in this thesis is shown in Figure 2.5. Although Figure 2.5 pertains to a three winding transformer, it can be extended to any arbitrary number of windings.

Until this point, distributed effects have not been considered. At microwave frequencies, the length of the windings may be comparable to the wavelength of the energy exciting the transformer. One way to deal with this is to use conventional coupled line theory. For pairs of lines, even-mode and odd-mode impedances and effective dielectric constants can be calculated, and a 2-port matrix representation (such as an s-parameter matrix) can be deter-

mined. The major difficulty with this approach is that few simulators support multiple-coupled line models. (SuperCompact version 2.0 [9] supports up to 10 coupled lines, and Touchstone [10] supports only pairs and triplets. Most versions of Spice [11] do not support any coupled lines.) The problem becomes especially difficult for time domain simulators, as the coupled line model must store the state of the line at many time points. Fortunately, the lumped approach is accurate for the short line lengths commonly found on MMICs. If greater accuracy is desired, then the coupled lines can be broken into smaller subsections.

In practice, each of the four sides of a transformer or inductor (such as the one in Figure 1.1) will be simulated with a model such as the one shown in Figure 2.5. Hence, an inductor will be simulated with at least $4N$ LC sections, where N is the number of turns. A schematic showing how a transformer (similar to Figure 1.2) would be modelled is shown in Figure 2.6. Since each six line transformer model has 30 current sources, the overall transformer model is very complex, but not beyond the capabilities of modern simulation tools. Since the user has the option of arranging the sections to his liking, and the user has access to all the corner nodes, this method of modelling offers great flexibility.

In general, a single pi section (consisting of a series inductor and two shunt capacitors to ground, similar to each section in Figure 2.5) differs from an ideal transmission line by less than 2 degrees in electrical length and less than .05 dB in transmission loss at an eighth of a wavelength. Multiple pi sections can be used if greater bandwidth is desired. A transmission line that traverses a 2 mm GaAs chip can be accurately simulated with one pi section at 3 GHz. At higher frequencies, more sections could be used, or poorer accuracy could be deemed acceptable. Figure 2.7 shows the error in magnitude and phase of S_{21} of a transmission line when modelled with various numbers of pi sections for various electrical lengths of line in a matched system. Lines unmatched to the characteristic impedance of the system will incur larger errors. These errors can, in theory, increase indefinitely at certain line lengths for highly mismatched systems, but for practical MMIC circuits, the error is seldom greater than a factor of 1.5 greater than the error shown in Figure 2.7. (For example, the error on a 110 ohm line (5um wide on a 125 um GaAs substrate) simulated in a 50 ohm environment is 6.8 degrees, as compared to 4.8 degrees as predicted by Figure 2.7.) If there

is doubt in the accuracy of a simulation, a designer can resimulate a circuit with transmission lines broken into more subsections. If the circuit's performance remains similar, then the designer can safely assume that the transmission line is being adequately simulated.

Since a minimum single turn inductor is modelled by at least 4 pi sections (one for each side), and inductors are rarely used below their quarter wave resonant frequency, inductors invariably have enough sections for an accurate simulation. For straight lengths of transmission line, however, one must make an estimate of the wavelength to calculate the number of sections required. For microstrip lines on GaAs, the ε_{eff} is roughly 7, and wavelength is 11 cm·GHz. For other materials, the safest estimate of velocity is to assume that $\varepsilon_{eff}=\varepsilon_r$. The number of sections required should be selected via Figure 2.7 given the length of line being simulated in wavelengths.

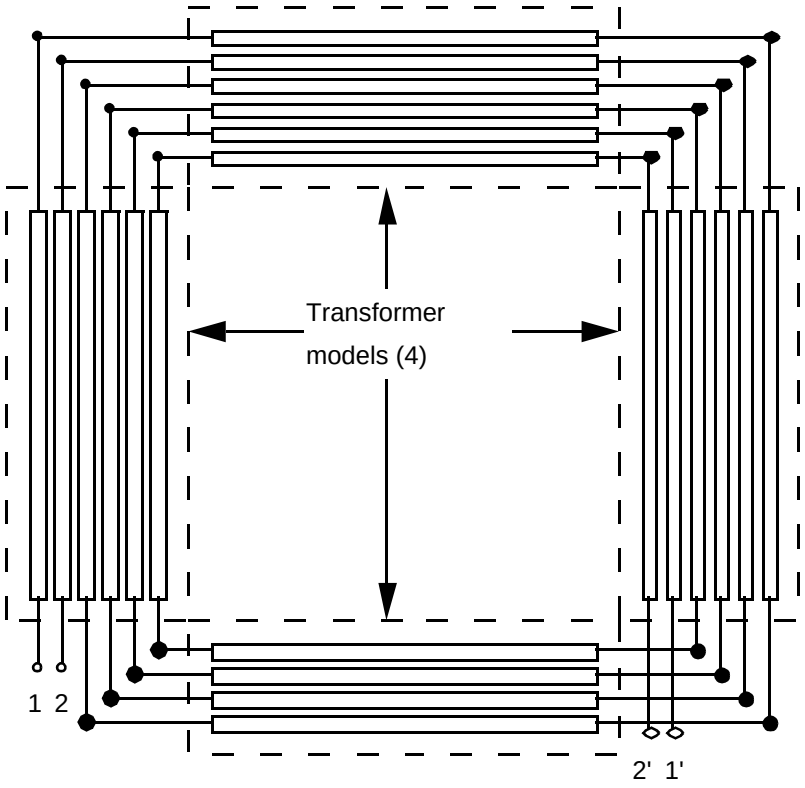

Figure 2.8. Simulation of a 2.75 turn transformer using four transformer sections, each section being described by a model similar to the one shown in Figure 2.5.

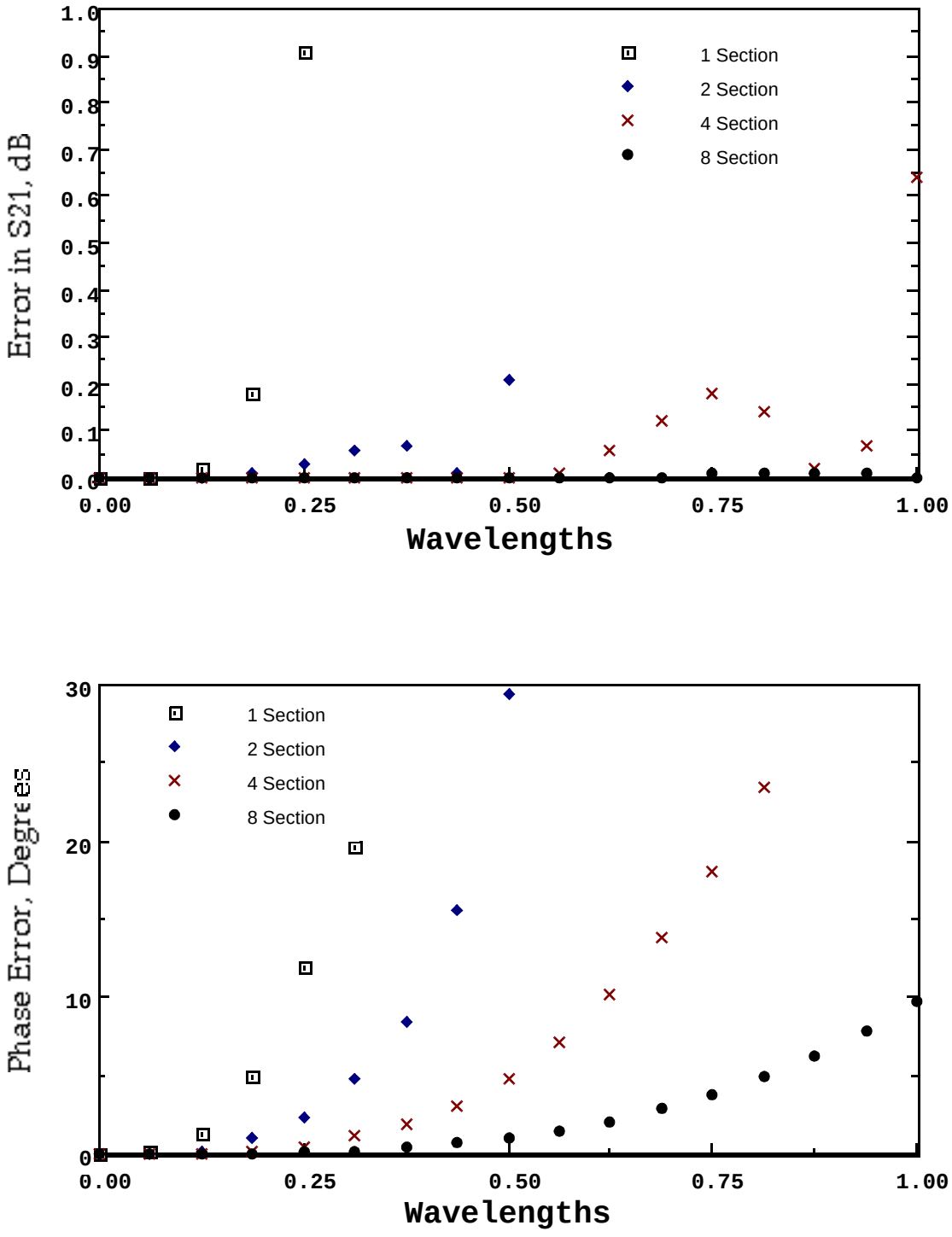

Figure 2.9. Error in magnitude and phase of S_{21} of a matched transmission line, when modelled with 1, 2, 4, and 8 pi sections.

At this point, we have determined an appropriate model for a simple transformer. Actual transformers when laid out may require more components to form an accurate model, especially at high frequencies. Transformers formed from parallel microstrip transmission lines will undoubtedly have bends when formed into the spiral configuration, and these bends may be modelled as a lumped capacitance to ground with an electrical delay [12]. The interconnections to the transformer will certainly add electrical delay, and they may also couple into the main coupled line section. Where two microstrip lines cross over each other (using a MMIC air bridge, for instance) there will be extra capacitance [13]. In any case, it can be seen that any of these effects can be modelled using four fundamental circuit elements: the resistor, capacitor, inductor, and the multiple coupled inductor, which itself is made up of inductors and controlled current sources. The next sections will be devoted to the determination of the electrical parameters of these elements based on the physical dimensions of the conductors.

2.3. Inductance and Capacitance Matrix

It is convenient to describe the capacitance and inductance associated with coupled transmission lines in terms of a matrix. Generally, the matrices quantify the inductance or capacitance on a per unit length basis, implying that the values are independent of length. For a system with N conductors, the capacitance matrix is an N by N symmetric matrix. The elements, termed the coefficients of capacitance, are defined below [14]:

$$\begin{bmatrix} Q_1 \\ Q_2 \\ . \\ Q_N \end{bmatrix} = \begin{bmatrix} C_{11} & C_{12} & . & C_{1N} \\ C_{21} & C_{22} & . & C_{2N} \\ . & . & . & . \\ C_{N1} & C_{N2} & . & C_{NN} \end{bmatrix} \begin{bmatrix} V_1 \\ V_2 \\ . \\ V_N \end{bmatrix} \tag{2.6}$$

where Q_N is the total charge on the N th conductor, and V_N is the voltage on the N th conductor relative to ground. The off-diagonal capacitance coefficients (mutual capacitance coefficients) are always negative because conductors must be of opposite polarity (relative to the common ground) to induce more charge on each other. Note that any capacitance matrix based on a physically realizable topology will be positive definite. In order to use this matrix in a circuit topology similar to the one shown in Figure 2.5, the following transformation [14] is used:

$$\begin{aligned} C_{Cii} &= \sum_{j=1}^{N} C_{ij} \\ C_{Cij} &= -C_{ij} \end{aligned} \tag{2.7}$$

where Cc_{ij} is the model capacitance between the ith and the jth conductor, or to ground if $i=j$, in the equivalent circuit model. This capacitance is often divided between two equal capacitors connected to either end of the conductor.

The inductance matrix for a system of *N* conductors is an *N* by *N* symmetric matrix. The elements of this matrix are defined as follows:

$$\begin{bmatrix} \Phi_1 \\ \Phi_2 \\ . \\ \Phi_N \end{bmatrix} = \begin{bmatrix} L_{11} & L_{12} & . & L_{1N} \\ L_{21} & L_{22} & . & L_{2N} \\ . & . & . & . \\ L_{N1} & L_{N2} & . & L_{NN} \end{bmatrix} \begin{bmatrix} I_1 \\ I_2 \\ . \\ I_N \end{bmatrix} \tag{2.8}$$

Where Φ_N is the flux linking the *N*th conductor, and I_N is the current through the *N*th conductor. Each diagonal inductance terms is the self inductance of the *i*th conductor with all other conductors open. The off diagonal terms are the mutual inductance terms. The inductance matrix provides the circuit values required in Figure 2.5 without any conversions.

It is often assumed that the inductance per unit length, and capacitance per unit length of a transmission line is constant with respect to frequency. This is equivalent to assuming that the characteristic impedance and velocity of propagation of the transmission line are constant with respect to frequency. This is known as the TEM (Transverse ElectroMagnetic) assumption. A transmission line that propagates only a TEM mode (a mode where both **H** and **E** fields are perpendicular to the direction of propagation) exhibits constant impedance and velocity with respect to frequency. Coaxial lines, striplines, and other media with homogeneous dielectric and two conductors are considered truly TEM below the frequency at which other modes can propagate (although the variation in the skin depth in the conductor causes changes in the inductance, and therefore characteristic impedance, at low frequencies [15]). Microstrip, and other media with inhomogeneous dielectric are not truly TEM media. As frequency changes, the distribution of the field in the different dielectrics changes, causing changes in transmission line parameters. This change in transmission line parameters with frequency is known as dispersion. In microstrip, dispersion causes the effective dielectric constant (ε_{eff}) to change from its DC value to the dielectric constant of the substrate as frequency increases. The frequency at which dispersive effects perturb a microstrip line to the point that ε_{eff} has increased from its DC value to the average of its DC value and $\varepsilon_{substrate}$ is given by (2.9) [16].

$$F_0 = \frac{Z_0}{2\mu h}\frac{1}{\sqrt{0.6 + 0.009Z_0}} \tag{2.9}$$

where F_0 is in GHz, and h is in cm. A microstrip line must be used well below this frequency if dispersive effects are to be avoided. Since the basic parameters of a TEM transmission line are constant with respect to frequency, the parameters can be calculated at DC.

2.4. Capacitance Calculations

The capacitance matrix can be obtained many ways. This section deals with several of the more popular techniques, and describes the technique used for this work in detail.

Conformal mapping may be used to map the actual cross-sectional detail of a transmission line to an imaginary cross-section that is more amenable to calculations. This technique has been successfully used for some simple microstrip structures. The advantage of this technique is that it may yield a closed-form expression for capacitance based on physical parameters. Unfortunately, it has not been used for multiple coupled lines such as the ones used in transformers and inductors. Frlan [7] uses a technique similar to this [17] to calculate self-capacitance, and the capacitance between adjacent lines in an inductor, and assumes that the rest of the capacitances are negligible.

Numerical techniques may be used to solve Laplace's equation for the electric field using, for example, a finite difference technique [18]. This technique has the advantage of being able to handle very general geometries, including bends, but the numerical work required makes it very slow. If this amount of computational work is to be done, then a complete full wave analysis may be more appropriate [3].

The technique used to calculate the capacitance matrix in this work is the method of moments (MOM)[14][19][20]. MOM can be used equally well on single lines or on multiple coupled lines. In this technique, one calculates the charge induced on all conductors if a potential of 1 volt is applied to one or two of the conductors with the other conductors grounded. Central to this calculation is the dielectric Green's function which gives the potential at a position relative to a line source of charge. This function can be relatively complex, as it must include the effects of the dielectric and the ground plane. The perimeter of each conductor is divided up into straight subintervals. A conductor with square cross-section would likely have at least 10 subintervals and more if high accuracy is required. A charge density is often assumed to be a linear function of distance along each subinterval. In other words, the charge density along the perimeter of each conductor is assumed to be a piecewise linear function of the distance around the perimeter. (As a result, one benefits

by using many subintervals around the square edge of a conductor where large peaks in the electric field, and hence charge density are expected. [19]) The charge density along each segment (which is presently unknown) multiplied by the Green's function is integrated to determine the potential at any point on the conductor. The potential on each conductor is known, however, so an error function can be formulated. By applying the least squares technique, the error is minimized, and the best fit can be found. The result is a set of coefficients that describes the piecewise linear approximation to the charge density around the perimeter of each conductor. By integrating this charge density, a capacitance can be determined since the potential is set at 1 volt. This procedure is performed first for all possible configurations where one conductor is excited by 1 volt, (and the others grounded), and then all possible configurations where two conductors are excited by 1 volt (and the others grounded). This set of $(N^2+N)/2$ capacitances can be combined to determine the complete capacitance matrix.

This technique does not yield a closed-form expression, but it can be relatively quick, and is not iterative, although the integration is done numerically. Green's functions are available for several conductor configurations. In the implementation used in this work, the Greens function used applies to a thin conductor of finite width directly over a grounded substrate. A program implementing the MOM for coupled microstrip lines was available for this work [21]. The accuracy of this program has been verified by comparing the capacitance that it calculates with the Bryant Weiss technique [20], and with SuperCompact [9]. Accuracy of better than 1% is possible for typical transmission line structures [19]. In structures where large differences in the widths of the conductors exists (a factor of 10 or more), larger inaccuracies, and possibly erroneous results can occur, but such structures are not often used in MMICs.

2.5. Inductance Calculations

In this section, methods for determining the self- and mutual- inductance of multiple parallel transmission lines will be discussed. Inductance can be calculated to good accuracy using closed-form expressions. Unlike capacitance, the inductance matrix can be derived by examining the set of parallel lines in pairs; in other words, the inductance of a pair of lines is not affected by an adjacent, unconnected line. The same is not true of the capacitance matrix where all lines must be considered simultaneously. Inductance can also be directly calculated using a moments method solution [22], but the technique is complicated by the fact that the potential field that must be matched is a vector field (A) rather than a scalar field (V). As microstrip lines are quasi-TEM structures, the inductance matrix can also be derived from a capacitance matrix.

2.5.1. Closed-Form Expressions

Grover [23] has collected many closed-form expressions for the inductance of segments, coils, and other shapes. These have formed the basis for many of the published papers on monolithic inductors, starting with a widely referenced paper by Greenhouse [24]. The technique has been refined by other authors [25] . The basis for many of these techniques is the formula for the mutual inductance of two filamentary parallel conductors of finite and equal length [23].

$$L = 2l\left[\ln\left(\frac{l}{d}+\sqrt{1+\frac{l^2}{d^2}}\right)-\sqrt{1+\frac{d^2}{l^2}}+\frac{d}{l}\right] \tag{2.10}$$

Where L is the mutual inductance in nH, l is the line length in cm, and d is the distance between the filaments in cm. This formula can be derived by determining the magnetic field surrounding a filamentary conductor carrying a DC current. This is done by integrating the Biot-Savart law over the length of a filament. The resulting **B** field is integrated from the position of the second conductor to infinity, as shown in Appendix A. This formula can be used directly to calculate the mutual inductance of pairs of approximately filamentary conductors (when separation is large compared to the conductor width).

When the mutual inductance of conductors of finite width located close to each other is required, the conductor width must be taken into account. If it is assumed that the length of the two conductors is much greater than the spacing, which is the case for most conventional distributed microstrip lines, then (2.10) simplifies to [23] :

$$L = 2l\left[\ln\frac{2l}{d} - 1 + \frac{d}{l} - \frac{d^2}{4l^2}\right] \tag{2.11}$$

Note that the last term of (2.11) is found by expanding (2.10) into a Maclaurin series. It is small enough that it is usually ignored.

In order to determine the mutual inductance of two conductors of finite width, each conductor is subdivided into filamentary conductors. The mutual inductance of the finite sized conductors is the average of the inductances between every pair of filaments. To do this calculation, it is necessary to integrate (2.10) or (2.11) over the cross-sectional area of the two conductors involved. The integration of (2.10) is intractable, but the integration of (2.11) yields the following:

$$L = \frac{2l}{\text{Area1}\,\text{Area2}}\int\int\left(\ln\frac{2l}{d} - 1 + \frac{d}{l}\right)d\text{Area1}\,d\text{Area2}$$

$$L = 2l\left[\frac{1}{w_1 w_2 t^2}\int\int\left(\frac{d}{l}\right)d\text{Area1}\,d\text{Area2} - \frac{1}{w_1 w_2 t^2}\int\int\ln(d)\,d\text{Area1}\,d\text{Area2} + \ln(2l) - 1\right] \tag{2.12}$$

Where one conductor's width and thickness are w_1 and t respectively, and the other conductor's are w_2 and t. The areas of the conductors are Area1 and Area2. The distance between the filaments is the variable of integration, d. The two resulting integrals have physical significance. The first one is the arithmetic average distance of every point within one conductor to every point within the other, and is known as Arithmetic Mean Distance, or AMD. The AMD of two rectangles is simply their centre-to-centre distance. The second integral represents the average of the logarithms of the distance between every point in each conductor, or the logarithm of the Geometric Mean Distance (GMD). Although the GMD can

not be calculated as easily as AMD, numerous formulae have been derived for the GMD between various cross-sectional areas [26][27]. In the case of conductors of rectangular cross-section, the exact value of GMD can be calculated. This lengthy equation is printed in Appendix B. Although it has not been widely used because of its length, the equation is easily implemented in a computer program. Rewriting (2.12) with AMD and GMD replacing the integrals, we get:

$$L = 2l\left[\ln\left(\frac{2l}{\mathrm{GMD}}\right) - 1 + \frac{\mathrm{AMD}}{l}\right] \tag{2.13}$$

Notice that because of the approximation used to derive (2.11), this equation is only accurate for parallel conductors that are much longer than their separation.

So far, only mutual inductance has been treated. The self inductance of a conductor can be calculated by finding the GMD and AMD of a conductor from itself and substituting these values into (2.11). Of course, the AMD is 0, but the GMD is finite, and given approximately by (2.14). Since a conductor is close to itself, the assumption that *d/l* is small is highly accurate. The self inductance of a conductor of width *w* by thickness *t* is given to high accuracy by (2.15):

$$\ln(GMD) = \ln(w + t) - 1.5 \tag{2.14}$$

$$L = 2l\left[\ln\left(\frac{2l}{w + t}\right) + 0.5\right] \tag{2.15}$$

These closed-form equations can not be used in every instance, and their accuracy is limited. If the conductor length is short relative to the space between conductors, then the approximation (2.11) can not be used. Instead, the general formula must be used, and it can not take into account the finite width and height of the conductors. Fortunately, when the ratio of gap to length for a conductor is large, the inductance is small and will constitute a small part of the total inductance of an inductor. In cases such as rectangular spiral inductors, the designer must decide whether to use (2.10) and accept the loss of accuracy because

of the width of the conductor or to use (2.11) and accept the loss of accuracy because of the short conductor length.

A more general form of (2.10) can be derived to calculate the mutual inductance of filamentary conductors each of arbitrary length, and without coincident ends. In fact, the lines need not even lie beside each other. The mutual inductance is given by [23]:

$$L = \alpha \operatorname{asinh}\frac{\alpha}{d} - \beta \operatorname{asinh}\frac{\beta}{d} - \gamma \operatorname{asinh}\frac{\gamma}{d} + \delta \operatorname{asinh}\frac{\delta}{d}$$
$$- \sqrt{\alpha^2 + d^2} + \sqrt{\beta^2 + d^2} + \sqrt{\gamma^2 + d^2} - \sqrt{\delta^2 + d^2}$$
$$\text{where } \alpha = l + \delta + m \ , \ \beta = l + \delta \text{, and } \gamma = m + \delta \qquad (2.16)$$

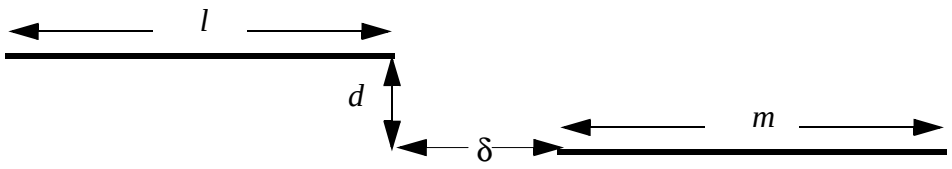

Figure 2.10. Plan view of parallel conductors for dimensional definitions for (2.16).

This equation can be simplified to (2.10) by setting $l=m$ and $l=-\delta$. This form is useful for calculating the coupling between adjacent, offset inductors.

The presence of a ground plane changes the self- and mutual-inductance of lines significantly. Even a cursory look at (2.11) indicates that as length approaches infinity, per unit length inductance also approaches infinity. From simple transmission line theory, it is known that the inductance per unit length of a transmission line is a constant. This inconsistency is due to the fact that the ground plane of the transmission line has not been considered. The boundary condition for the electric field stipulates that the electric field tangential to a conducting plane must vanish. One of Maxwell's equations stipulates the relation between electric and time varying magnetic fields:

$$\nabla \times \mathbf{E} = -\frac{\partial \mathbf{B}}{\partial t} \tag{2.17}$$

If Cartesian coordinates are used and the x and y components of the **E** field are assumed to vanish, then (2.17) simplifies to:

$$\frac{\partial \mathbf{B}}{\partial t} = \frac{\partial \mathbf{E}_z}{\partial x} \hat{a}_y - \frac{\partial \mathbf{E}_z}{\partial y} \hat{a}_x \tag{2.18}$$

From this equation one can deduce that the time varying **H** field must have no component normal to a conducting plane. Therefore, a current must be induced into the ground plane to cancel the **H** field caused by the current flowing in the wire above the plane. The current in the ground plane is modelled by an image conductor located on the opposite side of the ground plane to the real conductor. The image conductor carries a current in the opposite direction to the image conductor as shown in Figure 2.9. This current is in a direction that reduces self-inductance. The mutual inductance between adjacent lines is also reduced by this effect. The self inductance of the line is reduced by the mutual inductance between the

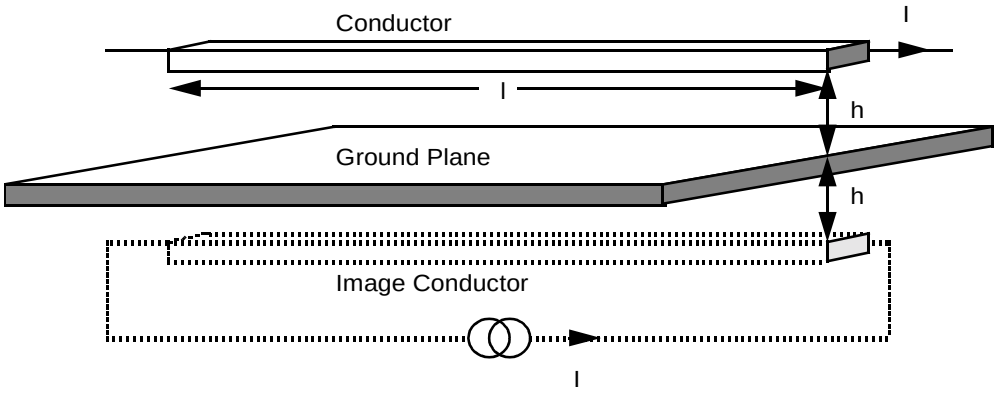

Figure 2.11. The effect of the image current in a ground plane.

lines. The self-inductance of a line separated from a ground plane can be calculated by subtracting (2.11) from (2.15) and assuming the d^2/l^2 term vanishes:

$$L = 2l\left(\ln\left(\frac{2h}{w+t}\right) + 1.5 - \frac{2h}{l}\right) \tag{2.19}$$

As the length of the transmission line is increased to infinity, the inductance per unit length reaches a limit given by (2.19). This effect, and its experimental verification is discussed in more detail in Chapter 3.

Another significant source of error incurred when closed-form equations are used is that the current flowing throughout the cross-sectional area of the conductor is assumed to be uniform. In fact, because of skin effect, and because of the high electric field along the edge of a microstrip line, charge will accumulate along the edges of the conductors. The charge density at DC can be calculated from the method of moments solution. The skin effect can be calculated by assuming that the conductor is split into numerous closely spaced filaments, each with a finite conductivity. The mutual coupling, and the finite conductivity result in an expulsion of current flow from the centre of the conductor at higher frequencies. The skin effect has a pronounced effect on losses, but the effect on self and mutual inductance is minimal. The effect of high electric field appears to be more noticeable, especially in mutual inductance calculations between closely spaced lines. One could take this into account by assigning a weighting factor in a numerical integration of the distances in a GMD calculation, but this has not been done in this work.

2.5.2. Inductance from the Capacitance Matrix

The other way to derive the inductance matrix is to use the fact that the microstrip is, to a good approximation, a TEM structure (see section 2.3), and that the inductance matrix does not depend on the substrate dielectric constant. If it is assumed that the substrate material has a dielectric constant of 1, then the velocity of propagation in that medium is ν, the speed of light. The speed of light also determines the ratio of capacitance to inductance:

$$\nu = \frac{1}{\sqrt{[L][C]}} \tag{2.20}$$

Therefore, the inductance matrix for that structure can be determined by inverting the capacitance matrix. This technique will be referred to as the Inversion of the Capacitance Matrix (ICM) technique. The ICM technique is especially elegant if a capacitance matrix is being calculated anyway; one need only re-run the capacitance matrix program assuming unity dielectric constant, and invert the result.

The ICM technique produces an inductance matrix for a different set of conditions than the closed-form equations. The closed-form equations were derived assuming that current flows throughout the cross-sectional area of the conductor. The ICM technique assumes that the current flows only on the surface of the conductors. The ICM technique assumes that a perfect TEM wave exists on the conductor. As a result, colinear conductors do not magnetically couple, and the inductance per unit length is constant for any length of line. The closed-form equations do not assume the propagation of TEM waves, so that colinear conductors do couple. Therefore, inductance per unit length is dependent on length, as (2.11) confirms.

The operational differences between these two approaches is explored in Chapter 3.

2.6. Loss Calculations

Techniques for calculating loss that are applicable to MMIC sized structures are not widely available. Because semi-insulating substrates are commonly used, the dielectric loss tangent is usually less than .001, and dielectric losses can be ignored. If semiconducting substrates such as silicon were to be used, then the substrate loss tangent would have to be included. Only conductor loss is considered in this analysis. A first-order approximation to conductor loss is to calculate the DC resistance of the conductors, and include fixed resistors with these values in series with the inductances shown in Figure 2.5. This procedure is accurate at DC, and should be accurate for conductors that have dimensions smaller than the skin depth. Usually, only the smallest conductors on digital MMICs are this small, and they are very lossy. Although they are lossy, such conductors can still be accurately described with the TEM approximation [28]. The more typical MMIC conductor has a thickness on the order of the skin depth, and a width of many skin depths. For example, the skin depth of gold at 4 GHz is 1.2 um, and a typical MMIC conductor is 2 um thick and 10 um wide. In these conductors, the currents tend to flow preferentially along the edges of the conductor (although the current in the middle of the conductor will not approach 0). In larger conductors, typically fabricated on ceramic or soft substrates, RF currents tend to flow along the surface of the conductor. If the conductor cross section is large enough, virtually no RF current flows in the central core. The classical theory on microstrip loss [29] assumes that the conductors are at least 3 skin depths thick. To date, no closed-form or simple numerical techniques have been devised to determine the losses of microstrip conductors with thicknesses comparable to skin depth. Numerical techniques have been applied to single microstrip lines, and the results have been tabulated for the geometries of interest to the MMIC designer. An article by Pettenpaul et al. [30] gives a table listing correction factors to the DC resistance, given the “normalized frequency” and the ratio of width to conductor thickness, based on numerical methods. He also gives empirical data in the form of two closed-form expressions, one valid below a w/t ratio of 2.5, and the other valid for higher ratios.

To implement this loss in a simulator, a frequency-dependent resistor must be used. SuperCompact allows only simple algebraic expressions to define component parameters, so the

two empirical loss expressions can not be used. Pettenpaul's second expression (equation 1b in his paper), valid for $w/t>2.5$ can be fitted over the entire range of tabulated data with sufficient accuracy. The empirical expression is:

$$R_{RF} = R_o\left[1 + K_1 x^{2(K_2 + K_3 x^2)}\right] \tag{2.21}$$

$$x = \sqrt{2F\sigma\mu wt} \tag{2.22}$$

where w is the width of conductor in um, t is the thickness of conductor in um, R_0 is the DC resistance of the conductor in ohms, σ is the metal's conductivity, F is frequency in Hz, μ is the permittivity of the conductor, x is the normalized frequency, and K_1, K_2, and K_3 are fitting parameters. Table 2.1 shows the fitting factors for various ratios of conductor width to conductor thickness. Figure 2.10 shows the AC resistance predicted from the empirical formula and the tabular results. The maximum error is less than 6% which is acceptable for a loss calculation. Notice that the loss is given for a line isolated in space over a ground plane. The effect of neighbouring lines is not included, and this will tend to make the loss prediction optimistic.

Table 2.1
Fitting factors used to calculate the DC resistance correction factor.

w/t Ratio	K_1	K_2	K_3
1 2	5.956121E-2	.9146308	-5.582820E-4
4 6	5.202810E-2	.9352023	-5.519648E-4
12	3.632865E-2	.9813440	-5.362747E-4
18	3.555208E-2	.9482391	-4.046604E-4
	4.062991E-2	.8202279	-7.854366E-5
	3.031919E-2	.7623477	1.296432E-4

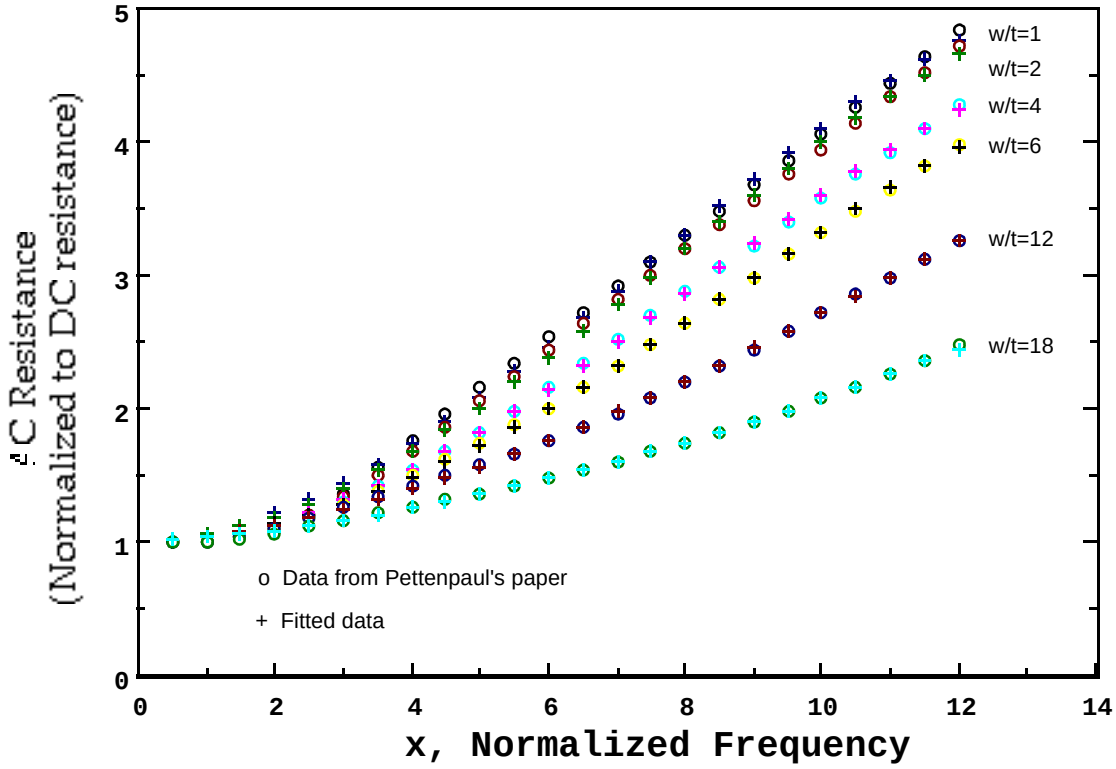

Figure 2.12. Normalized AC resistance vs. Frequency. Doted line is data from [30], solid line is data fitted with (2.21) and Table 2.1.

2.7. Program Integration

To conveniently examine the complex coupled line structures, an integrated program called GEMCAP (GEneral Microstrip Coupling Analysis Package) has been written. GEMCAP acts as a pre-processor to common circuit simulation programs such as SuperCompact [9], Touchstone[10], and Scamper[11]. GEMCAP accepts as input a standard “Netlist” in which special coupled-line descriptors have been embedded. GEMCAP calculates the capacitance and inductance matrices for the lines, and creates an equivalent circuit model that can be simulated by a circuit simulator. The program is written in FORTRAN, in 4 sections: the input, capacitance, inductance, and output sections. Their functions will be briefly described below.

The input to GEMCAP is in the form of two files: an input file that is in the form of a netlist, and a profile. The input file contains both elements and commands native to the simulator (either SuperCompact, Touchstone, or Scamper), and special commands that describe the coupled lines. The user must specify the substrate dielectric constant and thickness, the conductor thickness and resistance (ohms per square) and line widths, gaps and lengths. These descriptors are described in detail in Appendix C. Up to 20 coupled conductors can be handled, but the simulator usually imposes tighter restrictions. The profile file specifies analysis options, such as the type of inductance calculation that is to be done, capacitance calculation accuracy, etc.

The input segment of GEMCAP reads the input file, does simple checks on syntax, extracts parallel conductor information (length, width, spacing, etc.), and places the information into files that are used by the following program segments.

The capacitance program performs a MOM solution of the geometries fed to it by the input program. If the inductor matrix is to be derived by the ICM technique, then a second capacitance matrix is derived by assuming a dielectric constant of 1. The Green's function used is for an infinitely thin conductor over a uniform dielectric. Trapezoidal excitation is used where the charge around the conductor is assumed to be a piecewise linear function of the distance around the conductor. The user can specify the number of subsections that the con-

ductor is divided into in the profile. Typically, analysis with the conductor broken into 8 sections is suggested. The output from this program is a file that contains the capacitance matrix.

The inductance program is the most elaborate program, as it can derive the inductance matrix several ways. If the user has specified in the profile that the inductance matrix is to be derived by inverting the capacitance matrix, then the inversion is done here. If closed-form equations are to be used, then there are several options. If two conductors are long and close, so that width must be taken into account, then detailed GMD calculations are done to calculate the mutual inductance. If the two lines are offset from each other, then (2.16) is implemented. The flow chart shown in Figure 2.11 shows the overall process for calculating inductances most clearly. Note that the input to the inductance calculating program can contain parallel lines located anywhere on a plane; not just side by side. The output of the inductance program is a file containing the inductance matrix.

The output program reads the capacitance and inductance matrices and incorporates them into the equivalent circuit shown in Figure 2.5. The equivalent circuit is written to the output file using current sources, resistors, capacitors, and inductors native to the simulator to be used. It also calculates the values of resistors or frequency dependent resistors for implementing losses correctly. Lines in the input file that were not used by the input program are duplicated in the output file. The output file can be directly read into either SuperCompact, Scamper, or Touchstone.

The analysis of an inductor or transformer is done in three steps. First, an input file is written as described above. GEMCAP is invoked, and the four sections of program are automatically run. This part of the process runs without intervention. Finally, the simulator of the user's choice solves the netlist produced by GEMCAP. Restrictions in the complexity and size of the input file are imposed both by GEMCAP and the circuit simulator.

GEMCAP places the following restrictions on the geometries to be entered: No more than 60 segments, mutually coupled to each other, can be entered. These segments can be made up of blocks of side by side lines, each block containing no more than 20 lines. GEMCAP

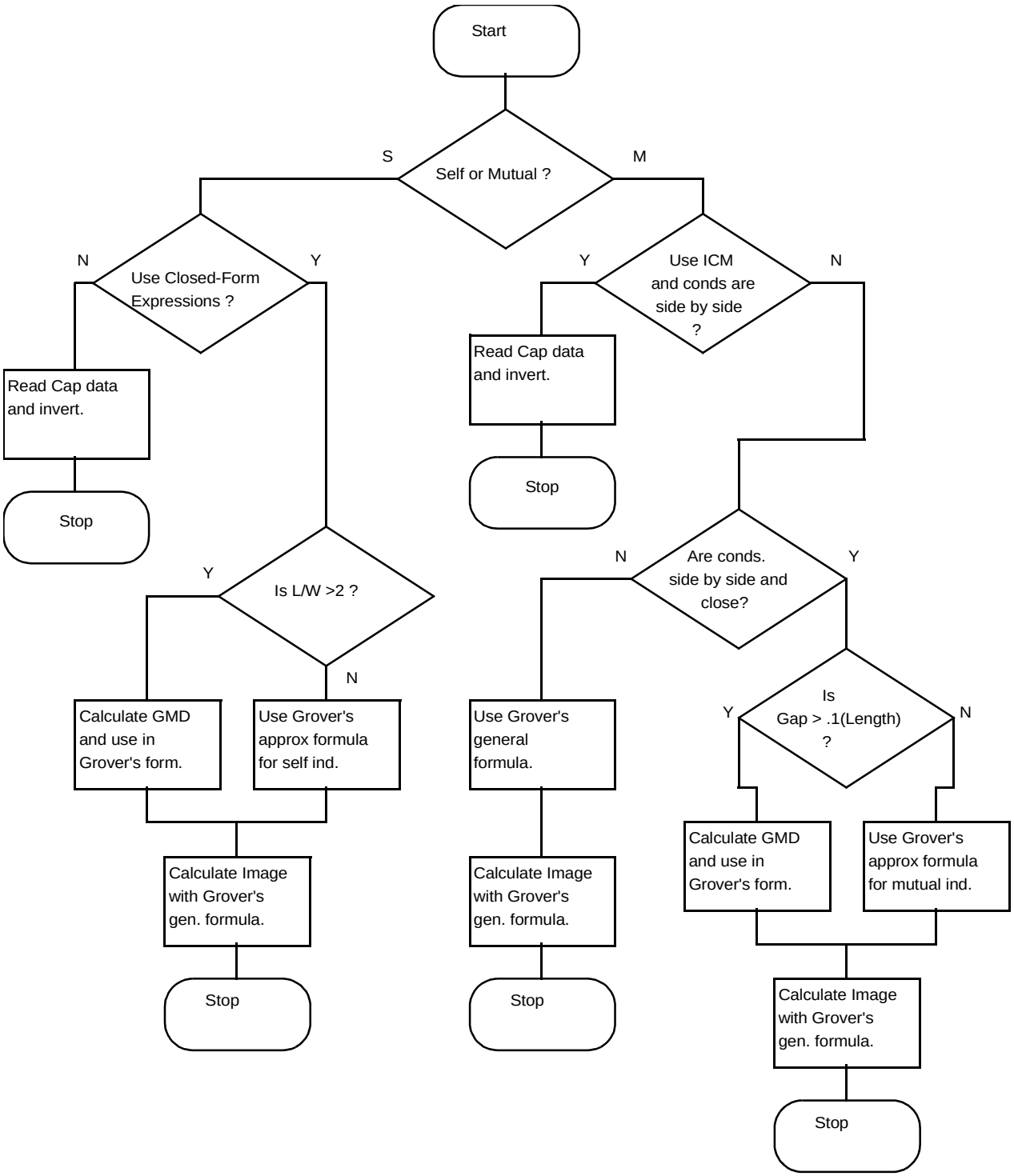

Figure 2.13. Flow Chart of GEMCAP inductance calculation.

can handle an unlimited number of 60 segment coupled line systems. To illustrate this, Figure 2.12 shows 6 blocks of 4 lines each, in a Lange coupler configuration. GEMCAP calculates the capacitance from every segment to ground, and between each side by side segment. It can also calculate the self inductance of every segment, and the mutual inductance between every pair of segments, regardless of position, although only the mutual inductance of close lines is usually included. Each arm of the Lange coupler could be divided into up to 7 pieces, and the total would be less than 60 segments. Each arm must contain no more than 20 parallel elements, however. More details are given in Appendix C.

GEMCAP will have limited accuracy when simulating coupled lines that have gaps wider than line length or line width greater than line length. The line width and gap restrictions are principally due to the assumption that current flow is uniform across the conductor. These configurations are dominated by end effects, and require full wave analysis for proper simulation. Substrate height restrictions stipulate that line width should be no more than the substrate height if the closed-form equations are to be used. The loss calculation is valid from w/t ratios of 1 to over 20. w/t ratios beyond this range will be pessimistic by a maximum factor of 2.5. The thickness of the conductor must be kept smaller than the gap between conductors and the width of the conductor, as the capacitance calculations assume an infinitely thin conductor, and the inductance calculations take conductor thickness into account approximately.

The circuit simulator usually provides a more severe restriction on the size of the circuits that can be analysed. SuperCompact [9] has a 50 node limit in Version 1.95 on an IBM mainframe, which implies that no more than 25 segments can be placed in a block. All 3 simulators have vague limits on the size of the file that can be accepted. Scamper is capable of handling the largest files. The Lange coupler, shown in Figure 2.12, containing 24 elements, and spiral inductors containing 36 elements have been successfully analysed in Scamper. For extremely complex topologies, such as some of the transformers described in Chapter 4, it is better to fit a model (similar to the ones in section 2.2) to the simulated data, rather than using the GEMCAP output in a circuit design.

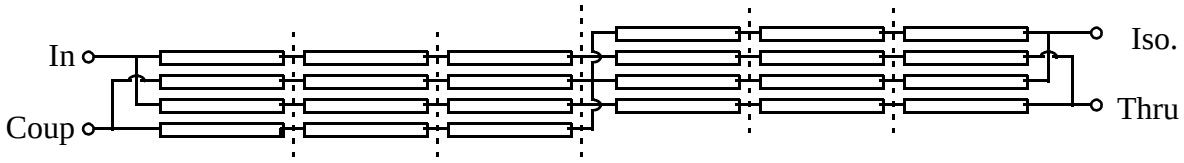

Figure 2.14. GEMCAP equivalent circuit for a Lange Coupler.

CHAPTER 3
GEMCAP VALIDATION

3.1. Introduction

This chapter deals with the use of GEMCAP in the analysis of familiar microwave elements such as transmission lines, couplers, and inductors. Simulated parameters will be compared to measured results, other simulators, and published results. The goal of the chapter is to validate GEMCAP and some of its underlying assumptions, and to determine its range of validity.

3.2. Simple Transmission Line

3.2.1. Analysis of a Transmission Line

The simplest structure for GEMCAP to analyse is a single microstrip transmission line. GEMCAP can process a file containing a physical description of the line to create a file that contains an electrical equivalent circuit of the line.

As a first example, assume that a line of width 20 microns and length 500 microns on a GaAs substrate is to be analyzed. The GaAs substrate has a height of 100 microns, and a dielectric constant of 12.9. The gold metallization from which the transmission line is fabricated is 2 microns thick, and has a resistance of .01 ohms per square. These parameters are representative of a typical line used on a MMIC. Figure 3.1 shows the input file that would be accepted by GEMCAP for eventual use with SuperCompact. The XSUB line describes the substrate. The XCON describes the conductor height and resistive losses. The WID line describes the width of the line(s), and the GAP line describes the spaces between them. Note that there is only one conductor in this system, so the information on the GAP line will be ignored. Further down in the file, there is a NUM statement that indicates the number of conductors in the system being simulated. The SEG statement indicates which nodes the conductor is connected to, and the conductor's length. The rest of the file is in standard SuperCompact notation.

When GEMCAP is run, it searches for a PROFILE file that sets various processing options. The PROFILE was configured to calculate the inductances with the closed-form equations described in Chapter 2.5.1. This file is described in Appendix C. If all other options are set to their default values, then the SuperCompact file shown in Figure 3.2 is produced. Notice that the SEG statement has been replaced with an equivalent circuit of the transmission line. The equivalent circuit is a simple pi type structure with a resistor in series with the inductor to simulate loss.

If the program is executed using the ICM technique to calculate the inductance, the answer is rather different. The series inductance for the same topology is .3704 nH rather than

```
* Substrate, Conductor and Line Dimensions
*
XSUB 12.9 100
XCON 2 .01
WID 20
GAP 10
*
* SuperCompact Data File
*
BLK
*
* Line Description
*
NUM 1
SEG 1 2 500
A:2POR 1 2
END
FREQ
STEP 1GHZ 10GHZ 1GHZ
END
```

Figure 3.13. GEMCAP input file for a single microstrip line.

```
 BLK
*  1 CONDUCTOR GROUP WITH 20.0 UM WIDTH AND 10.0 UM GAP
IND   1 401 L    0.3344415NH
RES   2 401 R    0.2500000
CAP   1   0 C    0.0292985PF
CAP   2   0 C    0.0292985PF
*  1 CONDUCTOR GROUP WITH 20.0 UM WIDTH AND 10.0 UM GAP
A:2POR 1 2
END
FREQ
STEP 1GHZ 10GHZ 1GHZ
END
```

Figure 3.14. GEMCAP output file for use with SuperCompact.

.3344 nH. Table 3.1 shows the impedances and effective dielectric constants calculated from the inductance and capacitance matrices produced by GEMCAP for various line lengths. Values calculated by the transmission line analyser in SuperCompact are also tabulated. From this table, it is apparent that the ICM technique and, for long lines, the closed-form equations agree well with SuperCompact. The predicted inductance of shorter lines calculated with the closed-form equations is less than with the other techniques. The capacitance matrix for all four GEMCAP runs is identical. This difference is due to the shortness of the line with respect to the substrate height.

Traditional transmission line theory assumes that the transmission line is infinitely long. When the capacitance matrices are calculated in the ICM solution of the inductance matrix, capacitance fringing effects at the line ends are ignored; the electric field is assumed to have no component in the direction of propagation. In order to determine the inductance from the capacitance matrix, both the electric and magnetic fields are assumed to have no z component (the TEM assumption). These assumptions are reasonable as long as the cross sectional area in which the field is confined is small compared to the length of the line. In the case of a microstrip line, the line length must be much greater than the substrate thickness. This is clearly not true for many MMICs. GaAs MMICs are made on substrates with thicknesses from 100 um to over 500 um, and overall chip sizes are often only 2000 um. Line length to substrate height ratios can be much less than unity.

If the standard (ICM) solution for the inductance is applied to such a problem, one should find that the measured inductance is lower than predictions. To see why, assume that a con-

Table 3.1
Simulated Impedances and Effective Dielectric Constants for Transmission Lines

Simulator	Length	Impedance	ε_{eff}
GEMCAP (Closed-Form)	200 um	70.8 Ohms	6.17
GEMCAP (Closed-Form)	500 um	75.5 Ohms	7.05
GEMCAP (Closed-Form)	50000 um	79.5 Ohms	7.81
GEMCAP (ICM)	any	79.6 Ohms	7.79
SuperCompact	any	79.2 Ohms	7.81

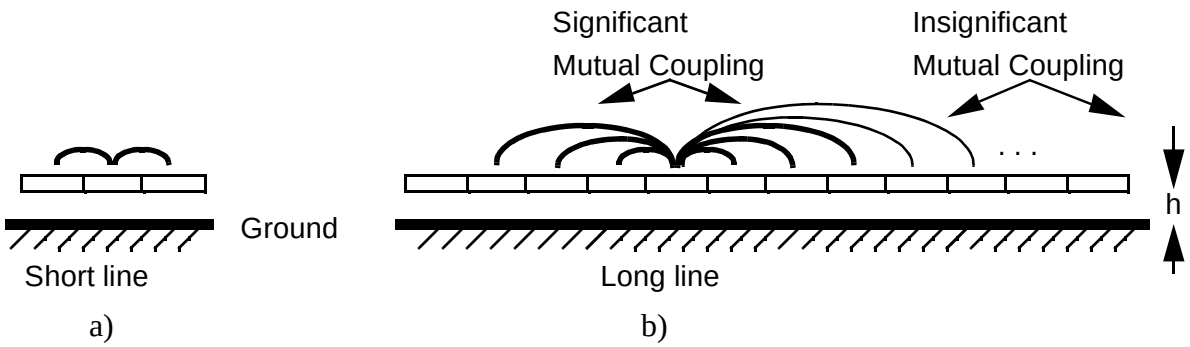

Figure 3.15. Comparison between a short line and a long line. Notice that the shielding effect of the ground plane prevents opposite ends of the line from coupling.

ductor is divided into pieces, each of which is *h* long, where *h* is the substrate height, as shown in Figure 3.3(a). The ground plane has a shielding effect such that conductors more than roughly 3*h* apart have negligible mutual inductance. On a long line, such as the one in Figure 3.3(b), virtually every segment is mutually coupled to 6 other segments, and this coupling acts to increase inductance per unit length. Segments that are farther apart have negligible mutual coupling. On smaller lines, many or all segments are coupled to fewer than 6 other segments, and the overall inductance per unit length is lower. This effect is predicted by (2.10) directly. Figure 3.4 shows inductance of a 20 um wide conductor over a 100 um thick substrate for various conductor lengths as predicted with the closed-form expressions. Also shown is the inductance that would be calculated by the ICM technique, which is exactly proportional to the length. Notice that the closed-form inductance appears to be offset from the ICM inductance by a fixed amount. At very long lengths, the two lines converge, as the offset becomes negligible compared to the length. Similar curves have been published previously [22]. These curves suggest that it might be possible to correct inductances calculated through the ICM technique by shortening the line by a fixed length.

The return path inductance also tends to make the inductance calculated with closed-form expressions low. As was mentioned in Chapter 2.5, the closed-form expressions calculate only the inductance of the line on the top surface of the microstrip, not the return path. This error is expected to be largest for short lines.

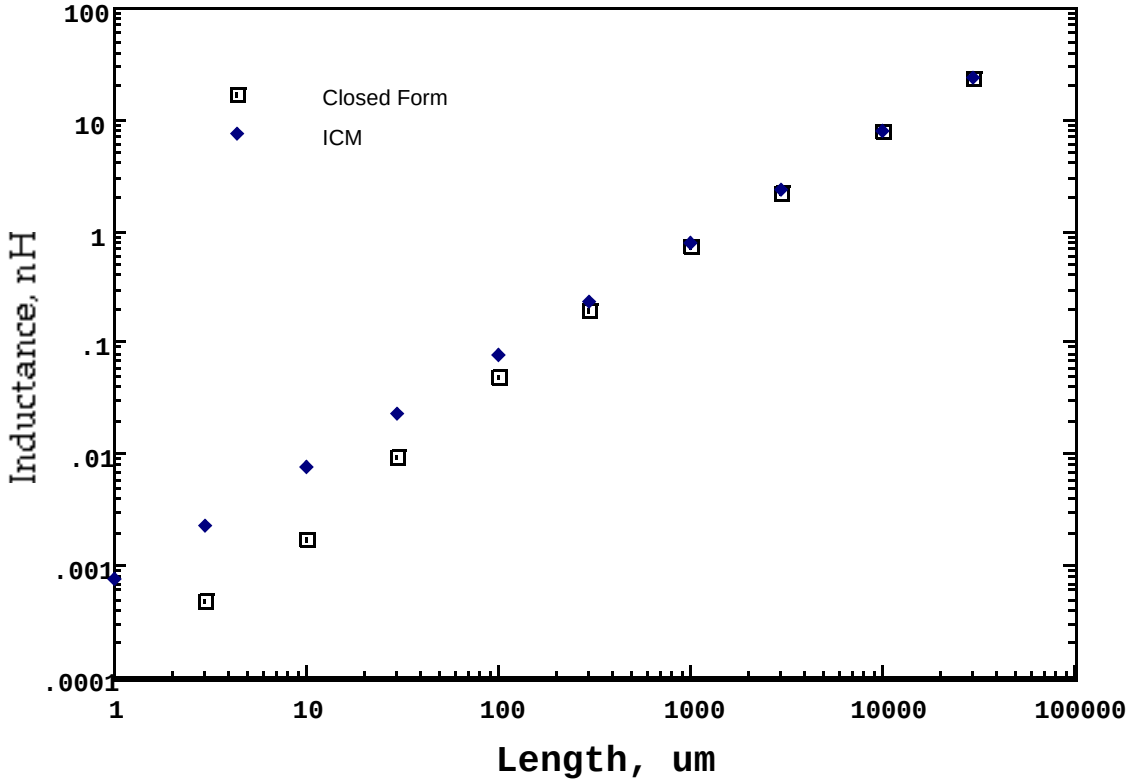

Figure 3.16. Inductance vs. length calculated with closed form expressions, and the ICM technique.

3.2.2. Experimental Verification of the Transmission Line Models

Several experiments were performed to try to verify these effects. It was expected that short lines (lines that have a length comparable to the substrate height) would have lower self inductance per unit length than longer lines, and that the closed-form expressions would be more accurate for short lines. The 1-port s-parameters of .125 inch wide lines on a .25 inch alumina substrate ($\varepsilon_r = 9.9$) with lengths of .5 inch, 1 inch, 1.5 inch, and 2 inch were measured. The far end of the line was shorted to the back-side ground plane with a wrap-around ground, as shown in Figure 3.5. The measurements were done from 150 MHz to 2 GHz. The experimental results along with simulated results from GEMCAP using both techniques and SuperCompact are shown in Figure 3.6. The GEMCAP (using ICM technique)

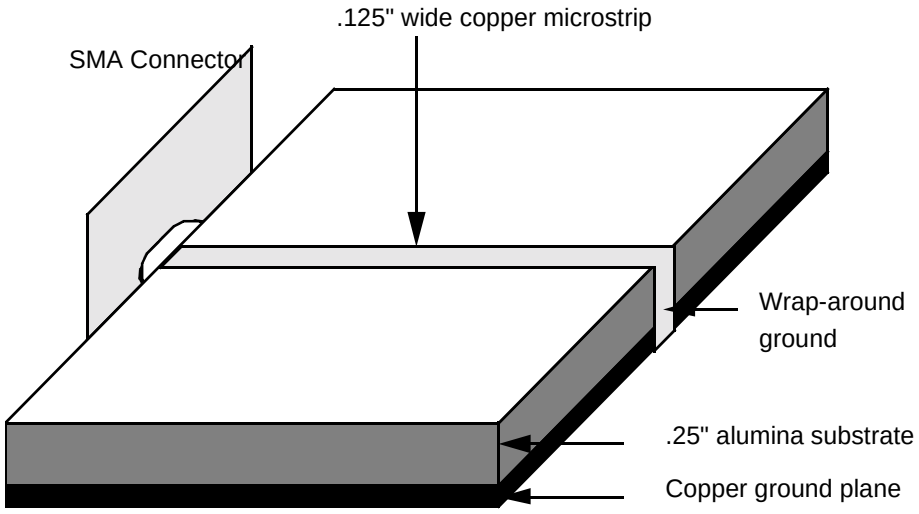

Figure 3.17. Basic microstrip one-port test fixture.

solution, and SuperCompact both predict constant inductance per unit length, as expected. The closed-form expressions predict increasing inductance per unit length for longer lines. The measurements suggest slightly decreasing inductance per unit length for longer lines. This series of experiments highlighted one of the problems with such experiments: any error in the position of the reference plane will change the slope of the curve. A 1 degree error in the position of the reference plane makes the measured results almost constant with respect to length. Because of uncertainties in calibration standards, and the wrap-around ground, 1 degree of accuracy was not achieved.

A second, similar, experiment was performed in a more controlled manner to try to resolve the discrepancies. The .25 inch substrate was difficult to work with, so air dielectric was used. In order to avoid the effect of wide lines, a 10 mil diameter wire approximating a filamentary conductor, was used instead of a flat stripline. The wire was suspended .25 inches over a ground plane by an SMA connector on one end and a grounded copper plate on the other. The one-port s-parameters were measured at 150 MHz for wire lengths of .2 to 1.0 inches. Special calibration standards were made from SMA connectors to avoid problems with the reference plane uncertainty. The graph of inductance vs line length is shown in

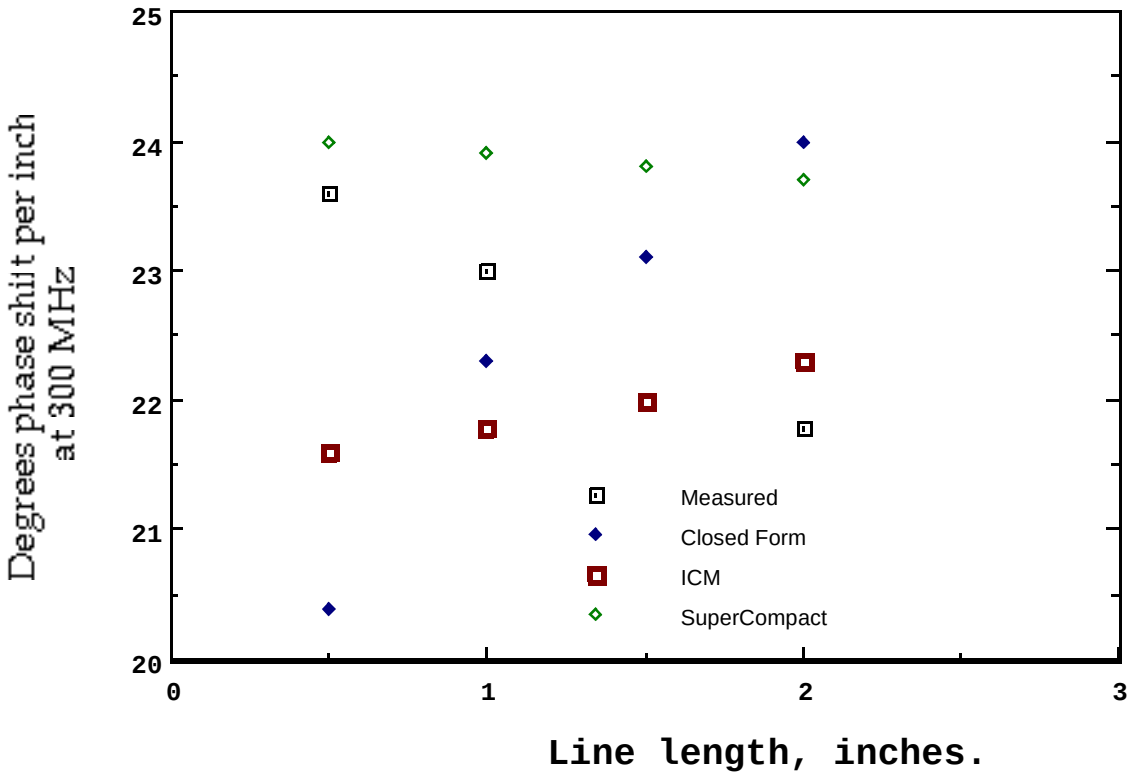

Figure 3.18. Simulated and measured angle of S_{11} at 300 MHz for microstrip test fixture, Figure 3.5.

Figure 3.7. Simulations using the closed-form equations suggested that the line would intersect the length axis at roughly .05 inches because of the short line effect. When a straight line is fitted to the measured data, the line extends almost exactly to the origin. (Note that if a 50 inch long line is simulated with closed-form equations, it does closely match extrapolated measured results.) A simulation using GEMCAP with the ICM option matches measured results quite well. The above experiment was repeated, but the end ground plate was replaced with another SMA connector, and two-port s-parameters were measured. Similar results were seen.

Two reasons for the disagreement have been investigated. In all of the above experiments, the current is returned from the end of the line by a wrap-around ground and the ground plane, both of which add extra inductance. If the effect of the ground plane inductance

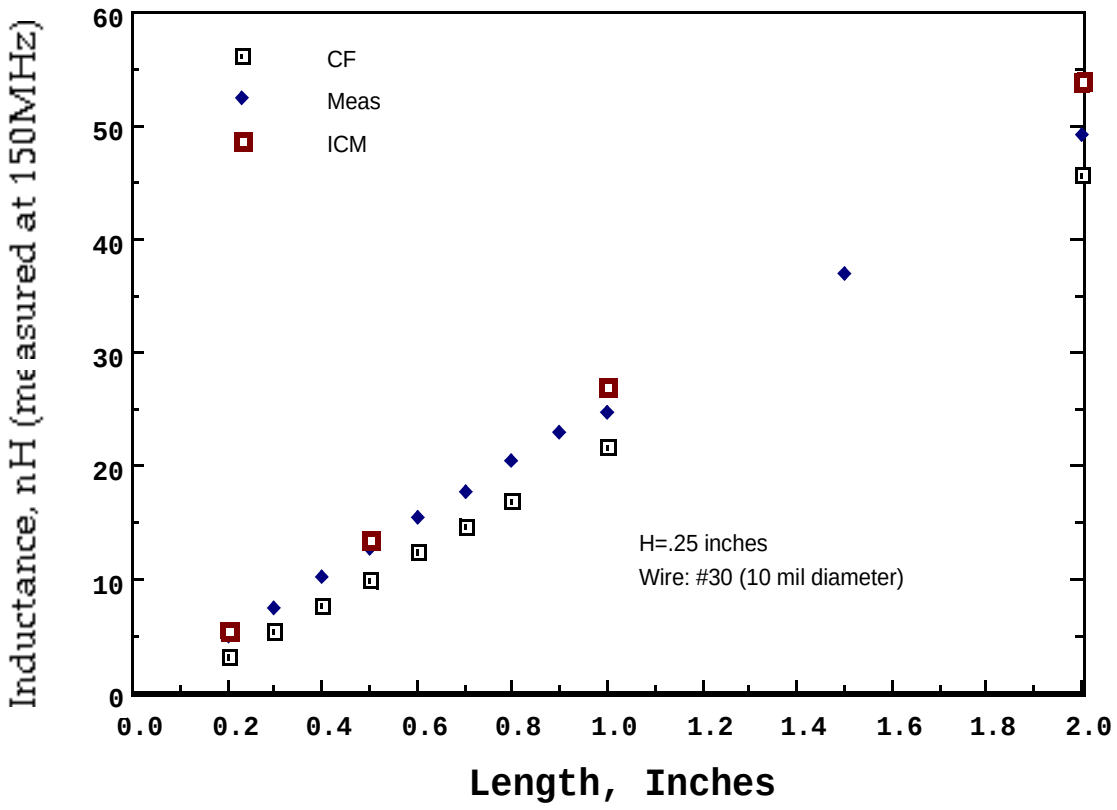

Figure 3.19. Measured and simulated inductance vs. length for a filamentary conductor .25 inches over a ground plane.

became more significant for short lengths of line, then enough line inductance might be added to account for the discrepancy. However, the most likely reason for the disagreement appears to be the effect of current induced into structures supporting the ends of the wire.

All measurements were made by placing the short transmission line between 2 planes (with the line perpendicular to both planes). One or both of the planes held an SMA conductor. These planes will have the same effect as the ground plane described in Chapter 2.5; the perpendicular component of the time varying **H** field must vanish at the conducting plane. When the ICM solution is performed, this condition is automatically satisfied as TEM waves are assumed to propagate, and by definition, a TEM wave will have no components perpendicular to the end plates. (Note that although the ICM solution seems to solve the

problem elegantly, it is inherently wrong, as current must flow perpendicular to the wire at the end. Any flow of current along one of the end plates will set up a perpendicular component to the magnetic field, which must be cancelled out by the electromagnetic wave impinging on the plate. Therefore, the wave is no longer TEM, and the ICM solution becomes invalid. The ICM solution is valid for long wires, as these end effects become a negligible part of the total inductance.) The closed-form solutions do not make any assumptions about the z- component of the magnetic field. The fact that the closed-form equations predict coupling between colinear lines (from (2.16)) indicates that there certainly is a z-component to the magnetic field. That being the case, the boundary conditions at the end plate must be satisfied. The simplest way to do this is to assume the existence of an image conductor colinear with the transmission line on the opposite side of the end plate. The direction of the current in this line is in the same direction as the current in the main line in order to cancel the perpendicular component of the magnetic field. In other words, the conductor is assumed to extend out, making it look more like an infinite conductor (which would support a TEM wave). Once again, this effect will be most noticeable on short lines where the centre to centre distance of the main line and its image is small compared to the ground plane height. Long lines are shielded by the ground plane so that the image conductor has little effect.

This theory has great ramifications on the experimental proof of the short line effects. If the end plates are made large, the image inductance must be taken into account, making the self inductance look larger, thereby masking the desired effects. If the end plates are made small, they will introduce significant inductance in series with the desired inductance, again masking the true self inductance.

To prove this theory, a third experiment was performed. In this experiment, the entire circuit is above a ground plane, and the ground plane does not form part of the circuit. The image current effects were reduced by eliminating one end plate, but the other end plate, the connector flange, could not be removed. Figure 3.8 illustrates the apparatus. The circuit is formed by a rectangular loop of 10 mil diameter wire. The width of the rectangle is fixed at .25 inches, and the length is varied from .25 to 1.0 inches.

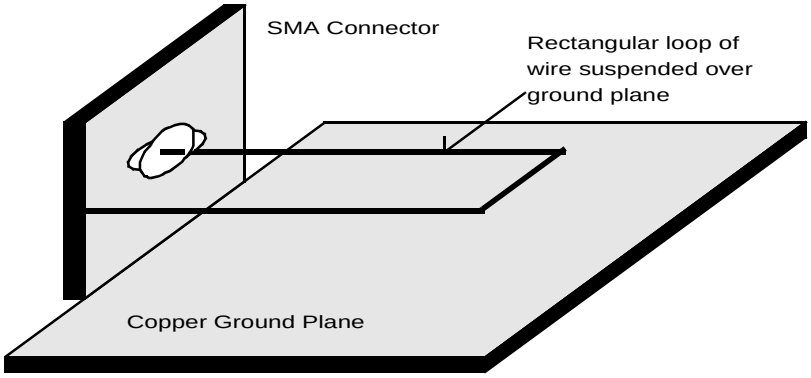

Figure 3.20. A simple loop over a ground plane.

The GEMCAP simulation of this circuit is more complicated than the previous examples. The GEMCAP equivalent circuit is shown in Figure 3.9. The mutual inductance between the parallel legs of the loop, and between the loop and the image conductors had to be considered. Note that current controlled current sources force the image inductors to have the same current as the main mesh.

Figure 3.10 shows the predicted and measured inductance of a .25, .5, .75, and 1 inch long loops. The closed-form equations with the image inductances included agree well with the measurement. The image inductor correction was not applied to the ICM solution, because this solution assumes that a TEM wave propagates, and therefore the boundary conditions are satisfied. If the corrections are applied, the ICM technique yields even less accurate answers.

From these experiments, one can conclude that the inductance of a short length of line that does not form a closed path can not be directly measured. However, the closed-form equations can be verified by looking at closed paths, and taking into account some of the second-

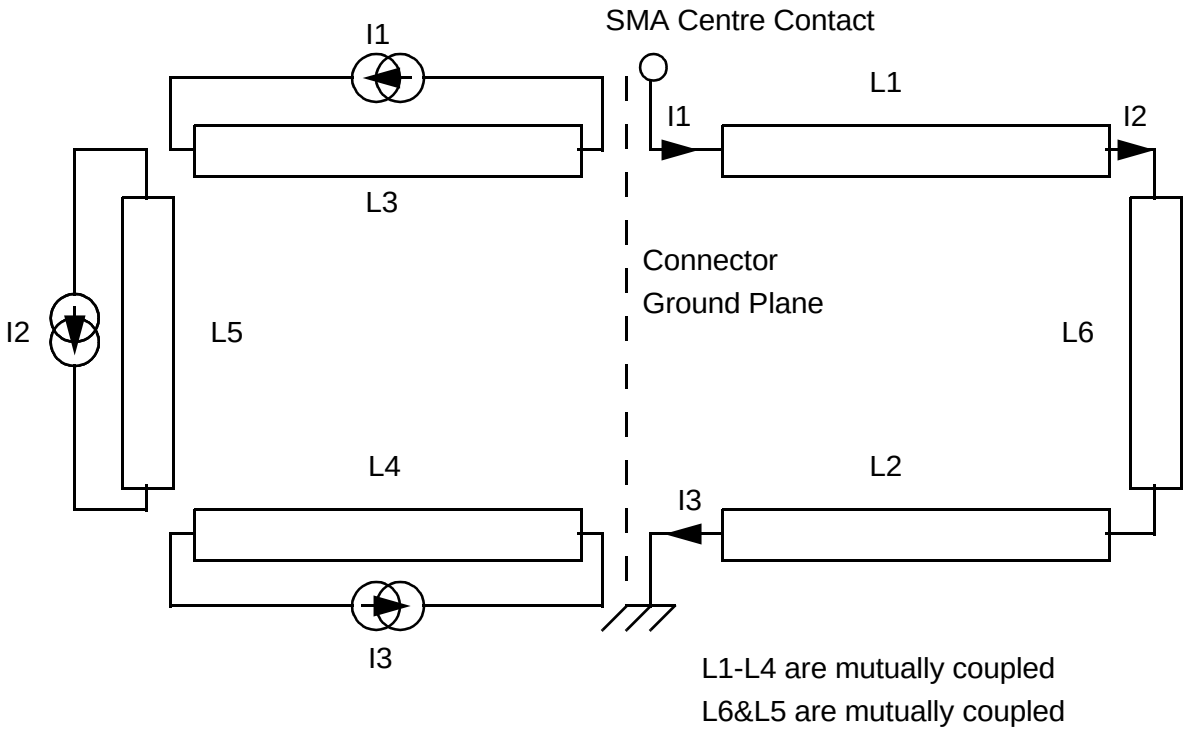

Figure 3.21. Equivalent circuit used to simulate the loop, with the effect of the image in the connector plane.

order effects. When these corrections are properly applied, the closed-form equations yield correct results, and the hypothesis that the inductance per unit length of a transmission line decreases for short lines is confirmed.

3.2.3. Transmission Line Loss Calculations

In the example in Figure 3.2, loss was modelled as a constant resistance in series with the inductive element. The resistance can be made frequency dependent to model the skin effect by enabling that option in the profile. The resistance of the resistor is calculated with (2.21). In order to create a frequency dependent resistor, an undocumented feature in Super-Compact must be used. The variable “F” is set by SuperCompact to the analysis frequency. The dispersive resistor call for Figure 3.2 is shown in Figure 3.11.

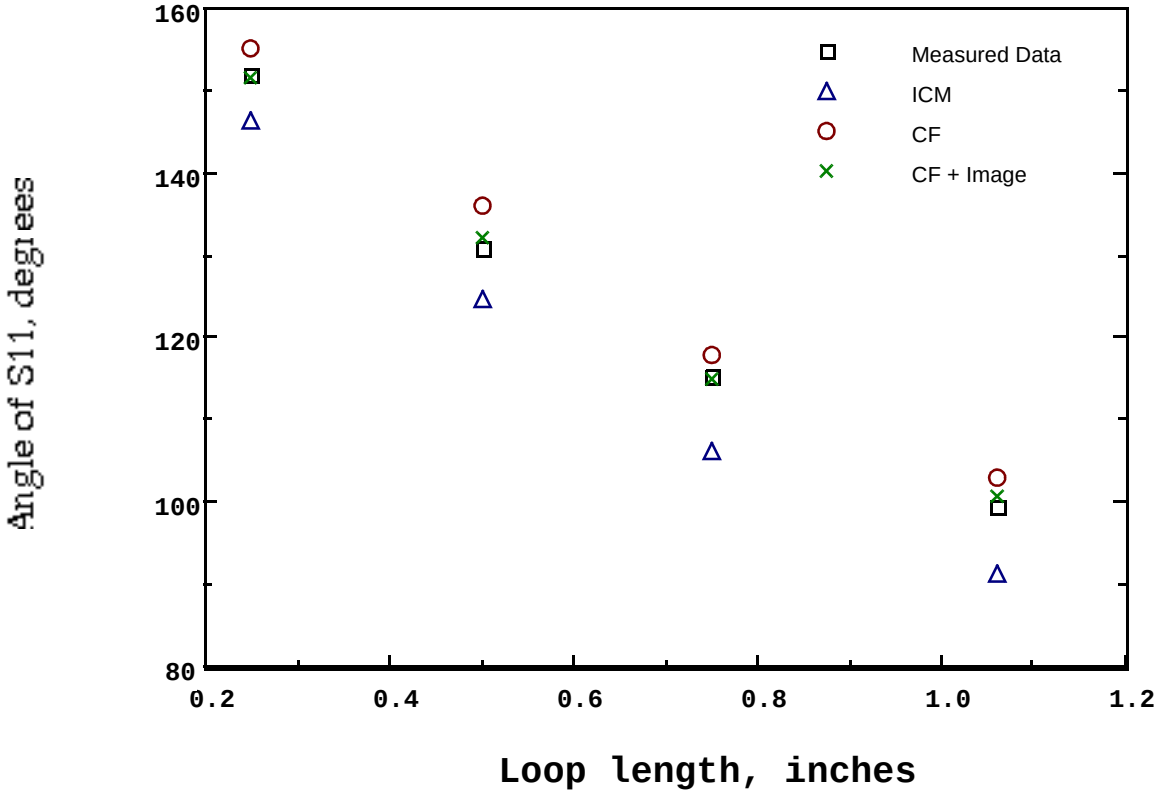

Figure 3.22. Angle of reflection coefficient (which can be related to the inductance) versus loop length, measured and simulated.

```
RES   2 401 R
+ (.25000E+00*(1+.40623E-01*(.50264E-08*F)**(.82023-.39479E-12*F)))
```

Figure 3.23. Frequency dependent resistor in SuperCompact.

At microwave frequencies, most of the current tends to flow along the edges of a conductor as a result of the skin effect. This can be illustrated with GEMCAP by breaking a wide conductor into many narrow pieces. In the example shown in Figure 3.12, the 20 um wide transmission line is broken into twenty sub-segments, each of width 1 um.The mutual inductance of every segment to every other segment is considered. To simplify the calculation, the capacitance to ground is ignored. The transmission line is driven by a high-fre-

quency ideal current source, and the current in each sub-segment is monitored. Figure 3.13 shows the current density (in amperes per micron) as a function of the distance from the edge of the transmission line. At low frequencies, the current is uniformly distributed along the width of the line. Above roughly 1 GHz, the current tends to accumulate along the edge of the line. Notice that this distribution is different from the charge distribution calculated in the MOM capacitance solution, as the current density distribution is highly frequency dependent. The effective AC resistance is calculated by dividing the voltage drop across the lines by the value of the current source. The predicted AC resistance of the segmented line increases with frequency. The AC resistance of a 20 um wide, 2 um thick, 500 um long gold conductor is plotted in Figure 3.14. The loss has increased by a factor of two over the DC value at 18 GHz. Note that the value of AC resistance from the segmented conductor simulation assumes that the current is uniform along any vertical line through the conductor. Pettenpaul [30] has calculated the AC resistance of a conductor with the skin effect taken into account on all four sides. This resistance is also plotted in Figure 3.14. This resistance is higher at high frequencies than the value calculated by segmenting conductors

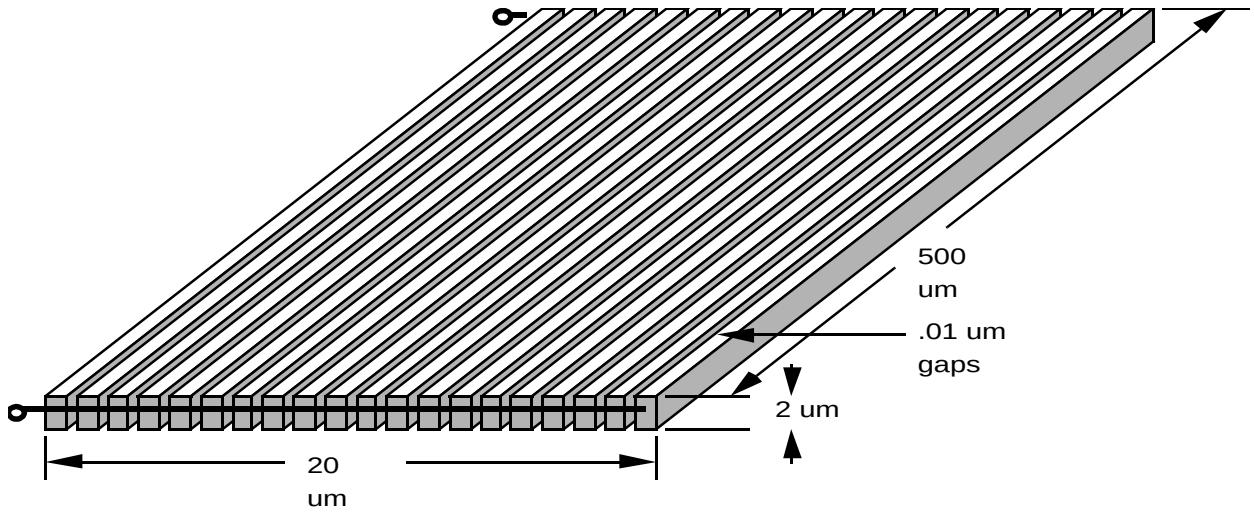

Figure 3.24. In order to determine the current distribution in a microstrip line, the line can be analysed as 20 parallel coupled microstrips that are connected in parallel.

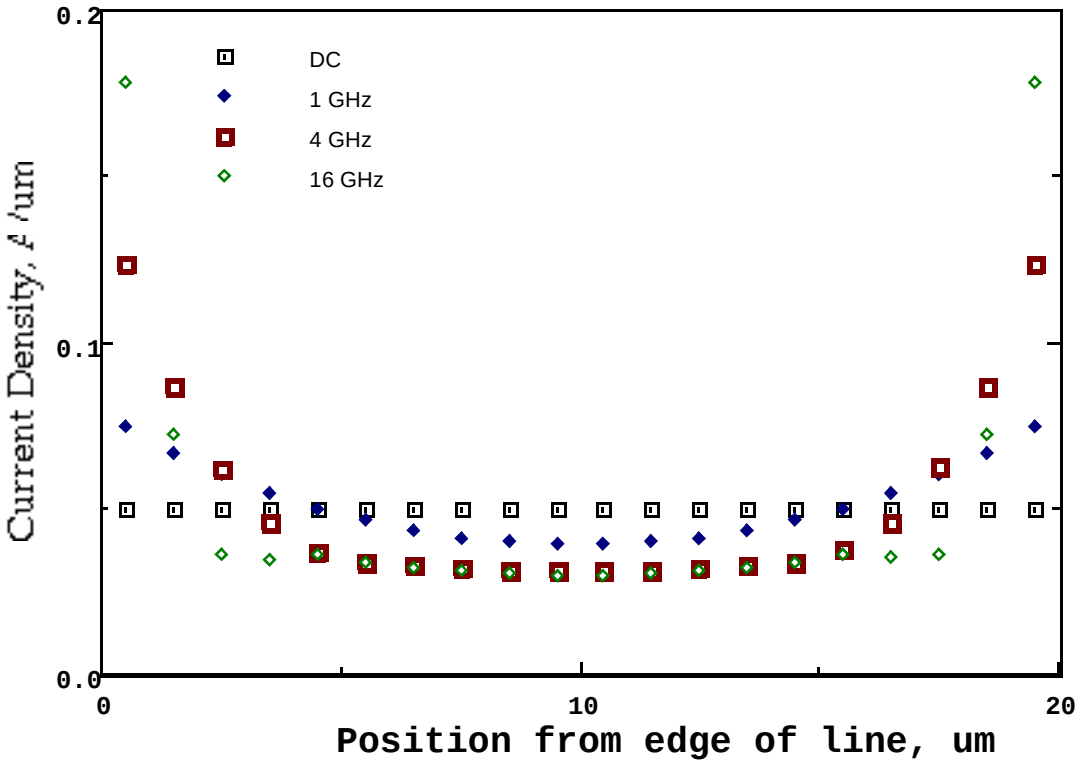

Figure 3.25. Simulated current distribution across a microstrip.

because of the skin effect on the thickness of the conductor, and because of the finite width of the segments in the segmented conductor simulation.

Very small MMIC conductors (with dimensions similar to the skin depth) will have uniform current flow through the cross-sectional area of the conductor. This implies that the loss of the conductor will be proportional to the area of the conductor. The surface roughness and the grain structure of the metal can have dimensions that are starting to be a significant fraction of the metal thickness, so these effects have a large effect on MMIC losses.

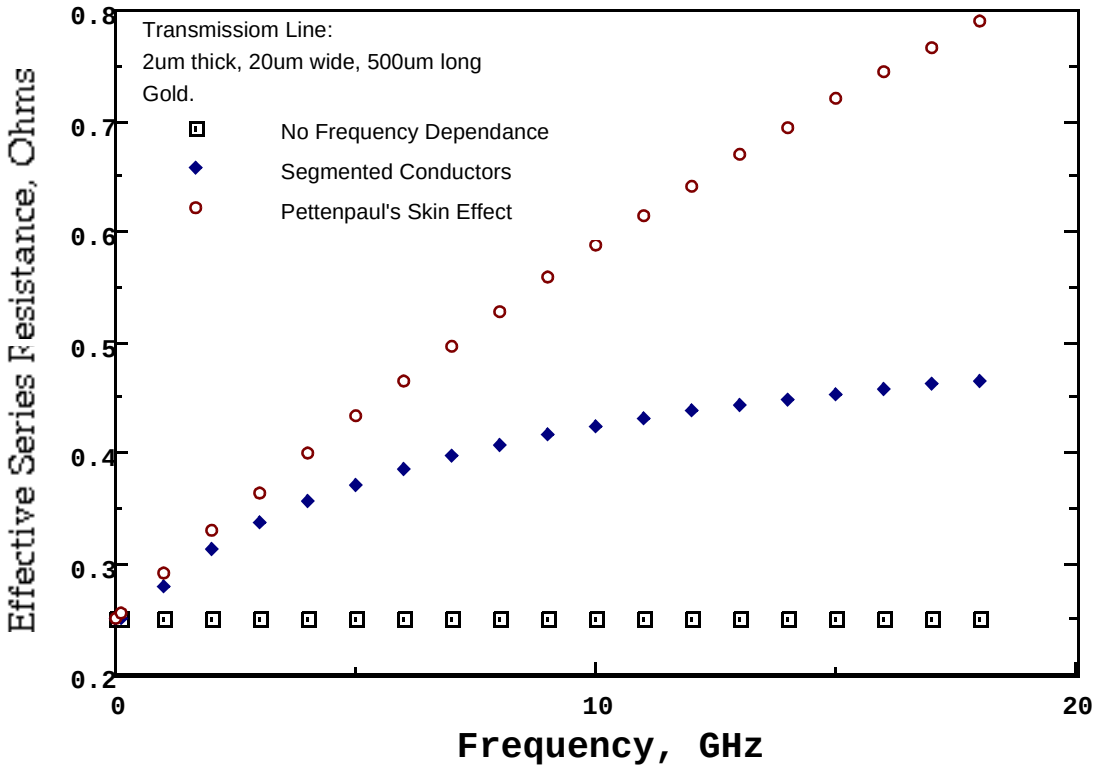

Figure 3.26. RF resistance of a 500 um length of microstrip line as calculated 3 different ways.

3.3. Coupled lines

In the preceding section, it was discovered that very few circuit elements can be considered using self inductance only. In fact, mutual inductance had to be used to explain the performance of the small inductive ring, and the skin effect demonstration circuit. The accuracy of mutual inductance calculations is crucial even for single port devices.

Many of the short line effects that were observed with the self inductance are also evident in mutual inductance. It is interesting to compare the inductance predictions of conventional transmission line theory and the ICM technique, with Grover's closed-form equations. For tightly coupled lines (lines where the gap between lines is smaller than the substrate height), the per unit length mutual inductance is constant for very long lines, but reduces when the line length approaches the height of the substrate. This effect is barely noticeable, as the close coupling masks the coupling from line ends. It only becomes noticeable when the line length is further reduced to be comparable to the gap, but this configuration is completely dominated by end effects and can not be solved using these techniques. For lightly coupled lines (lines where the gap is more than twice the substrate height), the per unit length mutual inductance is constant for long lines, but reduces when the line length approaches or falls below the gap width. In other words, classical transmission line theory fails when either the gap or the substrate height becomes a significant fraction of the line length. The reason for this reduction is the same as for the reduction in self inductance: in a long line, there is insignificant coupling between opposite ends of the line, so adding length does not change coupling per unit length. In a short line, there is coupling between opposite line ends so that increasing length adds a disproportionate amount of mutual inductance. As was the case with self inductance, Grover's closed-form equations predict the short line effects, and the ICM technique does not.

3.3.1. Coupled Line Measurement

It would be reassuring to measure the mutual inductance for lightly coupled conductors to verify this theory. This measurement is a difficult one, as the small coupling is easily masked by leakage inductance and capacitance. Several attempts were made to experimen-

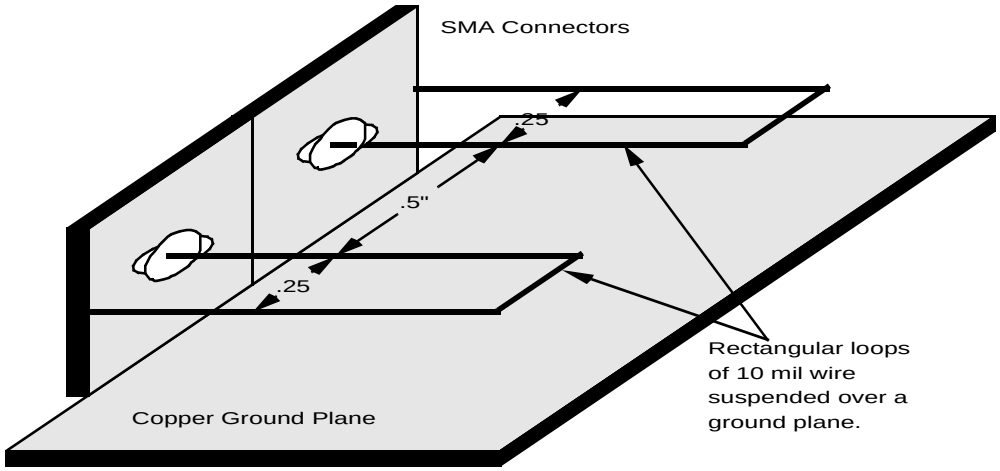

Figure 3.27. Two loops suspended over a ground plane.

tally measure the reduction in mutual inductance for short coupled lines, as was done for short transmission lines in Chapter 3.2. The configuration of the first attempt is shown in Figure 3.15. Two loops of 10 mil diameter wire were placed next to each other .25 inches above a ground plane. Most of the coupling between the loops occurs between the two parallel, adjacent lines separated by a .5 inch space. (A similar geometry employing a .25 inch thick ceramic substrate was employed, but the extra capacitive effects made the results difficult to interpret.) The measured S_{21} of this structure was compared to the S_{21} calculated by GEMCAP. The peak of the measured results matched the peak calculated by the ICM technique to within 2 dB, but at low frequencies (where very little coupling was predicted), measured coupling was more than 10 dB higher. The agreement with predictions made with closed-form equations was much worse. The predicted peak coupling was low by 12 dB. The reasons for these discrepancies are not known, although there may be coupling via the ground plane. This is elaborated on in the next paragraph. These measurements were dis-

turbing, because they indicated either that there was a large amount of stray coupling in the experimental set-up, or that, contrary to Grover [22], the closed-form equations fail to work for short line lengths.

A second test was done to try to measure mutual inductance directly. A high frequency current source was used to drive one of a pair of coupled lines while the voltage induced across the other line was measured. The ratio of the induced voltage to the current yields the mutual reactance, from which the mutual inductance can be determined directly. The test was done with long lines (22 cm long) at low frequency (5 MHz) so that dimensions could be measured easily, and parasitics could be controlled. The test was difficult, however, because lightly coupled structures were to be analyzed. An output voltage swing on the order of 2 mV p-p was expected for a current of 0.2 A p-p. Any leakage from the input to the output would mask the desired response. To minimize leakage, half-inch nickel plated steel plates were used as the ground plane and as a shield between the two halves of the test as shown in Figure 3.17. The thickness of the plates was necessitated by the large skin depth at 5 MHz, although .5 inch plates were far more than adequate.

The results of the testing were interesting, if not conclusive. When the lines were spaced by 8.7 cm, .625 cm over the ground plane, a voltage of 10 mV p-p was induced in the second wire. This voltage is approximately what the ICM technique predicts, but is 50% higher than the closed-form predictions. When the height was reduced to .1 cm over the ground plane, the induced voltage decreased to 5 mV, roughly as expected. When the height was reduced to 0 cm over the ground plane (i.e.: when the wire was taped to the steel plate so that only the wire's insulation separated it from the plate), the induced voltage increased to 11 mV, a completely unexpected result. One would have expected the overall mutual coupling to vanish, as the mutual coupling to the image inductance cancels the main mutual coupling. In fact, even if the wires were mounted entirely under the ground plane, a sizeable voltage was induced. This phenomenon was not electrostatic in nature, as it only occurred when the circuits at both ends were closed. The coupling was due to the non-ideal nature of the ground plane. The steel plate caused the current induced by the source wire to spread, and much of this spreading contributed to mutual inductance. Also, the magnetic permeability of the plate may act like the iron core of a transformer, providing magnetic coupling.

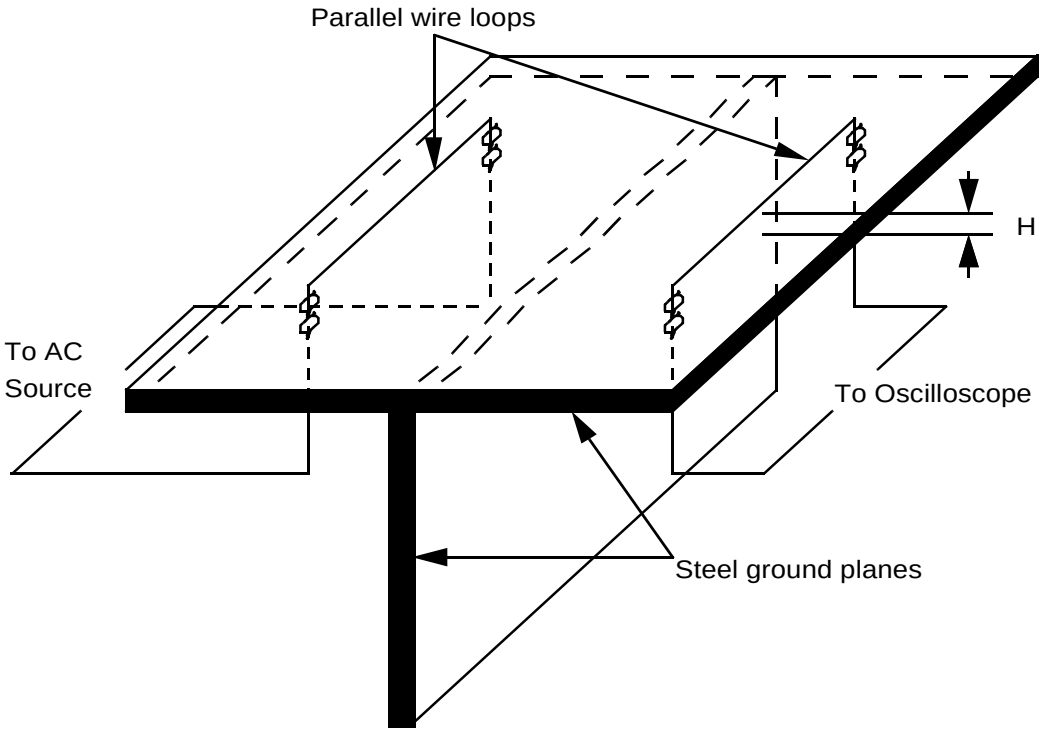

Figure 3.28. Apparatus for making measurements of mutual inductance between parallel conductors.

The mutual inductance due to this spreading is of the same phase as the desired mutual inductance. This experiment indicates a non-ideal ground plane may be a limitation to most transmission line models now in common use (ICM, closed-form, and conventional).

The results of this test with the wire elevated above the ground plane are summarized in Table 3.2. The predicted inductance values do not include the effect of the two .625 cm or 2.54 cm lines that support the 22 cm line, so 5% or 20% (respectively) should be added to the predicted values in Table 3.2. One can see from these results that measurements do start to deviate from the conventional (ICM) predictions in extreme cases. The fact that the measured results do not agree exactly with either equation may be due to the other stray coupling caused by the ground plane.

Table 3.2
Measured and predicted mutual inductances of lightly coupled lines.

Gap cm	Height cm	Mutual L (Meas.) nH	Mutual L (ICM) nH	Mutual L (Closed-Form) nH
8.7	.625	1.85	1.74	1.17
16.5	.625	0.56	0.50	0.25
16.5	2.54	1.66	1.98	0.97
25.5	2.54	0.56	0.85	0.31
34.5	2.54	0.26	0.47	0.14

All lines were 22cm long, .25mm diameter, and the measurement frequency was 5 MHz.

Direct verification of the mutual inductance calculations remains elusive. Indirect verification has been done by analysing real circuits and comparing the results obtained with the closed-form equations to those obtained with the ICM technique. The elements analysed in the following sections indicate that either technique can be used in many circuits, and care needs to be taken only when circuits are much shorter than the substrate height. When the length of the line is comparable to or less than the substrate height, the closed form expressions have proven to be more accurate. At long line lengths, either technique i
s suitable, although long, closely coupled lines simulated with the ICM technique agree better with measured data.

3.4. Inductors

3.4.1. Single Inductors

The next class of circuit element to be investigated will be the rectangular spiral inductor, similar to the one shown in Figure 1.1. This inductor can be analyzed using a series of transmission lines mutually coupled to each other. The first inductor to be analyzed will be a 2.75 turn, 1.2 nH nominal inductance unit, fabricated with gold air-bridges, 10 um wide with a 20 um pitch, on a 175 um GaAs substrate. This inductor is part of the TriQuint standard cell library, and has been measured and modelled by them [31]. Its dimensions are shown in Figure 3.17.

This element was modelled using the closed-form inductor equations in GEMCAP since the lines are short relative to the substrate height, and the ground plane does not form part of the return path. The GEMCAP input file that is used to simulate the inductor is shown in

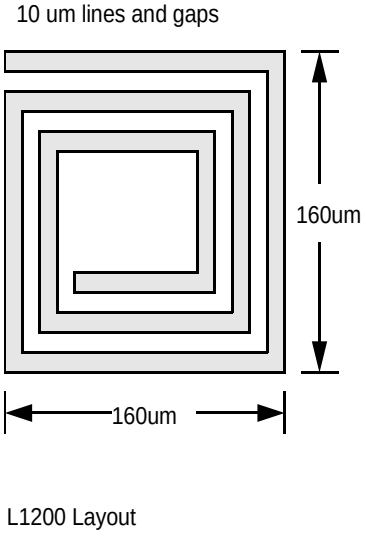

Figure 3.29. Layout of a 1.2 nH monolithic inductor. The inductor is held over the surface of the GaAs by posts at the corners.

Figure 3.18. The resulting file was simulated in SuperCompact, and the results are shown in Figure 3.19. The coil was simulated as a one-port with the centre terminal connected to ground. Also plotted in Figure 3.19 is the reflection coefficient measured by TriQuint using coplanar wafer probes. The angle of the reflection coefficient of an inductor is a good indication of its inductance. The inductance of an ideal inductor is related to the angle of the reflection coefficient by (3.1) and (3.2).

```
* INPUT FILE FOR A TEKTRONIX 1200PH INDUCTOR ON A 7 MIL SUB.*
BLK
XSUB 12.9 175
XCON 1 .04
WID 10  10  10  10  10  10
GAP   10  10  60  10  10
NUM  6
SEG 1 2 150
SEG 5 6 130
SEG 9 10 90
SEG 12 11 70
SEG 8 7 110
SEG 4 3 150
GAP 10 10 80 10
NUM 5
SEG 2 3 150
SEG 6 7 110
SEG 10 11 70
SEG 9 8 90
SEG 5 4 130
A:2POR 1 12
END
FREQ
STEP 2GHZ 18GHZ 1GHZ
END
OUT
PRI A S
END
```

Figure 3.30. GEMCAP input file for the inductor shown in Figure 3.17.

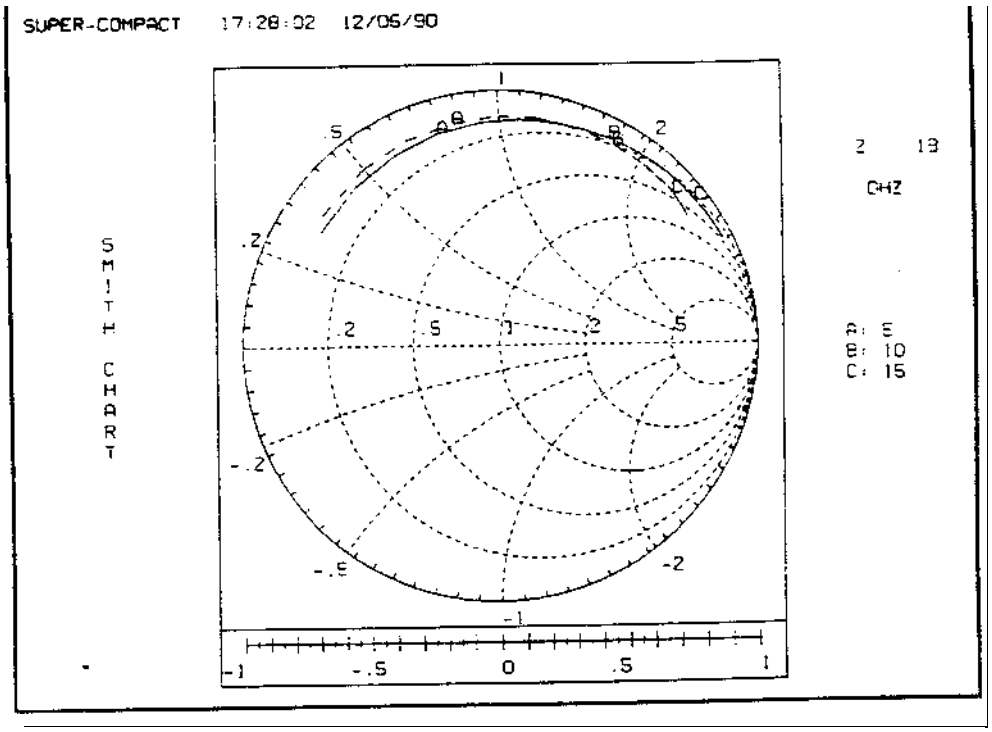

Figure 3.31. Simulated (solid line) and measured (broken line) S_{11} from 2 GHz to 18 GHz for the 1.2 nH inductor in Figure 3.17. Simulation was performed using GEMCAP with the closed form expressions for inductance. Markers A, B, and C are at 5 GHz, 10 GHz, and 15 GHz.

$$\text{Angle}_{S11} = \text{acos}\frac{(\omega L)^2 - Z_0^2}{(\omega L)^2 + Z_0^2} \tag{3.1}$$

$$\omega L = Z_0\sqrt{\frac{1 + \cos(\text{Angle}_{S11})}{1 - \cos(\text{Angle}_{S11})}} \tag{3.2}$$

where Z is the system impedance, L is the inductance, and ω is the angular frequency. GEMCAP's prediction of the angle of S_{11} is low by about 4 degrees at 5 GHz which is an error in inductance of less than 6%. The measured loss of the inductor is higher than the prediction. In fact, the measured reflection coefficient increases up to roughly 13 GHz, and then decreases. The simulated reflection coefficient increases monotonicaly up to at least 18 GHz, which is what would be expect for a simple series L R model of an inductor. The error may be caused by the porous nature of plated gold. Other factors that might increase

the loss could include dielectric loss and radiation. Dielectric loss was investigated as a possibility, but the loss tangent of the dielectric would have to be increased to roughly 0.1, which is an unreasonable figure for GaAs. This underestimation of loss is a common problem in GaAs circuitry, and it can be seen in many other devices. More work needs to be done in the area of loss simulation with attention paid to non-ideal metals, skin effect, surface roughness, and other second order effects.

When GEMCAP is run with the ICM option for the calculation of the inductance matrix, the phase of the reflection coefficient is about 11 degrees lower than the measured value. This supports the theory that short lines are modelled with more accuracy with the closed-form expressions. It is interesting to examine the effect of the various elements in the inductance calculation. Table 3.3 summarizes the effects tested.

Table 3.3.
Simulated and measured angle of S_{11} under various analysis assumptions.

Inductance calculation technique	Angle of S_{11} @ 5GHz	Error in S_{11} angle degrees.
Actual measured value [31]	101.0	-
Simulation ignoring all mutual inductance.	122.4	21.4
As above, but adding mutual inductance from adjacent neighbours.	101.5	0.5
As above, but including mutual inductance from every segment on each side.	96.9	-4.1
As above but with mutual inductance from opposite side included.	105.1	4.1
As above, but with the ground plane image inductance added. (A full simulation)	105.3	4.3
Use ICM solution	89.6	-11.4

These simulations indicate that the ground plane has relatively little effect on the inductance of this inductor. This inductor is small, and was fabricated on a rather thick substrate, so the image inductor is actually much further away than the adjacent sides. Furthermore, the image inductor acts to increase mutual inductance from one side of the coil to the other, and to decrease the self inductance of all sides. As these two effects tend to cancel, the net effect of the image inductor is small. The capacitive and inductive coupling between opposite sides of the coil has a significant effect on the inductance. This coupling reduces the overall self inductance of the coil by 10%. The mutual inductance between non-adjacent conductors on the same side of the coil acts to increase self inductance by 10%. The mutual inductance between adjacent conductors is a very significant effect, accounting for 20% of the overall inductance. From this, we can conclude that this inductor has about 20% more inductance than the sum of the inductances of the segments. If the inductor were to be unwound and stretched out, the long line would have more inductance per unit length than the segments, and it would have as much inductance as the inductor did. Inductors do offer a space advantage over transmission lines, but there is little performance advantage.

The principal reason that the phase is not being accurately estimated is likely the air-bridge structure used to fabricate the inductor. There is approximately 1.5 microns of air between most of the metallization and the surface of the wafer. This air gap lowers the effective dielectric constant slightly, and reduces coplanar capacitance compared to the computer predictions (GEMCAP assumes that the dielectric under the inductor is uniform). As the capacitance causes the inductor to resonate, the reduction in capacitance will increase the angle of S_{11} around resonance, yielding the measured results.

3.4.2. Coupled Inductors.

As a second test of the program, a 2.57 nH inductor from the Harris GaAs foundry library [32] will be examined. This inductor is fabricated on 125 um thick GaAs in 3 um thick gold metal. Unlike the TriQuint inductors, the metal is placed directly on the GaAs surface. The 2.57 nH inductor has 4.5 turns, and its overall dimensions are 225 um by 250 um. A model has been supplied by Harris, and test cells employing these inductors have been measured with a network analyser. This modelling effort is complicated by the fact that there is a

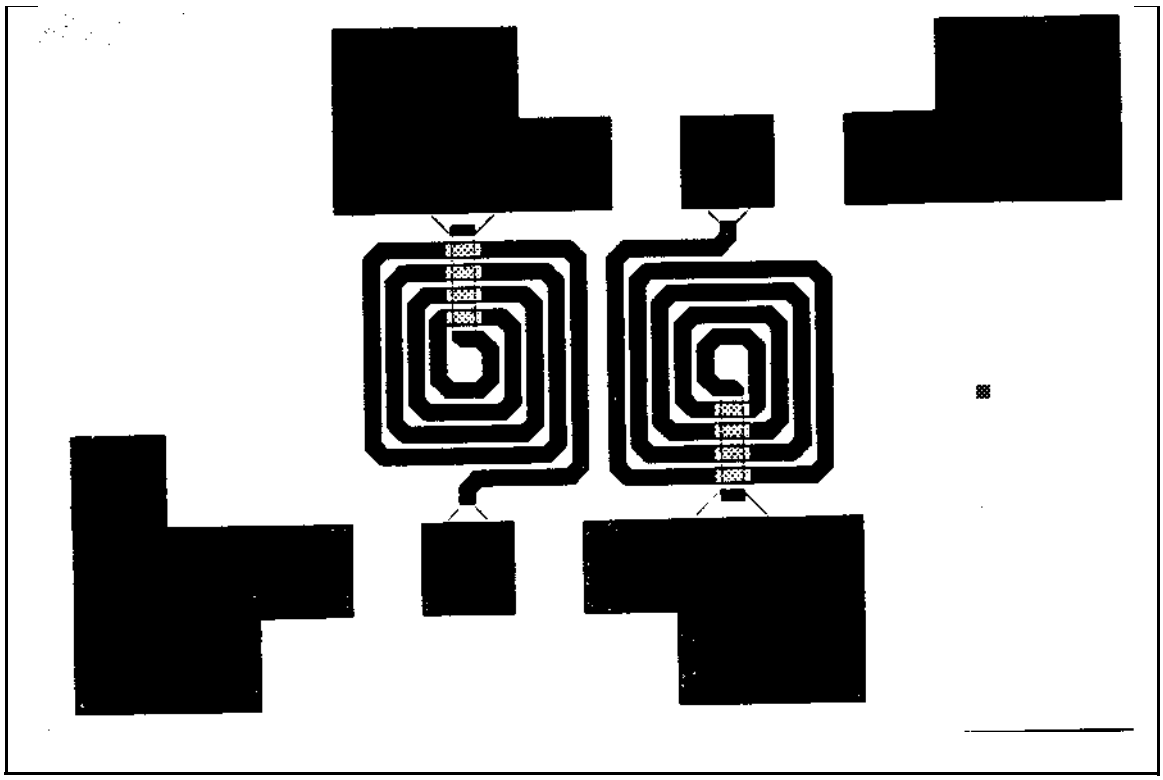

Figure 3.32. Layout of a pair of 2.6 nH inductors.

second inductor located next to the measured inductor, as shown in Figure 3.20. The second inductor introduces a resonance in the reflection coefficient of the first inductor. GEMCAP can be used to determine both the characteristics of the inductors, and the coupling between the two inductors.

A single inductor was modelled using GEMCAP with the closed-form expressions for inductance. Exactly the same profile file was used as in the example earlier in this chapter. The effect of the interaction between opposite sides of the inductor was included. The resulting data file was run on SuperCompact. The magnitude and angle of the reflection coefficient of the inductor as a one-port is shown in Figure 3.21, along with data supplied by Harris. The angle of the reflection coefficient agrees extremely well with GEMCAP's predictions, being within 2 degrees at 18 GHz. The magnitude of the reflection coefficient does not agree as well for two reasons. The gold in the Harris process is deposited with an electroplating process, and electroplated metal tends to have higher loss than bulk gold. The

match between modelled and measured results is especially bad at low frequencies. This is because the Harris model has no mechanism for including the loss due to skin effect. In order to get a good fit to measured data at high frequencies, Harris has added loss beyond the DC resistance, making the inductor's loss at low frequencies unreasonably high.

In order to verify the Harris model, the inductors were measured using coplanar waveguide wafer probes. At 11 GHz, there is significant interaction between the inductors; when one inductor is left open, the other inductor exhibits noticeably higher return loss. The interaction between these inductors can be modelled with GEMCAP. To keep the circuit size manageable, the mutual inductance from opposite sides of each inductor is ignored. The mutual inductance between all segments in the adjacent sides of the two inductors is modelled, however. The resulting circuit file is too large to be run in SuperCompact. Instead, the file was simulated in Scamper, and the results were transferred to SuperCompact in the form of a two-port s-parameter data file.

The measured and modelled reflection coefficients of one inductor with the second inductor open-circuited are shown in Figure 3.22. The second inductor causes a high Q peak in the return loss of the measured inductor at 11 GHz, which coincides with the self resonant frequency of the inductor. Notice the good agreement between theory and measurement at all points including the area where there is interaction between the inductors. Also notice the improved agreement in return loss. The agreement could likely be improved if the coupling between opposite sides of the inductors was included.

When the second inductor is terminated in 50 ohms, the behavior of the system is more benign. Figure 3.23 shows the one-port s-parameters of the inductor with the second port terminated in 50 ohms. The return loss is greater than the case where the inductor was isolated because of the energy coupled into the second inductor. The plot of S_{21}, describing the interaction between the inductors, is shown in Figure 3.24. The flat nature of this coupling is remarkable considering the high Q peak visible in Figure 3.22.

The ability of this program to analyse the interaction between inductors will enable designers to evaluate compact circuit topologies quickly and efficiently. No other program, other

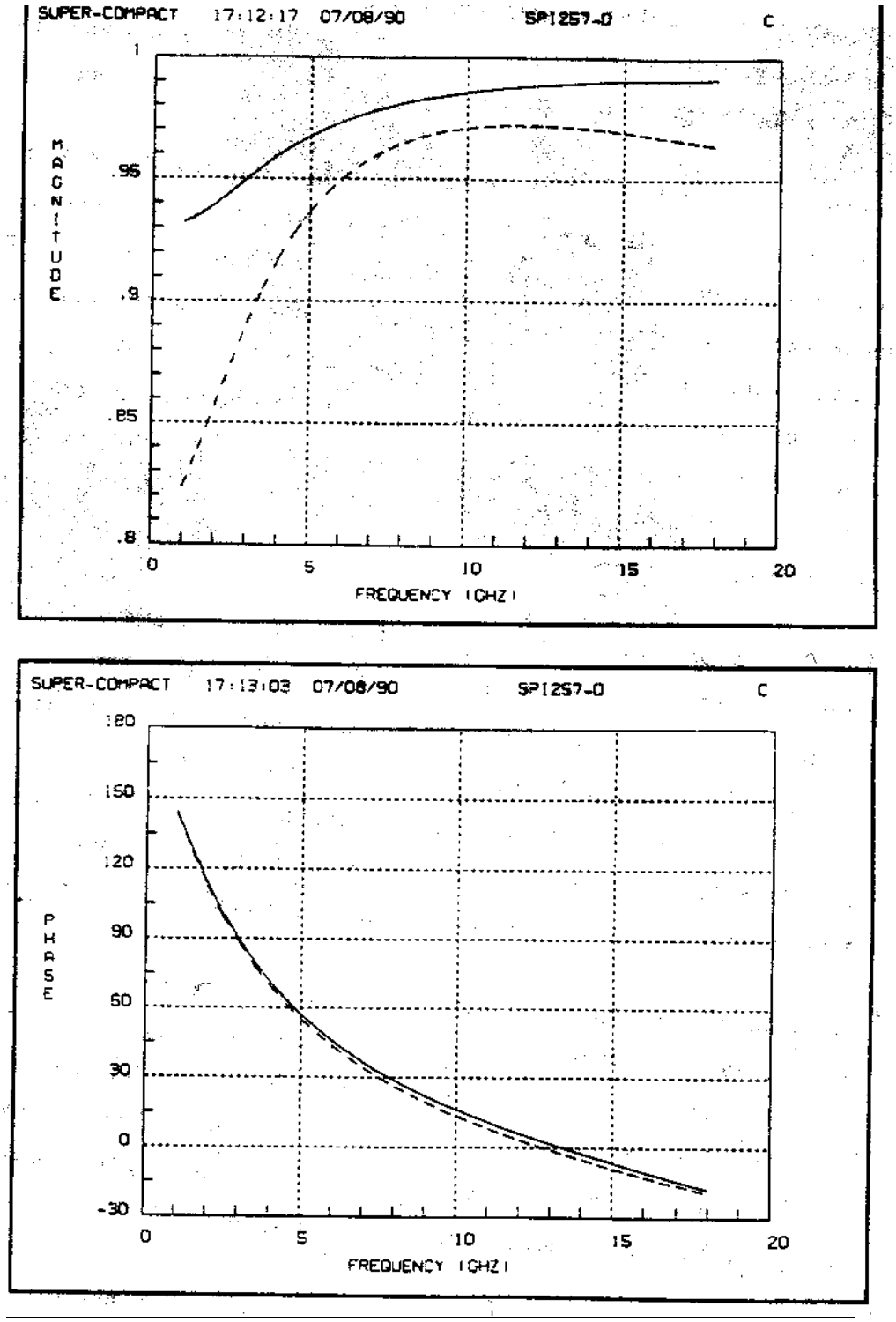

Figure 3.33. Magnitude and phase of reflection coefficient of an isolated 2.6 nH inductor. The solid line is the simulated (with GEMCAP) result, and the broken line is generated from the model supplied by Harris.

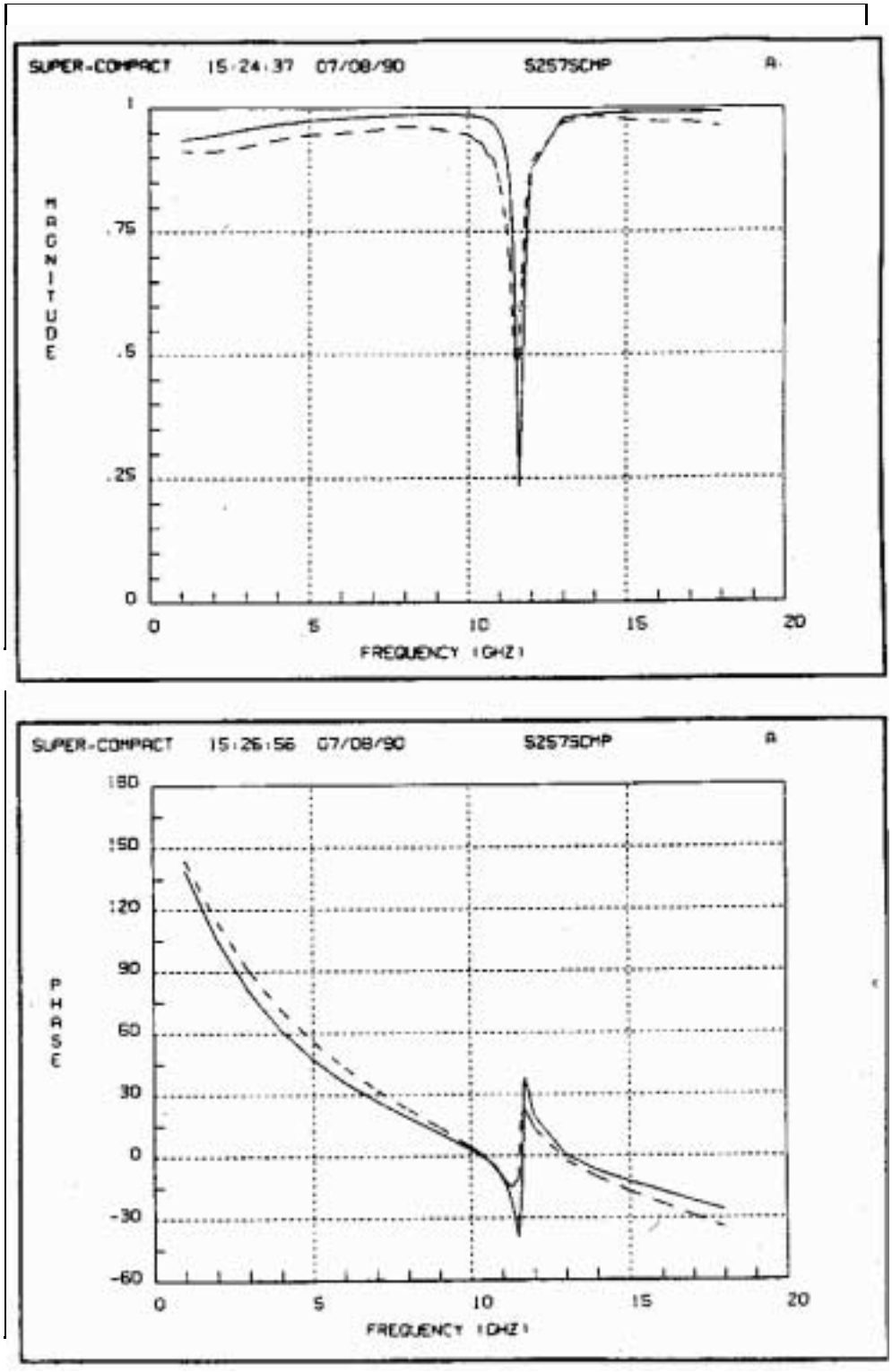

Figure 3.34. Magnitude and phase of reflection coefficient of a 2.6 nH inductor next to a similar unconnected inductor, as seen in Figure 3.20. The solid line is the simulated (with GEMCAP) result, and the broken line is measured.

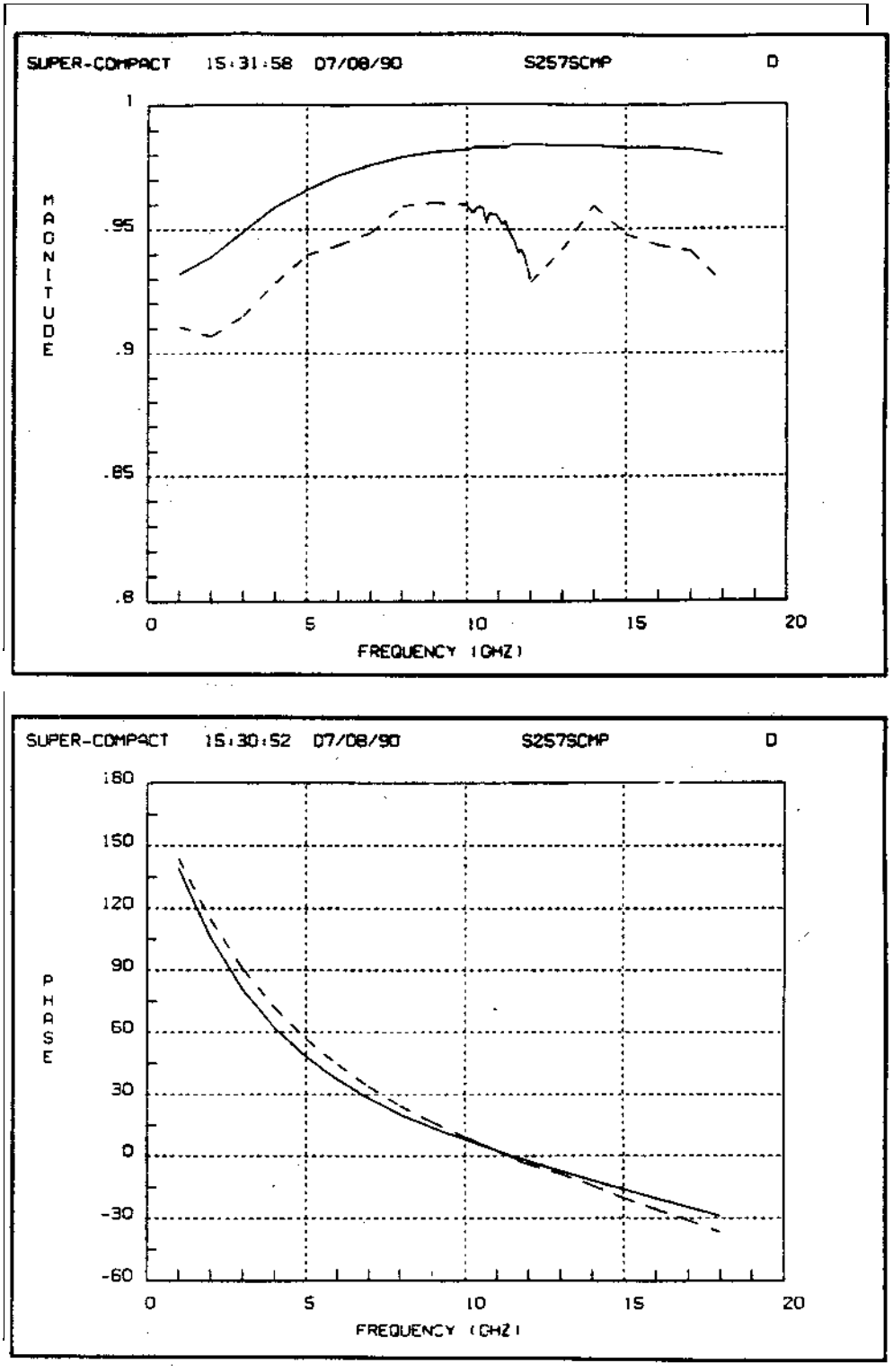

Figure 3.35. Magnitude and phase of reflection coefficient of a 2.6 nH inductor next to a similar inductor terminated with 50 ohms. The solid line is the simulated (with GEMCAP) result, and the broken line is measured.

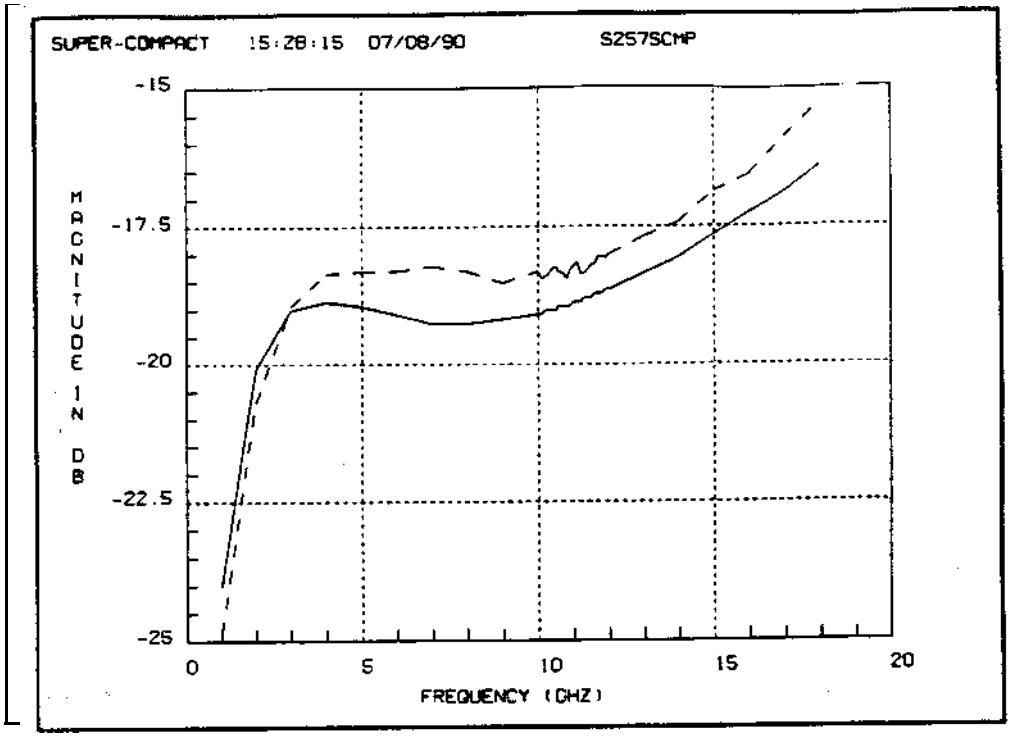

Figure 3.36. S_{21} of the coupled inductors shown in Figure 3.20. The solid line is the simulated (with GEMCAP) result, and the broken line is measured.

than cumbersome field theoretical algorithms, has been able to do this. To aid the MMIC designer, Figure 3.25 illustrates the coupling (S_{21} in a 50 ohm system) versus spacing for various 2 and 4 turn inductors on 125 um and 500 um substrates. The inductors had outside dimensions of 200 um or 400 um, and had 10 um wide lines, and 5 um wide gaps. The winding that ends in the centre was grounded. These graphs were calculated with GEMCAP. Close inductors on either substrate have similar S_{21}, but the S_{21} drops off more rapidly with distance on a thin substrate. This proves that the ground plane provides shielding between the inductors. Notice that the size of the inductor has little bearing on the amount of coupling. If the inductors are simulated in higher impedance systems, the coupling becomes more of a potential problem. The 4 turn, 200 um square inductors on 125 um substrate, spaced at 10 um has -10 dB peak S_{21} in a 200 ohm system, and -5 dB in a 500 ohm system. Fortunately, the inductive reactance of the inductors at that frequency is quite low, and their use in such a system is unlikely.

The graphs in Figure 3.25 can be used as a guideline to inductor placement, but if space becomes critical, the pair of inductors should be simulated in their entirety.

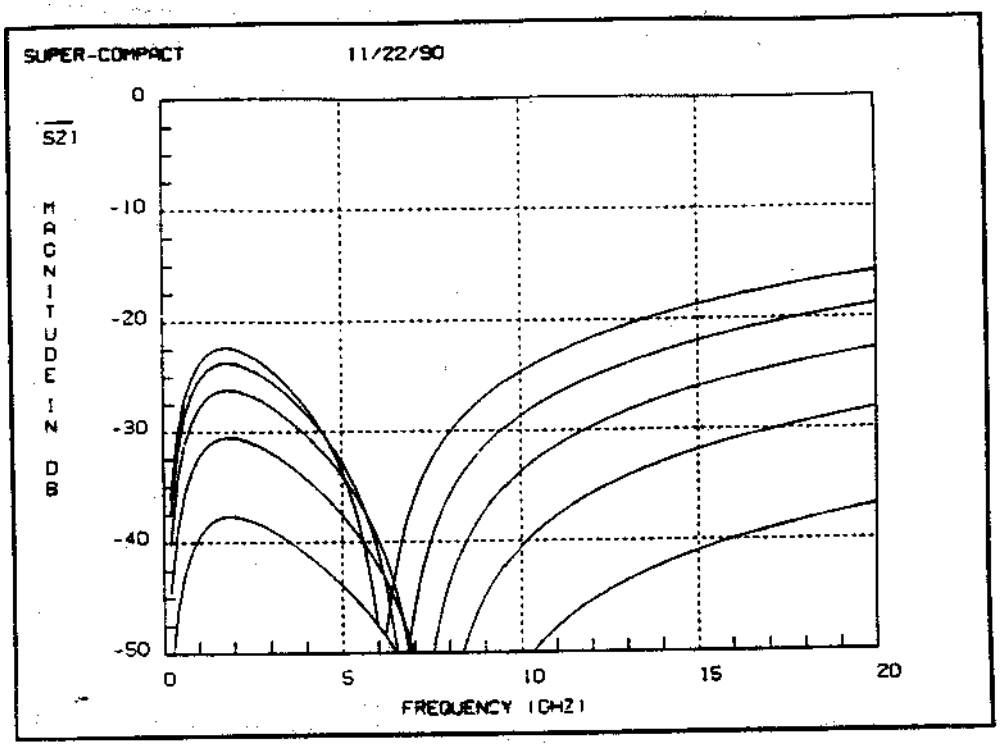

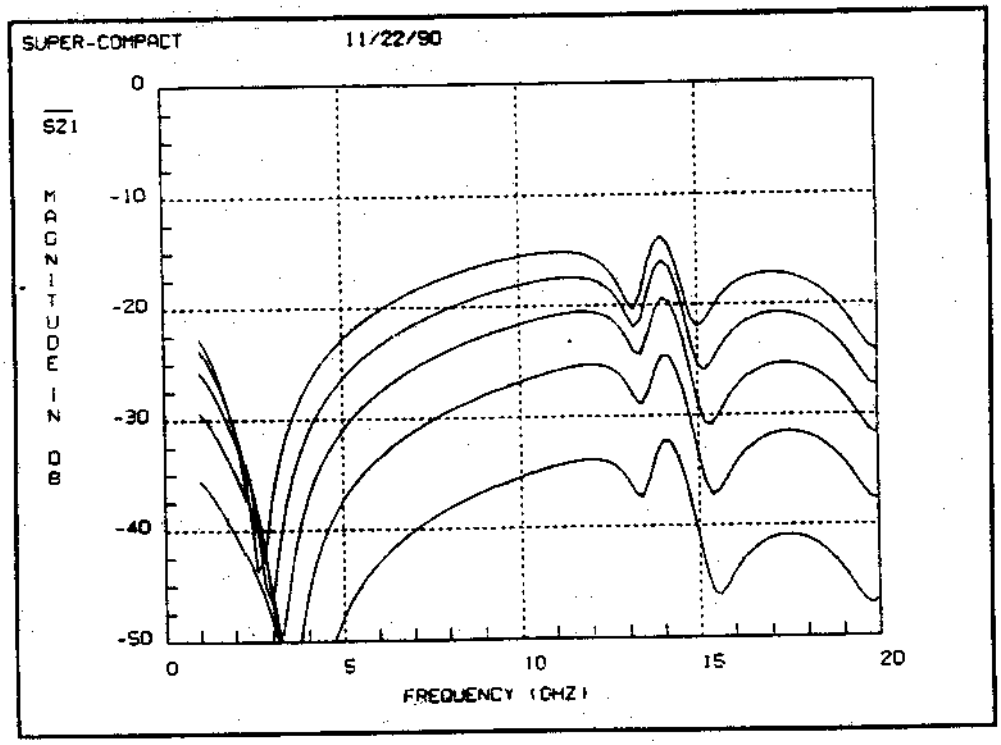

Figure 3.37a and b. Simulated coupling between pairs of identical four turn inductors located next to each other in a 50 ohm system. On each graph, the lines are for 10, 20, 40, 80, and 160 micron spacing (top to bottom) between inductors. Substrate height is 125 microns. Overall dimensions are 200 microns (upper trace) and 400 microns (lower trace).

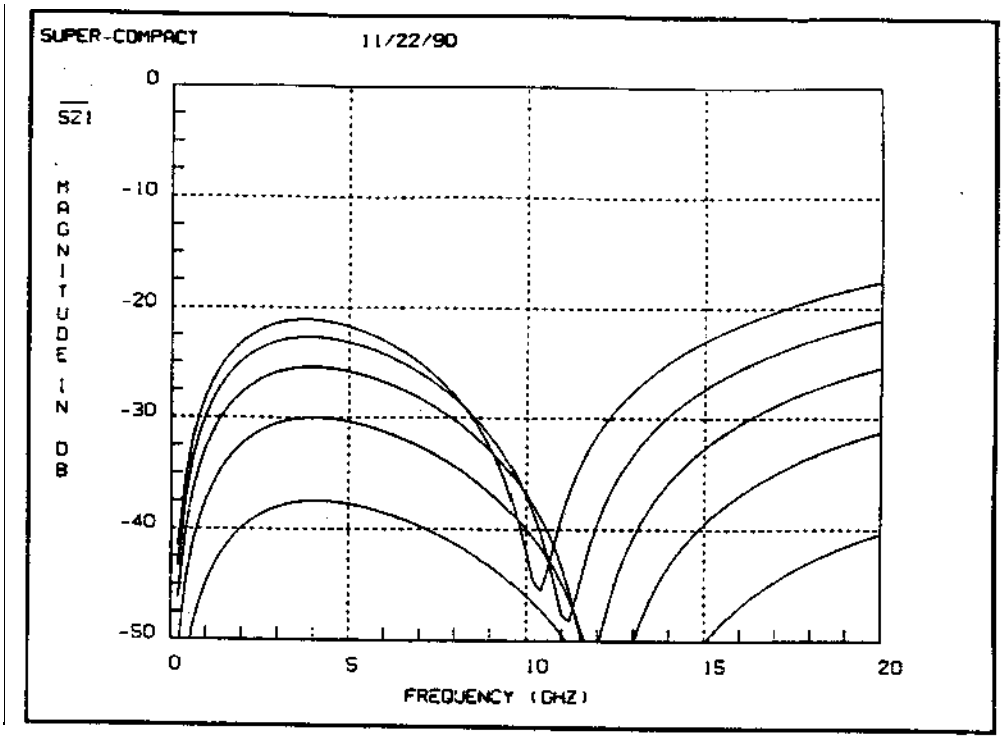

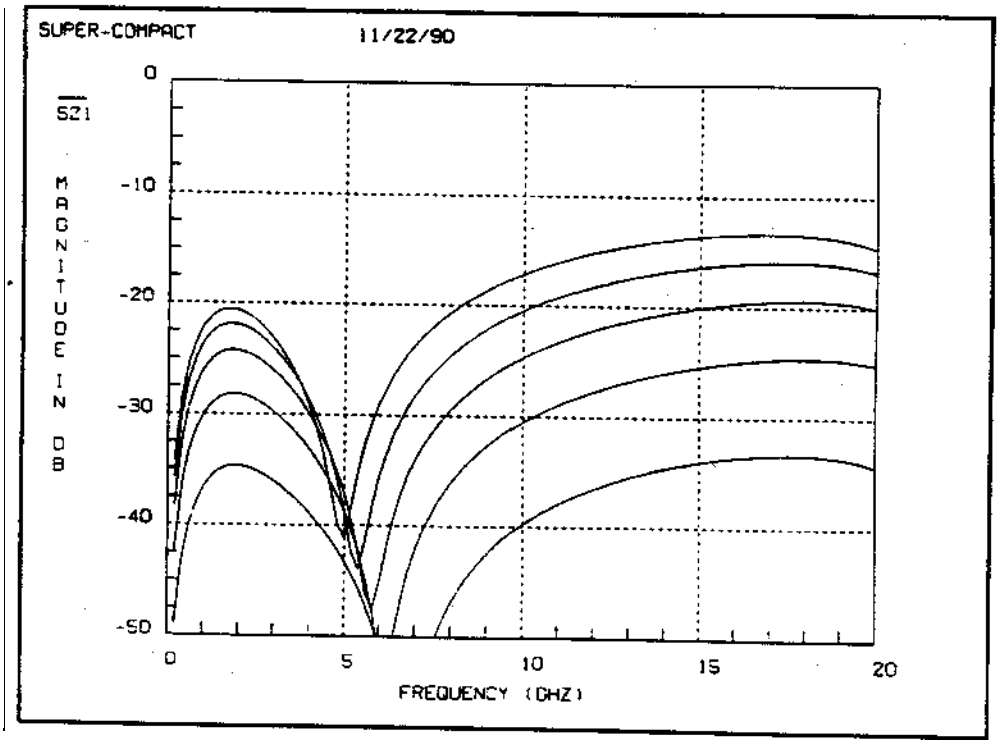

Figure 3.25c and d. Simulated coupling between pairs of identical two turn inductors located next to each other in a 50 ohm system. On each graph, the lines are for 10, 20, 40, 80, and 160 micron spacing between inductors. Substrate height is 125 microns. Overall dimensions are 200 microns (upper trace) and 400 microns (lower trace).

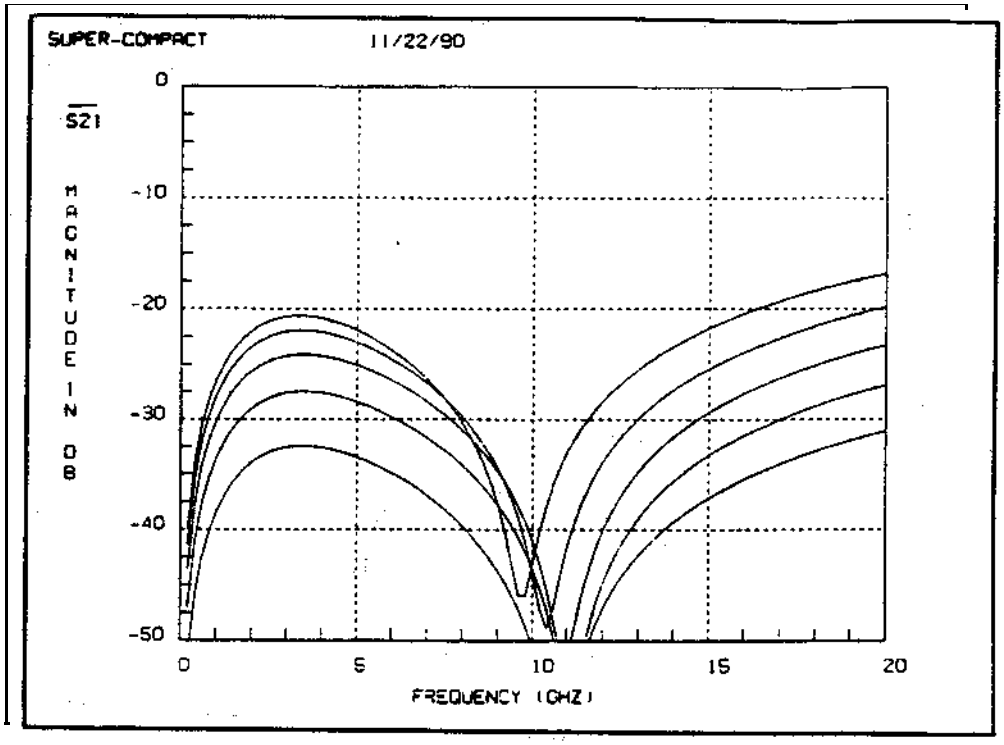

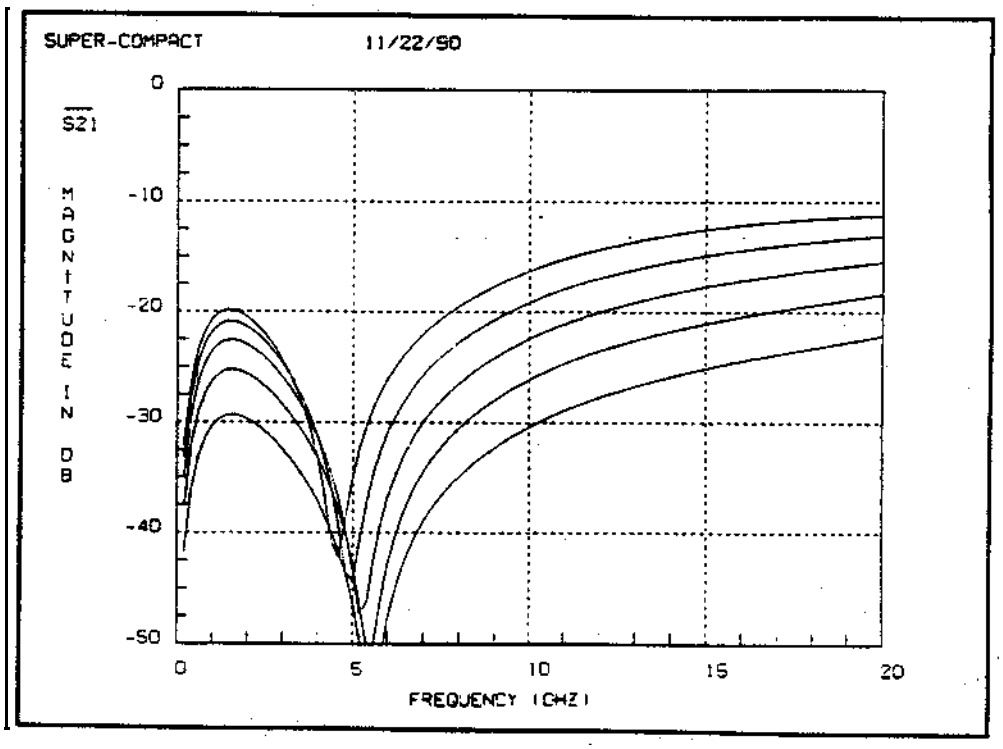

Figure 3.25e and f. Simulated coupling between pairs of identical two turn inductors located next to each other in a 50 ohm system. On each graph, the lines are for 10, 20, 40, 80, and 160 micron spacing between inductors. Substrate height is 500 microns. Overall dimensions are 200 microns (upper trace) and 400 microns (lower trace).

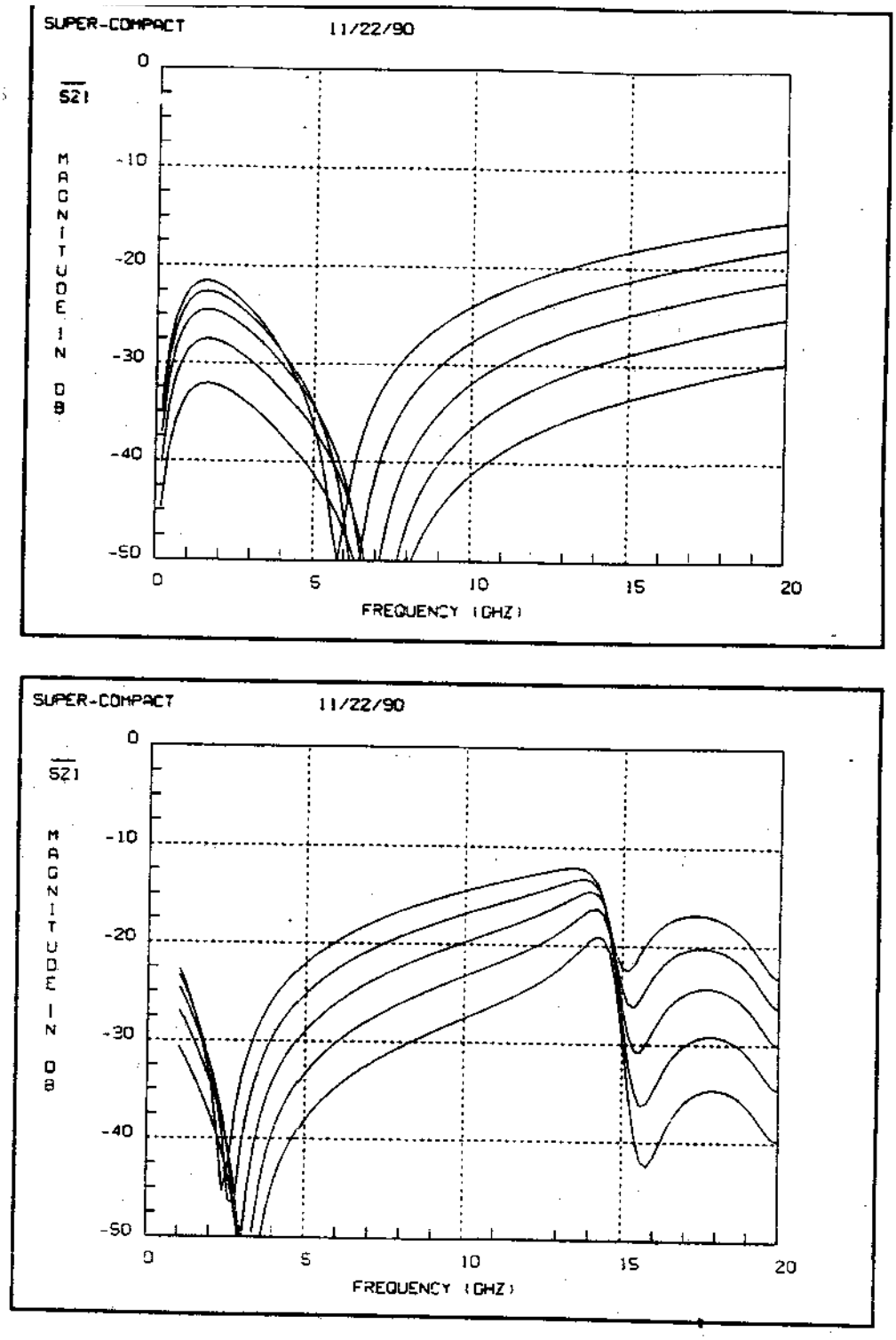

Figure 3.25g and h. Simulated coupling between pairs of identical four turn inductors located next to each other in a 50 ohm system. On each graph, the lines are for 10, 20, 40, 80, and 160 micron spacing between inductors. Substrate height is 500 microns. Overall dimensions are 200 microns (upper trace) and 400 microns (lower trace).

3.5. Lange Couplers

GEMCAP can be used to analyse linear coupled line structures. This section will illustrate the use of GEMCAP in the analysis of a Lange coupler. This Lange coupler was fabricated on GaAs, and its performance has been published [33].

Since the coupler is a quarter wavelength long at mid-band, it could not be analyzed in single sections. To insure sufficient accuracy up to 8 GHz (where the coupler would be about half a wavelength long), at least 4 sections would be required. To test the capabilities of the simulator on a complex circuit, the coupler was broken into 6 sections along its length; three to the right of the centre air-bridge connections, and three to the left. The circuit topology that was used is shown in Figure 2.12. The resulting file was too big to be analyzed with SuperCompact, so Scamper was used.

When the ICM technique was used to calculate the inductive coupling, excellent agreement with the published results was obtained, as shown in Figure 3.26. The coupler is slightly over-coupled. When the closed-form equations are used in the simulation, 0.5 dB more over-coupling is predicted. The large difference between the two techniques resulted because of the thick (4 um) metallization used for the coupler. The closed-form equations take metal thickness into account in the inductance calculation, but the ICM technique does not. The self inductance of the conductors, as predicted by the closed-form equations, is lower than that by the ICM technique, so the coupling coefficient is higher. The inductance is underestimated by the closed-form equations, however, because of the assumption that current is flowing uniformly throughout the cross-sectional area of the conductor. In fact, at 6 GHz, the skin effect will cause most of the current to flow on the surface of the conductor, and particularly on the surface closest to the ground plane. This causes the closed-form predicted self inductance to be lower than actuality, and the closed-form predicted coupling higher. (Note that GEMCAP corrects the loss calculations for the skin effect, but does not correct inductance calculations for skin effect.) If the conductor height is reduced to 1um, ICM and closed-form calculations yield similar results. The fact that GEMCAP can model a Lange coupler proves the usefulness of this technique for distributed structures.

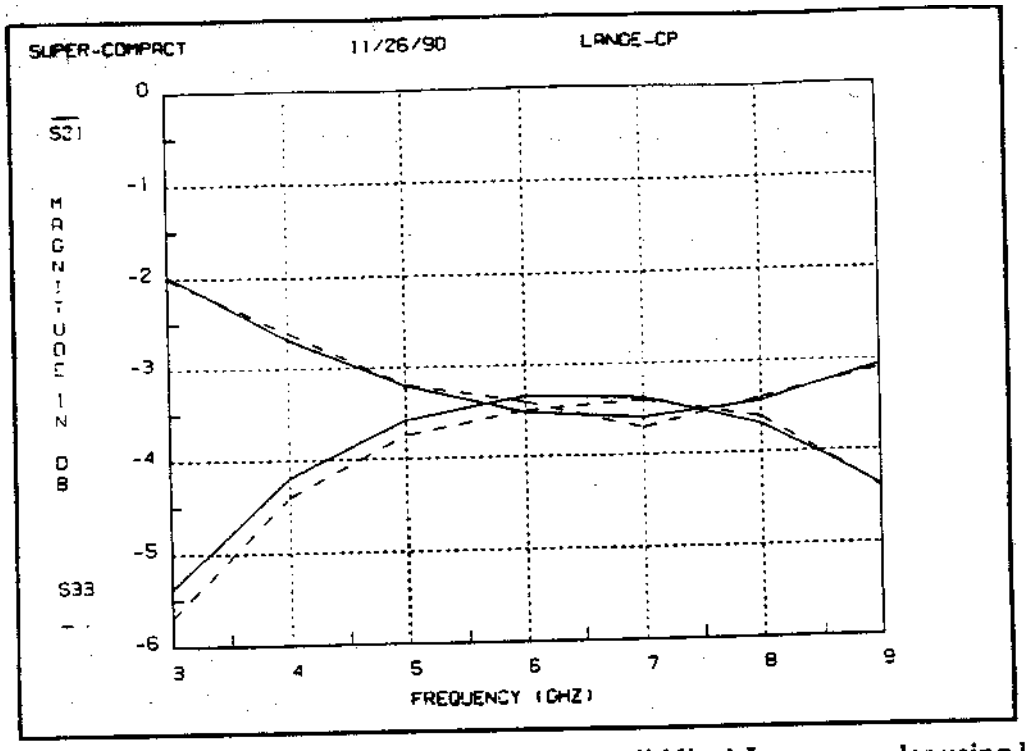

Figure 3.38. Measured (broken line) and simulated (solid line) Lange coupler using ICM tech. Upper traces are the through port.

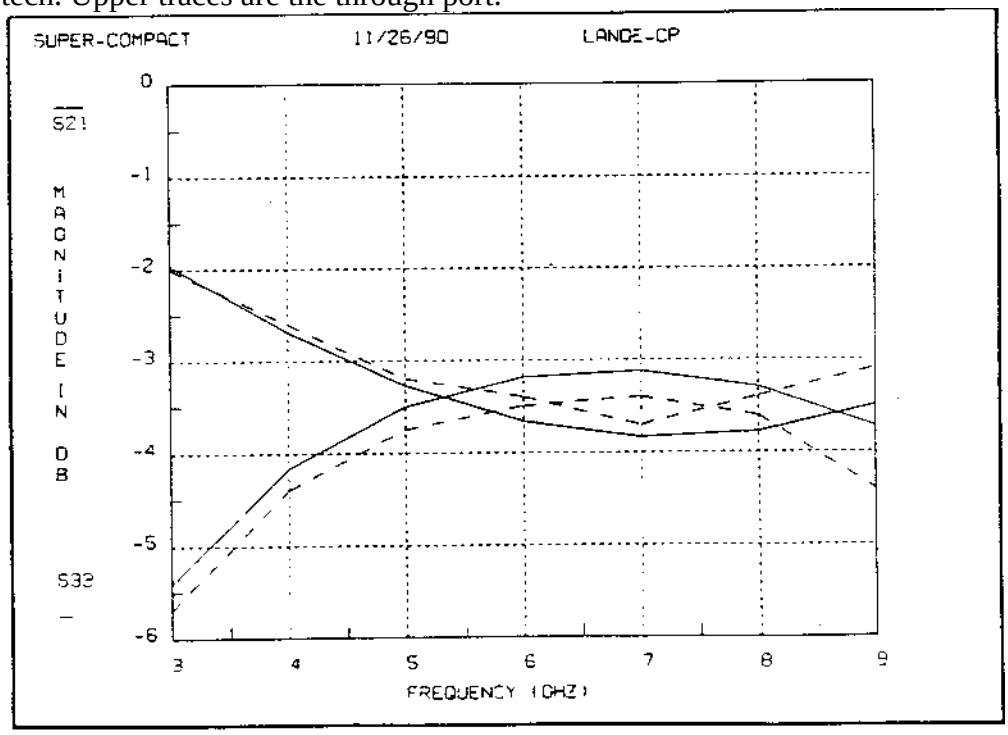

Figure 0.1. Measured (broken line) and simulated (solid line) Lange coupler simulated with closed form inductance calculations. Upper traces are the through port, and lower traces are the coupled port.

SuperCompact was also used to simulate the Lange coupler. Surprisingly, its predictions were even less accurate than either of the GEMCAP predictions. SuperCompact predicted 0.9 dB of overcoupling, with incorrect centre frequency.

3.6. Conclusions

The varying characteristics of the two different ways to calculate the inductance matrix stimulated efforts to determine which is most useful. In comparing simulations done both ways to measured data, it was observed that the closed-form techniques tended to give more accurate simulations for devices made of short elements, such as MMIC spiral inductors, and that the ICM technique lead to more accurate answers for longer lines, especially if they are close.

The measurements done in this chapter indicate that for large microstrip structures, the closed-form expressions predict inductance less accurately than the ICM method. The reason for these results appears to be the return path. As Grover's formula [23] is based on the Biot-Savart law, the current's return path is assumed to be at infinity. This is similar to analysing hypothetical current sources and sinks, separated by a finite distance, connected by a wire over a ground plane. The ground plane, even if it is of infinite extent, will have some inductance associated with it. The ICM formulation will take into account the inductance of the return path (at least the return path parallel to the microstrip). In order to improve the accuracy of the closed-form inductance equations, there is a need to calculate the inductance of the ground plane. Since the current in the ground plane will not be uniform or even unidirectional, this inductance will be difficult to calculate. Fortunately, in many cases, especially MMICs, the calculation of this inductance will be unnecessary, as the return path is not through the ground plane. Note that this additional inductance is not the same as the image inductance due to currents induced in the ground plane. The image inductance exists whether or not the ground plane forms part of the return path.

In conclusion, the most accurate inductance results will be achieved if careful consideration is given to which technique is most appropriate in a given situation. If there is a long return path through the backside metal, then the ICM technique should be used. If the elements are short (the same length as the substrate height or less) or if the ground plane does not form part of the circuit, the closed-form equations should be used.

CHAPTER 4
MONOLITHIC TRANSFORMER DESIGN AND MODELLING

4.1. Introduction

This chapter will explore the design of spiral monolithic transformers using GEMCAP as a simulation tool. Published examples of monolithic transformers, and some monolithic transformers that have been designed by BNR and fabricated by GaAs foundries will be considered. The characteristics of these transformers will be examined and compared to discrete transformers. One of the most promising applications of monolithic transformers is their use in baluns. The special requirements of baluns will be discussed, and transformers designed to meet these requirements will be presented.

4.2. Transformer Layout

A monolithic transformer in its most basic form consists of two inductors inter-wound to promote mutual inductance. Figure 4.1 shows several possible transformer layouts. The transformer shown in Figure 4.1a, which is a plan view of Figure 1.2, is basically an inductor in which the single conductor has been split into two parallel conductors. This results in a transformer that has unequal primary and secondary self inductances. Both the primary and secondary windings have ends that terminate in the middle of the transformer, which may be inconvenient for layout. Figure 4.1b illustrates a transformer in which the primary and secondary self inductances are identical because of the inherent symmetry of the transformer. A transformer of this nature has been described in the literature [7]. Figure 4.1c illustrates a transformer in which all four terminals are brought to the outside, making interconnection to the rest of the circuit more straight-forward. Another advantage of transformers of this design is that their symmetry allows the centre-tap position to be calculated exactly. Many other designs can be envisioned for special applications. Transformers can be made with more than two windings. Ratios other than 1:1 can be fabricated. For example, Figure 4.2 shows designs for a 3:1 transformer, and a 3:2 transformer. If it is more convenient for layout purposes, rectangular, octagonal, or circular transformers could be made.

Transformers are often used as two port devices, requiring that two of the transformers nodes be grounded. If the two grounded connections are wound in the same direction (clockwise, for example) then the transformer is said to be wired in a non-inverting configuration. Conversely, if the two grounded connections are wound in opposite directions, then the transformer is said to be in an inverting configuration. Windings that are wound in one of the two orientations are sometimes marked with a dot.

a)

b)

c)

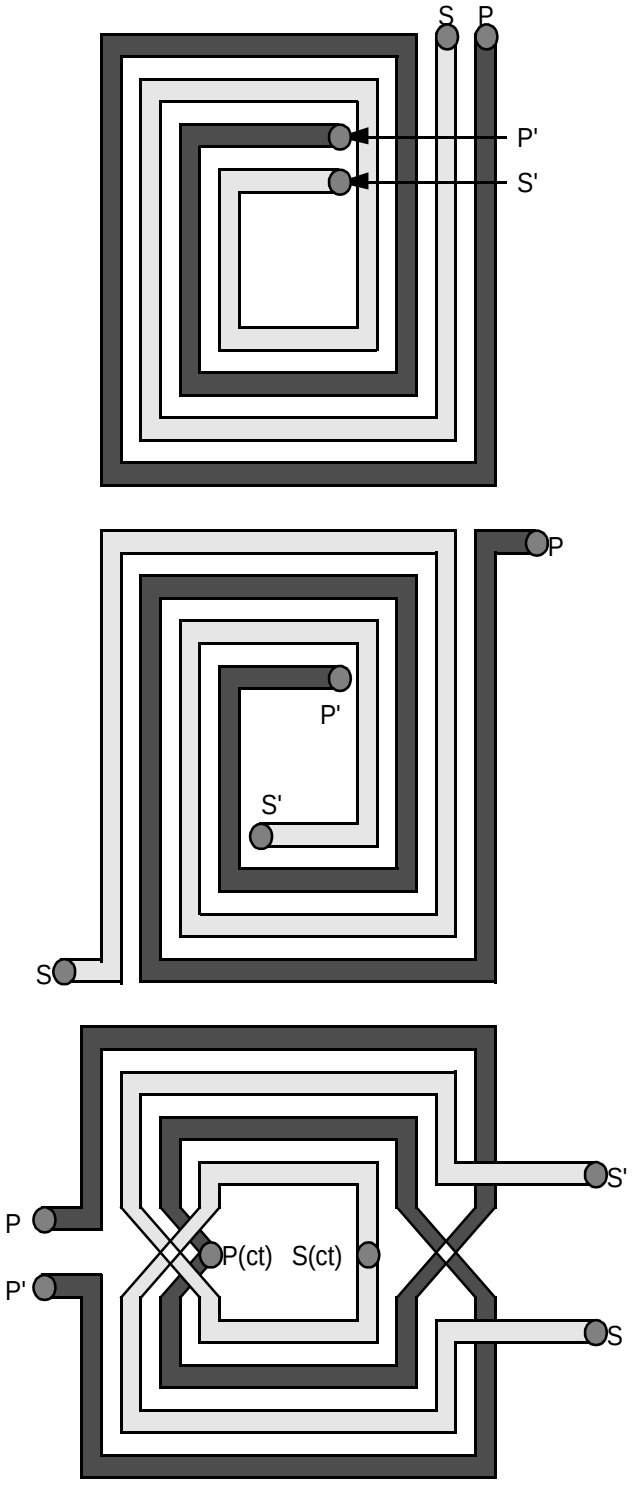

Figure 4.1. Three basic implementations of monolithic transformers.

a)

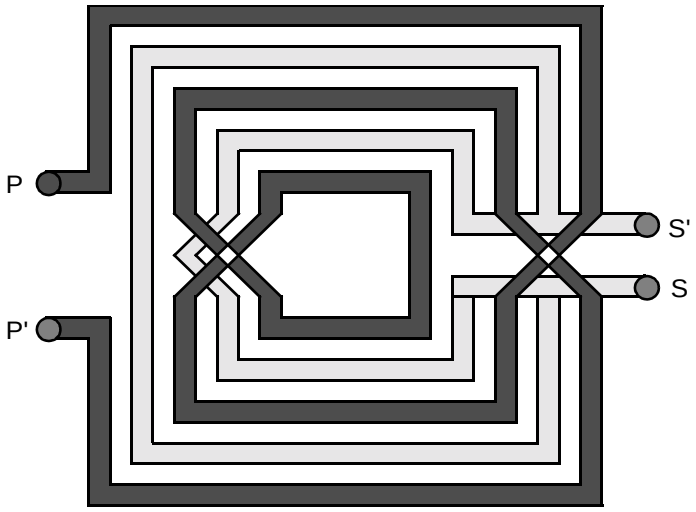

b)

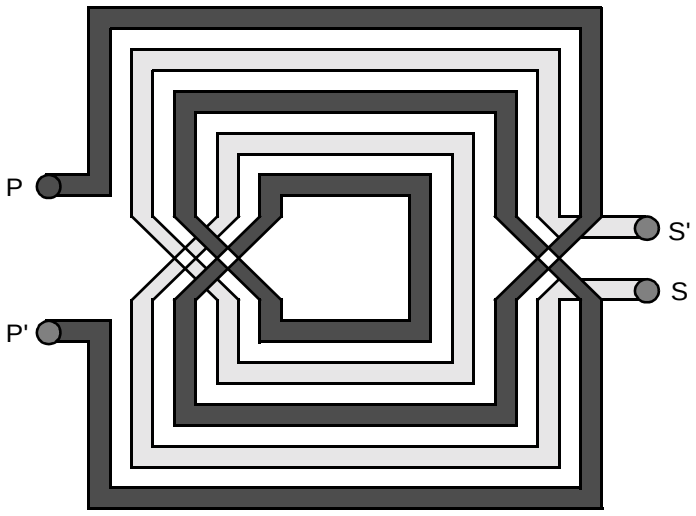

Figure 4.2. 3:1 and 3:2 monolithic transformer layouts.

4.3. Analysis of a Basic Monolithic Transformer

GEMCAP was used to analyse a number of monolithic transformers. One of the few published designs [7] was simulated with GEMCAP to establish its validity. This transformer is similar to the transformer shown in Figure 4.1b and measures 200 um square. The ends of the windings that are in the centre of the transformer are grounded. The input file for this transformer is shown in Figure 4.3. Coupling between opposite sides of the transformer was included. The measured and modelled coupling (S_{21}) and return loss (S_{11}) is shown in Figure 4.4. The agreement between measured S_{21} and GEMCAP is within .07 magnitude, and 5° angle. It is useful to examine the characteristics of this first monolithic transformer.

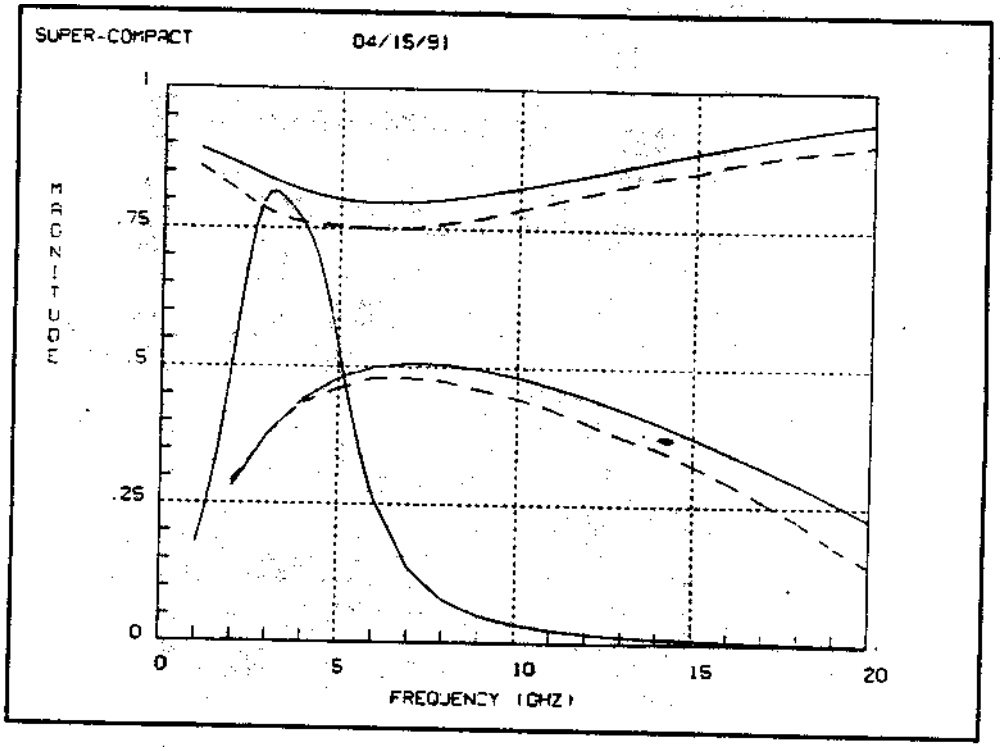

Figure 4.4. Simulated (solid line) and measured (broken line) S_{11} (upper pair) and S_{21} (lower pair) of the Frlan transformer [7]. The simulated (narrow) response with both windings resonated with parallel capacitors is also shown.

```
BLK
XSUB 9.8 250
XCON 1 .02
WID 10 10 10 10 10     10 10 10 10 10
GAP   10 10 10 10   70   10 10 10 10
NUM 10
SEG 4 10   206
SEG 21 20  175
SEG 31 30  136
SEG 41 40  100
SEG 51 18   42
SEG 17 63   42
SEG 52 53  100
SEG 42 43  136
SEG 32 33  175
SEG 22 3   206
NUM 10
SEG 2 4    100
SEG 22 21  190
SEG 32 31  151
SEG 42 41  121
SEG 52 51   81
SEG 63 40   81
SEG 53 30  121
SEG 43 20  151
SEG 33 10  190
SEG 3 1    100
```

```
TRL 1 19 W=72UM P=200UM SUB
TRL 2 29 W=71UM P=200UM SUB
TRL 17 18 W=10UM P=60UM SUB
TRL 17 36 W=10UM P=100UM SUB
TRL 18 37 W=10UM P=100UM SUB
TRL 36 0  W=72UM P=100UM SUB
TRL 37 0 W=72UM P=100UM SUB
A:2POR 19 29
END
FREQ
1MHZ
STEP 1GHZ 20GHZ 1GHZ
END
OUT
PRI  A  S
END
DATA
SUB: MS H=250UM ER=10
END
```

Figure 4.3. GEMCAP input file for Frlan transformer [7].

4.3.1. Loss and Mismatch

The magnitude of S_{21} of the monolithic transformer reaches a maximum of about .5 or 6 dB. This degree of transmission loss is quite poor, especially when compared to transmission line transformers wound on ferrite cores, which may have a maximum S_{21} of about .1 dB in a 50 ohm system. The principal reason for this is the poor coupling factor observed in monolithic transformers, as the match (S_{11}) is poor. The coupling can be improved over a narrow bandwidth by resonating out the self and part of the mutual cou-

pling with shunt or series tuning capacitors. Figure 4.4 shows the simulated S_{21} of the transformer with the primary and secondary windings resonated with capacitors, for optimum coupling at 3 GHz. Good coupling, -1.8 dB, is observed at the centre frequency, but the bandwidth is narrower. With the tuning, the return loss at both ports improves to better than -30 dB, so one can conclude that the 1.8 dB of loss is purely dissipative.

If one measures the resonant frequency of the primary, with the secondary open, one finds that the resonant frequency is much higher than the frequency at which maximum coupling occurs. The side-by-side coupled inductors that were examined in the last chapter had peak coupling when either inductor was self-resonant. The reason for the difference in behavior between the two systems is because of the nature of the coupling between the inductors. The coupling between the side-by-side inductors is principally inductive. The largest current flows through the inductor when it is excited at its resonant frequency, so the coupling is largest at that frequency. The coupling between the windings of the transformer is due to both capacitance and inductance, so it behaves like a coupled line structure. The nulls depend on which end of the coupled arm of the coupler is grounded.

The other significant shortcoming associated with monolithic transformers is their high loss, even when tuned. The transformer described by Frlan [7], for example, had a simulated dissipative loss of 1.8 dB, when tuned (Figure 4.4). This loss is very high, especially if the transformer is to be used at the input of a low noise circuit, or at the output of a high power circuit. This loss is entirely due to the conductor loss of the transformer windings. This loss can be reduced by widening the conductors, but only at the expense of reduced mutual coupling (if the gap is kept constant) or increased parasitic capacitance (if the conductor centre to centre distance is kept constant). The loss could also be reduced by increasing the thickness of the metallisation, up to the point where skin depth dominates metal loss behavior. The conductor thickness can not be arbitrarily increased without considering the extra difficulties with photolithography. Most processes use the thickest metal possible for the design rules; thicker metal can be used only if the either the process, the design rules, or the yield can be changed. Typical GaAs MMIC processes use gold metallisation thicknesses from 1.0 micron to 4.0 micron thick. If the gold conductors are increased to a thickness of 5 skin depths in the above example (from 1.0 micron to 7.5 micron), the dissipative

loss would decrease to .25 dB. Although this loss is acceptable, this thickness of metal is not practical in most MMIC processes.

4.3.2. Monolithic Transformers in Other Configurations

Some of the more interesting properties of monolithic transformers were not addressed in [7]. One of the main uses for transformers is in baluns. In a simple balun, two transformers are wired in opposite polarities, as shown in Figure 4.5. To achieve a perfect balance, the transformers must have the same performance whether they are used in inverting or non-inverting mode. The characteristics of monolithic transformers in both configurations have never been published. The transformer in Figure 4.6 was measured both in the inverting and non-inverting cases, corresponding to each transformer in Figure 4.5. This transformer was designed at BNR, fabricated by TriQuint Semiconductor, and characterized at BNR with microwave coaxial wafer probes.

The non-inverting measurement was made directly with coplanar waveguide probes. The measurement of the inverting configuration was done by breaking the air bridges in the ground ring surrounding the transformer, and wirebonding the centre pad of one probe pad set to one of the grounds on the other set. The probe grounds were therefore connected

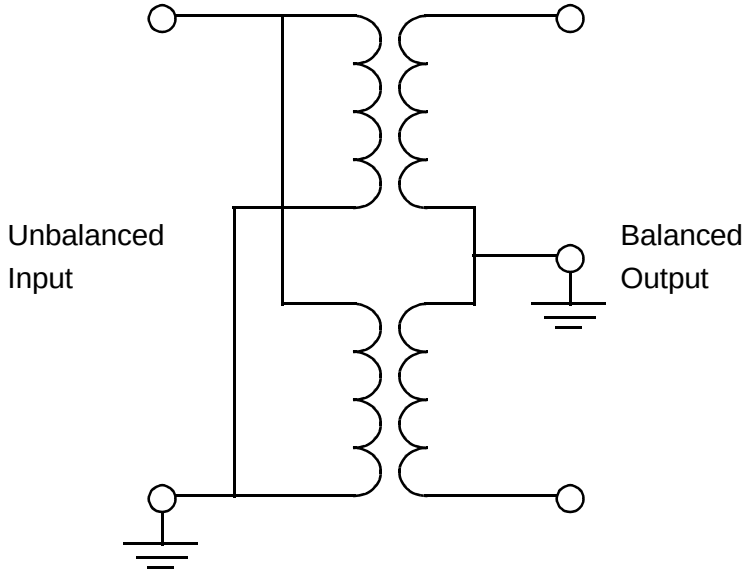

Figure 4.5. Schematic of an elementary balun, made of two transformers.

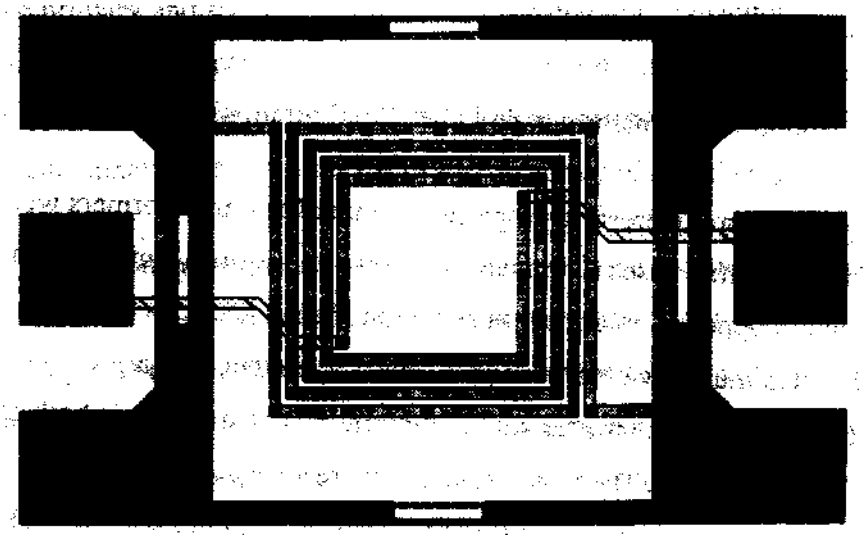

Figure 4.6. Physical layout of the 2-turn transformer. The lines are 10 um wide, spaces are 5 um wide, and the central hole is 150 um square.

together by this wirebond. This arrangement is the cause of the ripples in the inverting measurement. It also causes large inaccuracies in measurements of S_{11} and S_{22}, as one of the probe grounds is left floating, and the probes are not used in the same configuration in which they are calibrated. The actual setup for the modified transformer measurement is shown in Figure 4.7.

Measurements and simulations of this and other transformers fabricated at BNR indicate a large difference in performance between configurations, aside from the expected 180 degree phase difference. Figure 4.8 shows the simulated and measured magnitude and phase of S_{11} and S_{21} of the transformer in both configurations. At low frequencies, the coupling is low, but both configurations are similar. At higher frequencies, the coupling deviates significantly. The reason for the difference lies in the interwinding capacitance.

Intuitively, it would appear that a transformer with perfectly symmetrical windings should have equal performance in both configurations. If there was no interwinding capacitance, this would be true. In the non-inverting connection, the voltage gradient along the primary

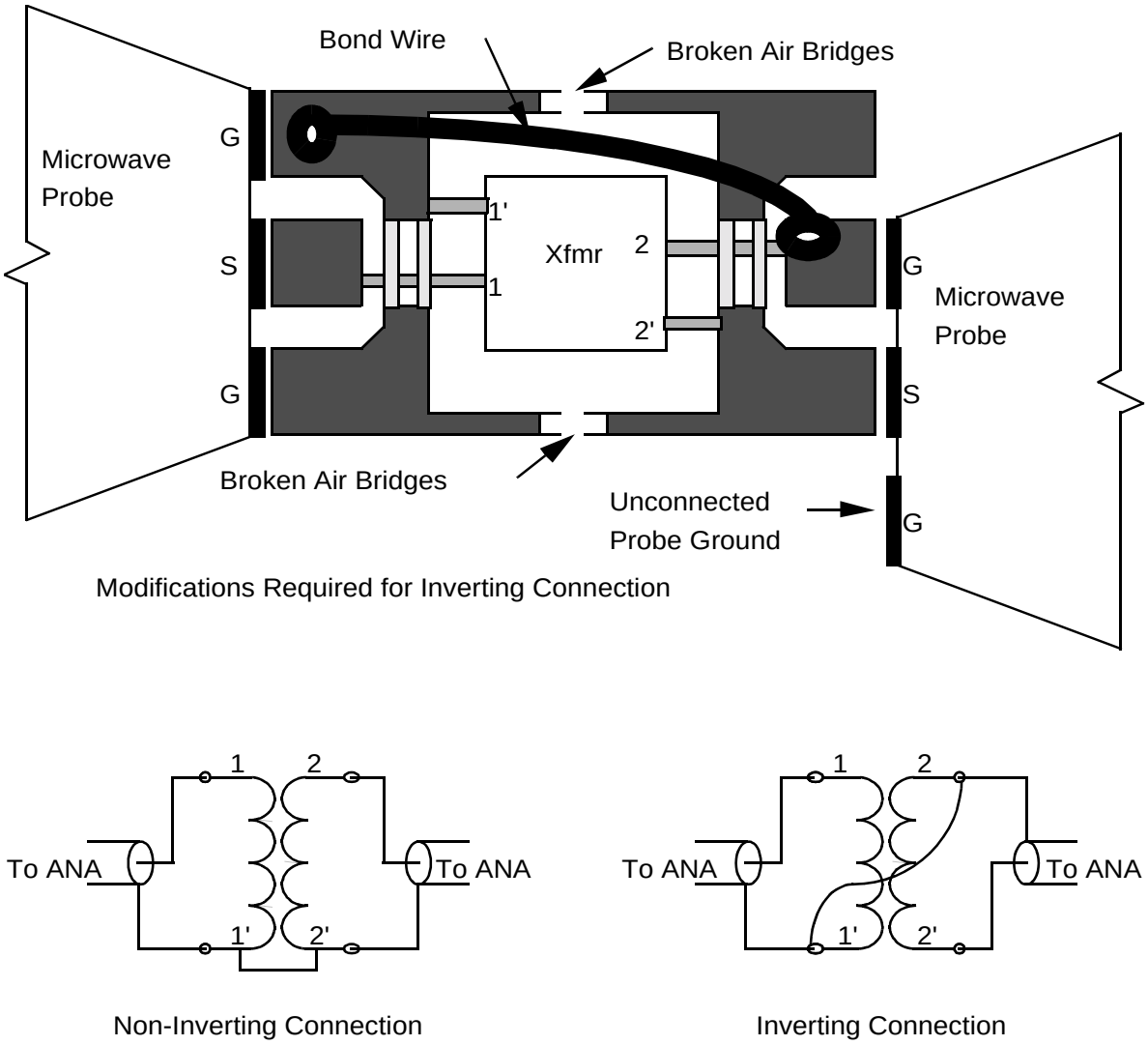

Figure 4.7. Modifications made to the transformer in Figure 4.6 so that it could be measured in the inverting configuration. The transformer in Figure 4.10, which is in the inverting configuration in its unaltered state, is modified in a similar manner so that it can be measured in its non-inverting configuration.

winding is the same as the gradient along the secondary, as seen in Figure 4.9a. The interwinding capacitance has no voltage across it. In fact, if poor coupling tends to reduce the output voltage, the interwinding capacitance would tend to increase the output swing. In the inverting connection, the voltage gradients are different, and there is voltage across the

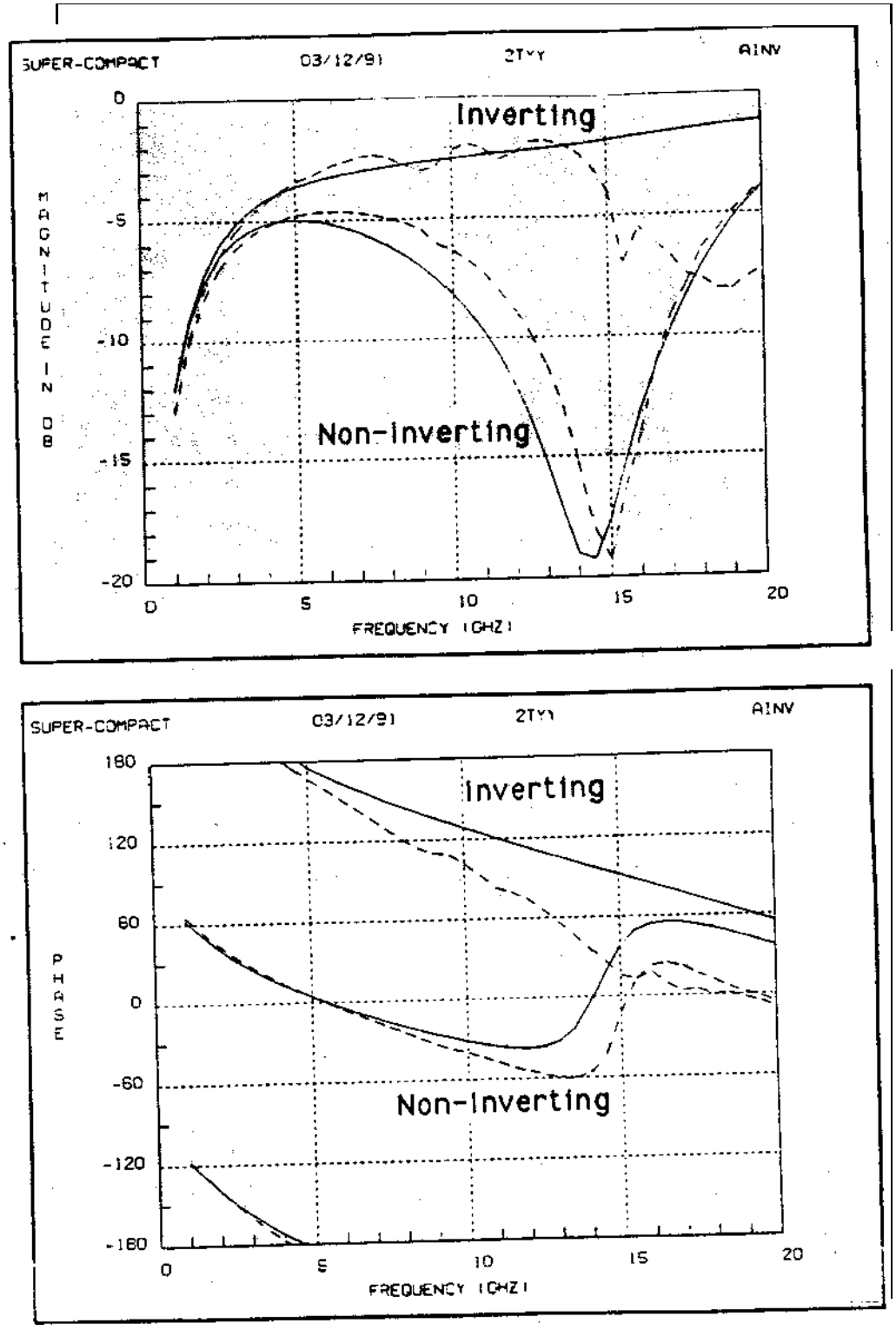

Figure 4.8a. Magnitude and phase of S_{21} of the two turn transformer (shown in Figure 4.6). The solid lines are simulated data, and the broken lines are measured data.

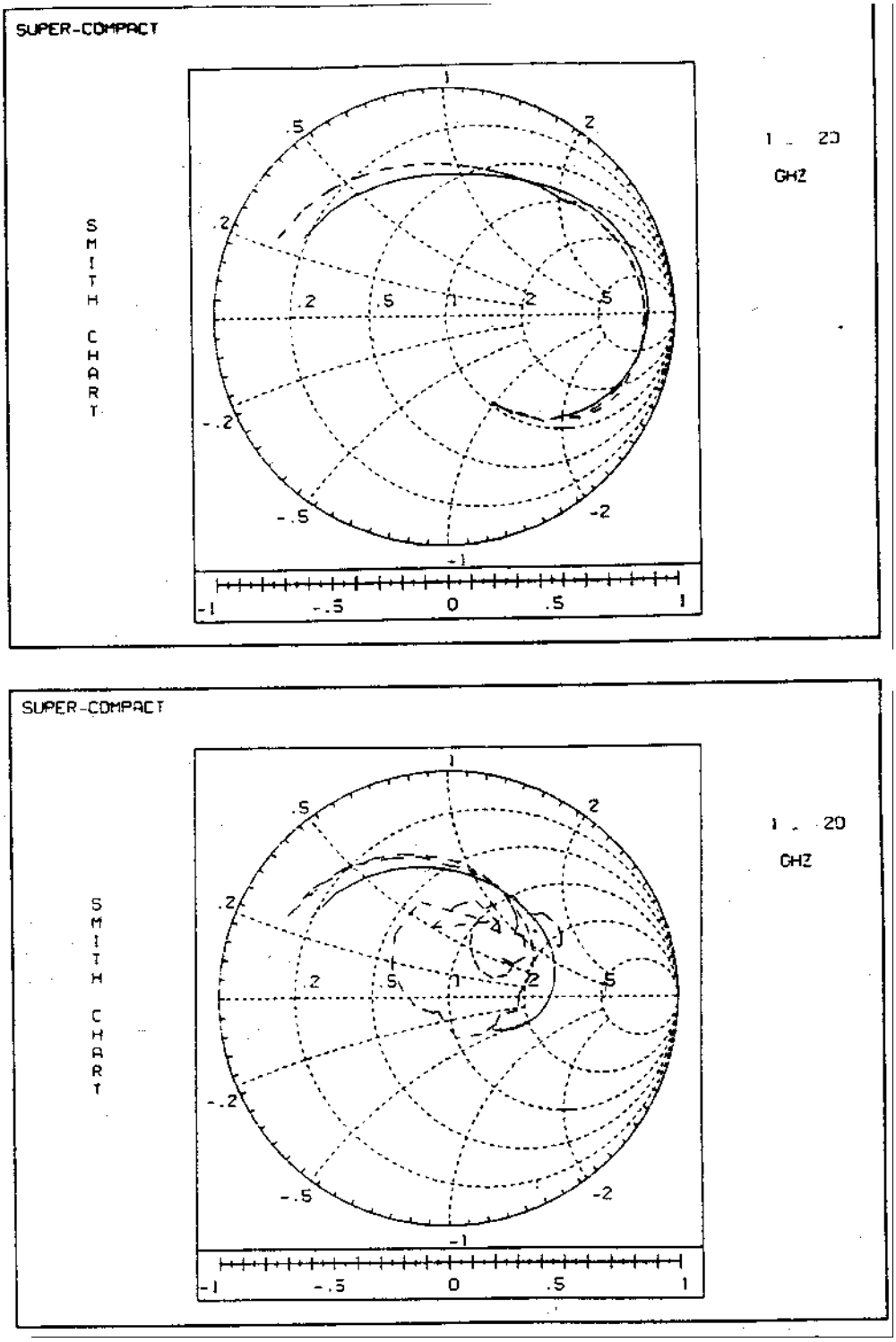

Figure 4.8b. Measured (broken line) and simulated (solid line) S_{11} of the transformer shown in Figure 4.6 from 1 to 20 GHz. The upper trace is the non-inverting response, and the lower trace is the inverting response. The two measured traces are for ports 1 and 2, which ideally should be equal. Notice that the two measured responses in the lower graph are quite different at high frequency because of the awkward probe arrangement.

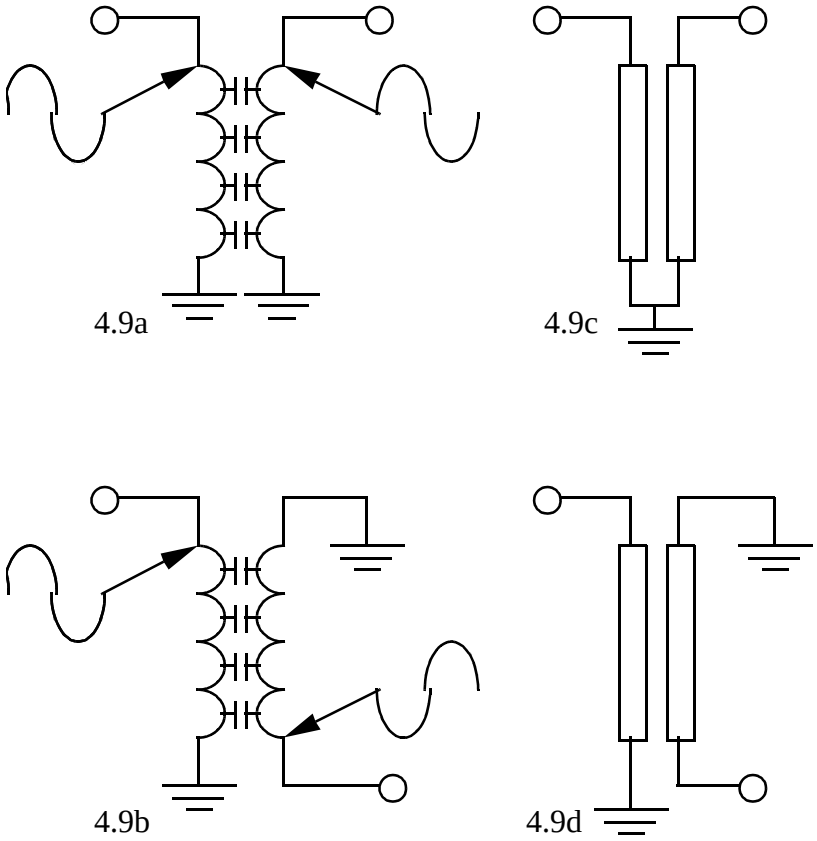

Figure 4.9. The effect of the interwinding capacitance in a transformer wired in various configurations. The drawings at the right are the coupled line equivalent circuits.

interwinding capacitance as seen in Figure 4.9b. The capacitance tends to reduce the output swing. From this analysis, one would expect better performance from the non-inverting transformer, but a further complication arises. The low coupling factor and the physical length of the transformer introduce an additional phase shift in the voltage on the secondary winding. At the self resonant frequency, roughly a 180 degree phase shift in S_{21} (relative to the DC value) has occurred. This makes the voltage gradients along the two windings more similar on the inverting transformer configuration. In fact, measured transformers have wider band performance when operated in the inverting mode.

Another way of considering the problem is by looking at the transformers as a coupled transmission line wound into a spiral. A pair of coupled lines driven as shown in Figure 4.9c

has a dip in S_{21} at its quarter wavelength frequency. When driven as shown in Figure 4.9d, there is a peak in coupling when the lines are a quarter wavelength long. A winding of a transformer exhibits “parallel” resonance at the frequency at which it is a quarter wavelength long. Even though this resonance occurred at 18 GHz in the 2 turn transformer, the imbalance is visible at frequencies as low as 4 GHz. The comparison between transformers and coupled lines is very appropriate, even at low frequencies. A 1:1 transformer (even an audio transformer) is a special case of the coupled line, where the line is much shorter than the wavelength. At high frequencies, coupled lines are accurate models of monolithic transformers. The monolithic transformers studied in this chapter are capable of much tighter coupling than straight coupled lines of a similar geometry (the ratio of even to odd impedance can be twice as high in a spiral design) and are therefore more useful in broadband circuits.

The difference between the configurations can be avoided several ways. The ideal solution would minimize the interwinding capacitance. In monolithic designs, this can only be done at the cost of mutual inductance, for example by increasing the gap between the lines. The loss of mutual inductance usually offsets the gain in balance, as more tuning is required to achieve high S_{21}. Another solution is to operate the transformer at a lower frequency where the reactance of the stray capacitance is higher. As the primary and secondary shunt inductive reactances are so low at such frequencies, the primary and secondary windings are usually made parallel resonant. The result is a fairly narrow band transformer, but the amount of coupling is greatly increased. Another solution would be to add an extra capacitance to the non-inverting transformer to try to make it more similar to the inverting transformer. This will be explored in another section. Transmission line transformers can be made to use the interwinding capacitance to advantage, but such transformers can not be made on a monolithic circuit.

4.4. Symmetrical Monolithic Transformers

An attempt was made to fix the imbalance problem before the problem was properly understood. The transformer in Figure 4.1c was designed to address the problem. The capacitance between either terminal of the primary winding and either terminal of the secondary winding is the same. In conventional designs, such as the design in Figure 4.1b, most of the capacitance is between like terminals (i.e. between terminals connected to windings wound in the same direction) of the primary and secondary, because the parts of the windings connected to the like terminals run side by side.

Several transformers of both designs (similar to Figures 4.1b and 4.1c) have been fabricated and measured. The layouts of these transformers are shown in Figures 4.6 and 4.10. Notice that the transformer in Figure 4.10 can be measured in its inverting configuration without modifications. To measure it in the non-inverting mode, the air bridge in the ground ring must be removed, and a bond wire placed from one port's former signal pad to the other port's ground pad. Note that the transformer in Figure 4.6 was designed in the non-inverting

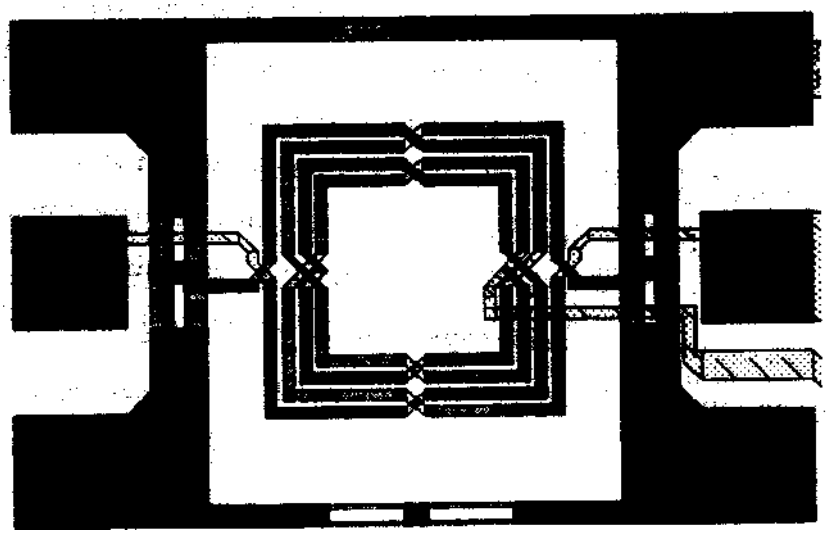

Figure 4.10. Physical layout of the 2-turn symmetrical transformer. The lines are 10 um wide, spaces are 5 um wide, and the central hole is 150 um square.

configuration (and must be modified to me measured in the inverting mode), and the transformer in Figure 4.10 was designed in the inverting mode (and must be modified to be tested in the non-inverting mode). Figure 4.7 illustrates the changes more clearly if the difference between the two designs is considered. Figure 4.11 shows the S_{21} of 2-, and 3-turn transformers in both inverting and non-inverting configurations. Figures 4.11a and b apply to designs similar to Figure 4.1b with 10 um lines and 5 um spaces, central ("hole") dimensions of 150 um, fabricated on a 500 um GaAs substrate. The transformers in Figures 4.11c and d have similar dimensions, but are laid out as shown in Figure 4.1c. A phase shift of 180 degrees has been added to the phase of the inverting response so that the two phase plots could be compared easily.

Notice that the response of the inverting and non-inverting configurations agree well at low frequencies, but degrades quickly at higher frequencies. The non-inverting response always shows a dip, where the inverting response is more benign. The phase difference also degrades suddenly at roughly the same frequency as the dip in magnitude. All of this occurs because capacitive coupling becomes dominant.

These measurements indicated that the imbalance problem in the new design was virtually the same as in conventional designs. This can be explained simply: when the transformer is used in the non-inverting mode, the voltage averaged over the primary is similar to the voltage averaged over the secondary (ignoring high frequency phase shift effects). The two averaged voltages will be different, and, in fact, of opposite polarity when the transformer is used in inverting mode. Notice that the difference in phase between the two configurations above the first resonance is less for the symmetrical (Figure 4.10) design. This is likely a result of the redistribution of the capacitance.

Although this form of transformer does not provide identical responses in both configurations, it can be used to advantage as all four terminals are accessible from the outside of the transformer, and the centre tap can be located exactly. This transformer is ideal for use in balanced circuits. In section 4.7, a transformer similar to this forms the basis for a symmetrical balun that is a significant improvement over other designs.

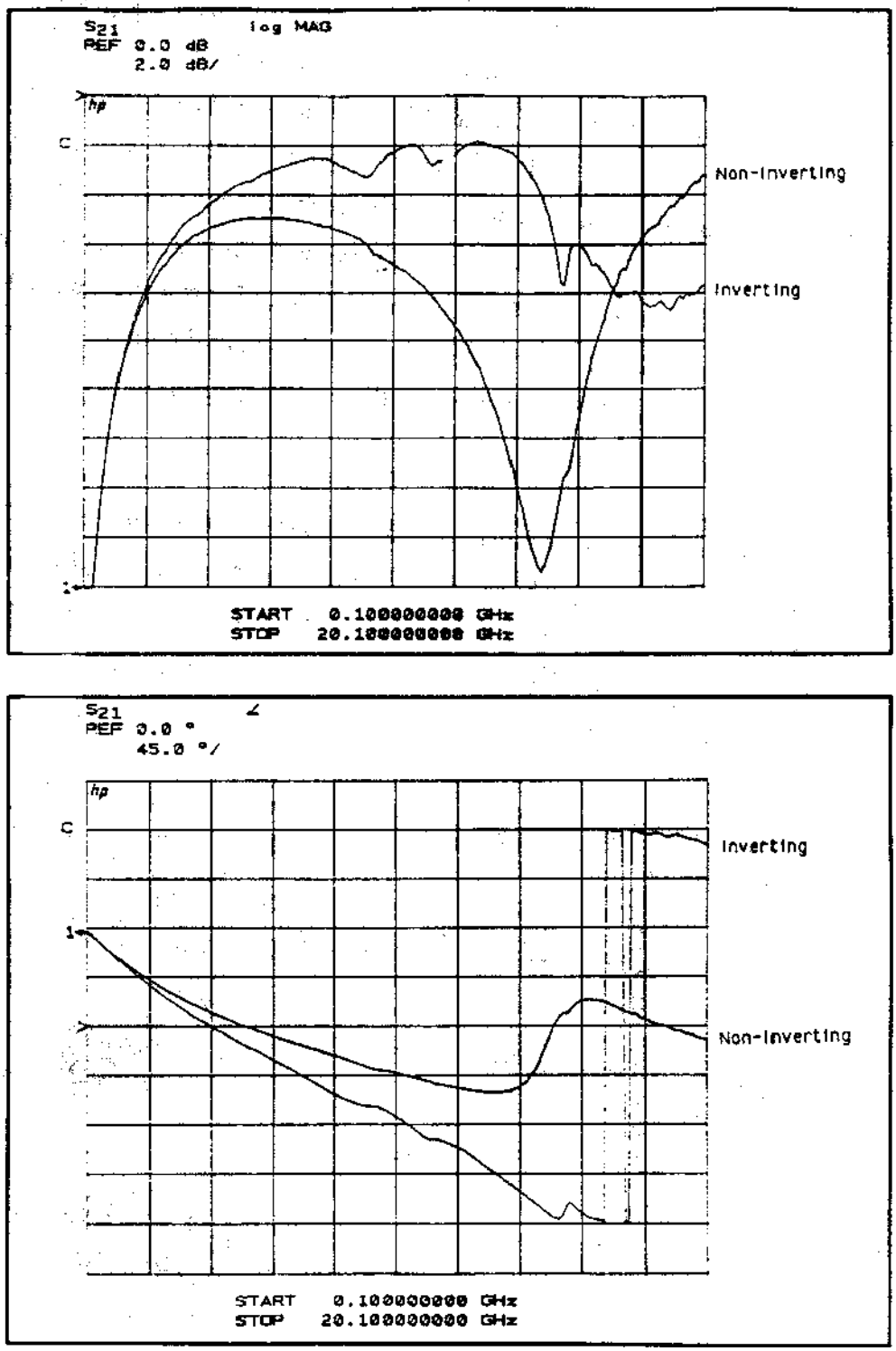

Figure 4.11a. Measured response of a two turn transformer of the form shown in Figure 4.6. The transformer measures 290 um by 260 um, with lines and spaces of 10 um and 5 um respectively. 180 degrees has been added to the phase of the inverting response.

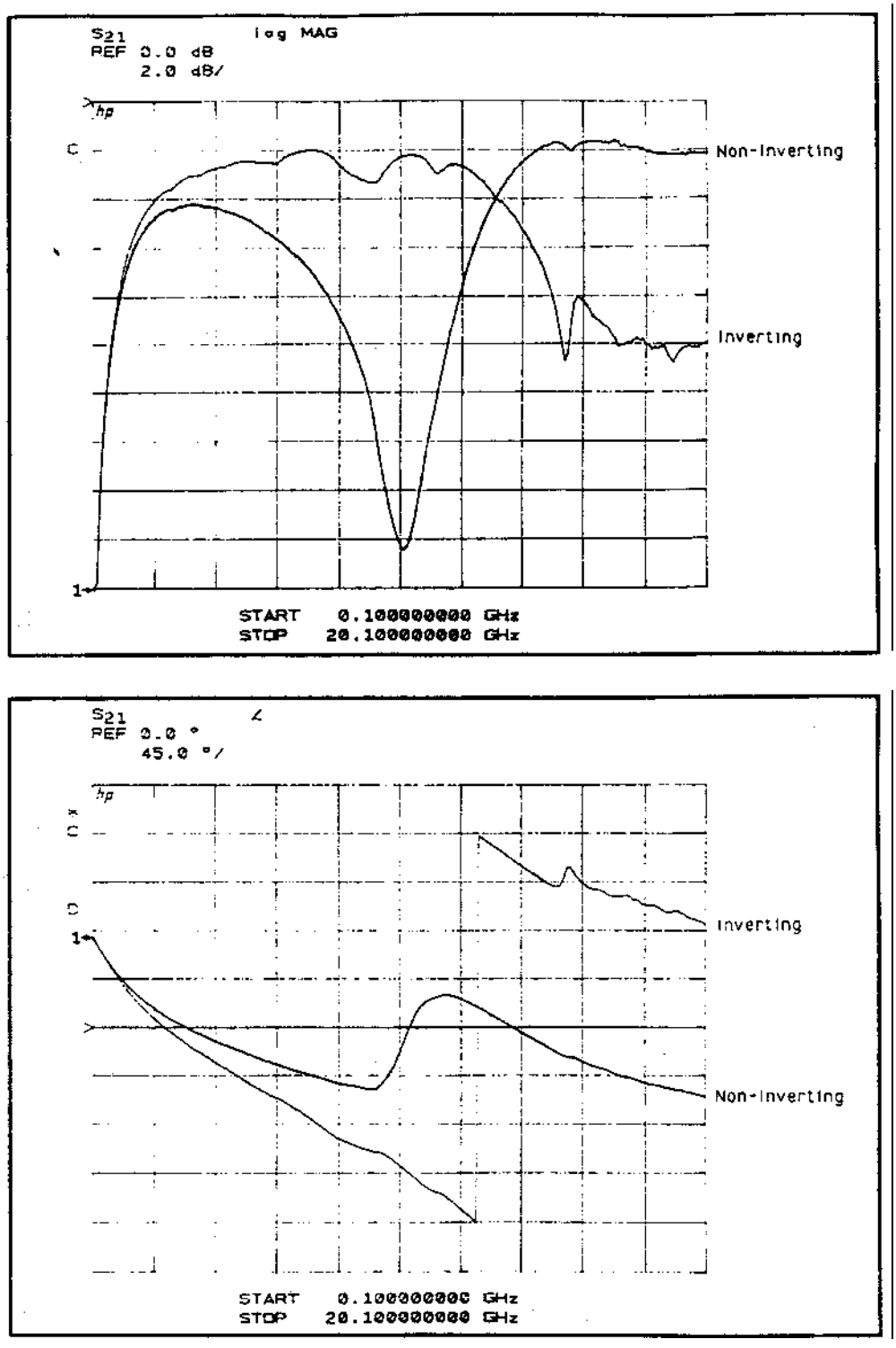

Figure 4.11b. Measured response of a three turn transformer of the form shown in Figure 4.6. The transformer measures 350 um by 320 um, with lines and spaces of 10 um and 5 um respectively. 180 degrees has been added to the phase of the inverting response.

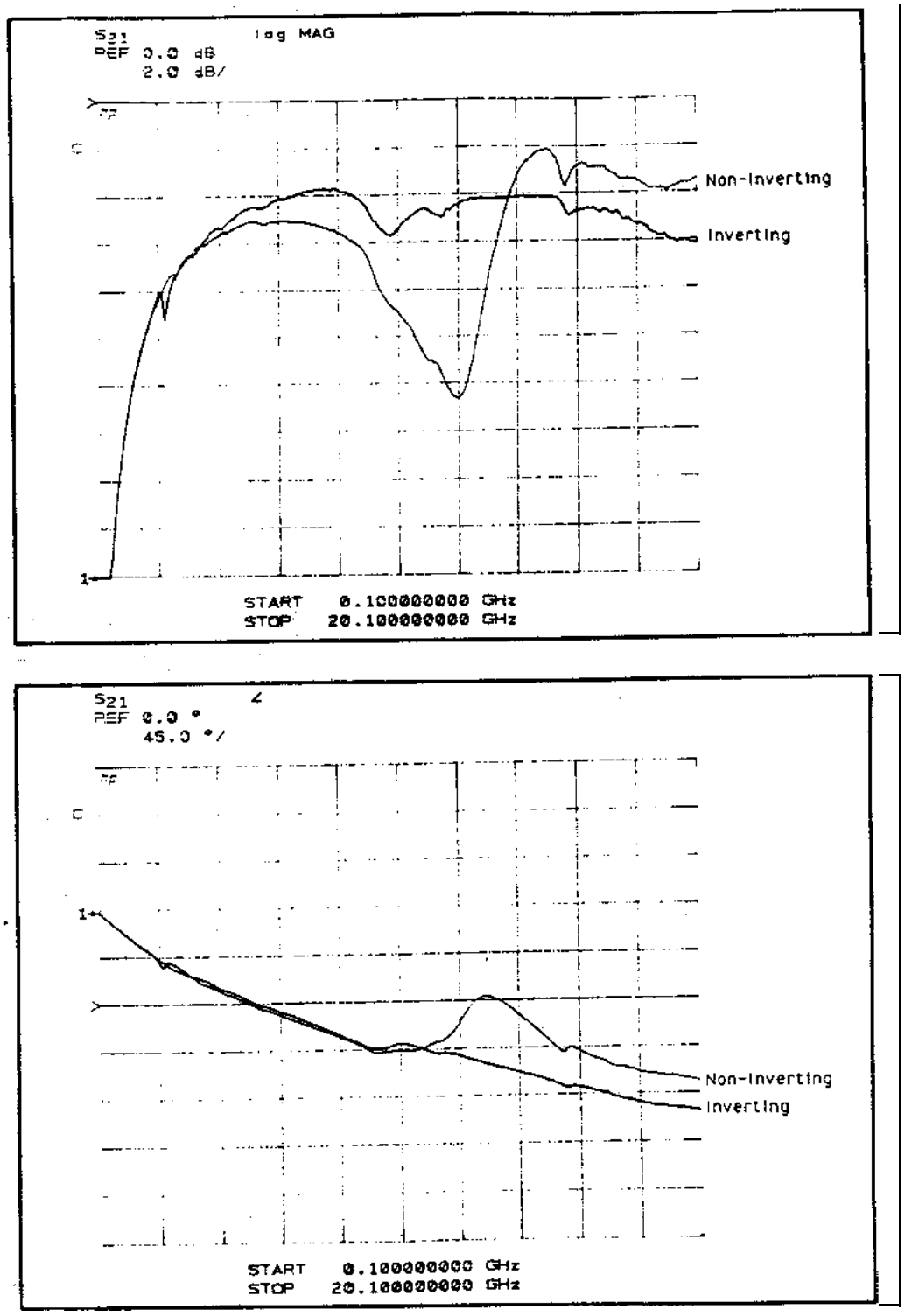

Figure 4.11c. Measured response of a two turn transformer of the form shown in Figure 4.10. The transformer measures 260 um by 260 um, with lines and spaces of 10 um and 5 um respectively. 180 degrees has been added to the phase of the inverting response.

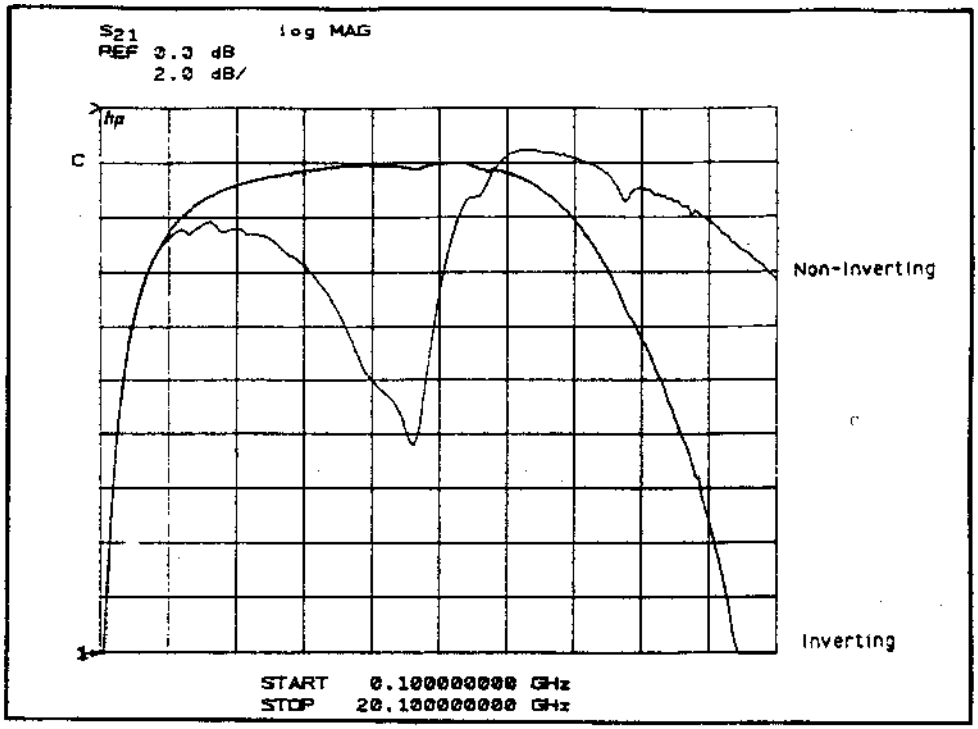

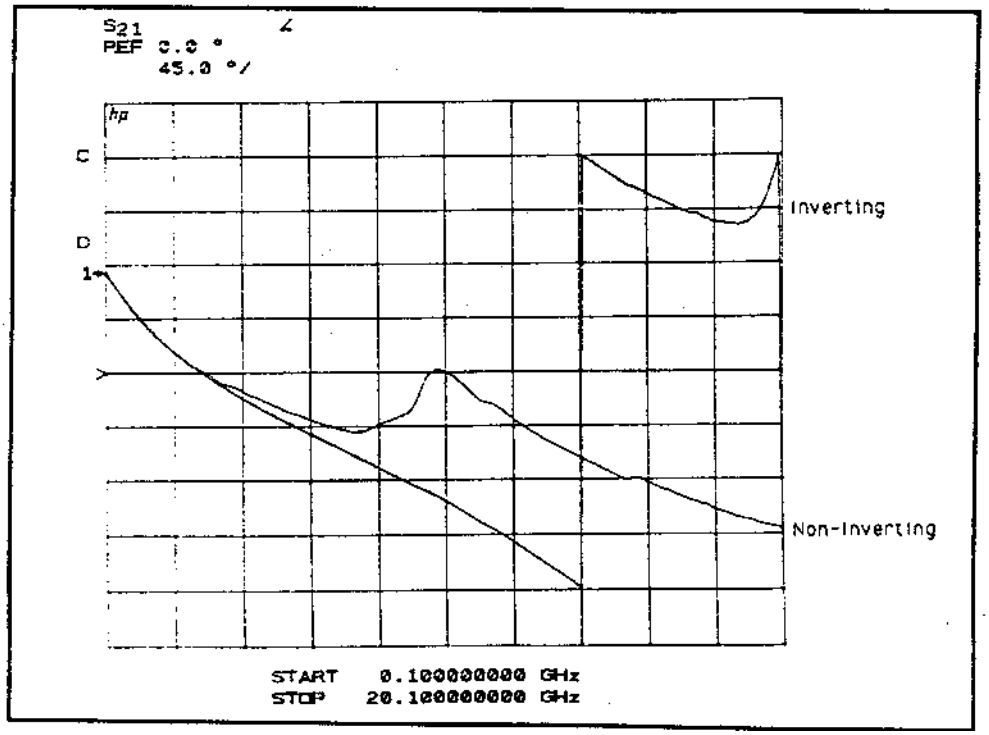

Figure 4.11d. Measured response of a three turn transformer of the form shown in Figure 4.10. The transformer measures 320 um by 320 um, with lines and spaces of 10 um and 5 um respectively. 180 degrees has been added to the phase of the inverting response.

4.5. Transformer Design

One of the goals of this study was to determine a monolithic transformer design technique. This section first discusses how to determine what electrical parameters a transformer should have, and then discusses approximate techniques for determining physical sizes.

4.5.1. Selecting Transformer Parameters

Given a certain transformer structure, a designer needs to know how to arrive at an optimum transformer. In general, this involves attaining the widest bandwidth and lowest loss, in minimum space requirements. To achieve this optimum, it is usually necessary to maximize coupling factor and select an optimum resonant frequency.

The model in Figure 2.2 illustrates the effect of the coupling factor. The inductive reactance of the shunt inductor (representing the mutual inductance) must be greater than the system impedance, Z_0 to avoid loading the generator excessively. The inductive reactance of the series inductors must be less than the load impedance to avoid excessive reflection. The inequalities in (4.1) and (4.2) describe this relation.

$$2\pi MF > R_0 \quad \text{therefore} \quad 2\pi MF_{\text{lower}} = R_0 \tag{4.1}$$

$$4\pi F(L-M) < R_0 \quad \text{therefore} \quad 4\pi F_{\text{upper}}(L-M) = R_0 \tag{4.2}$$

$$\text{Fractional bandwidth} = \frac{F_{\text{upper}}}{F_{\text{lower}}} = \frac{k}{2(1-k)} \tag{4.3}$$

Where F is the frequency of operation, M is the mutual inductance, L is the self inductance, k is the coupling coefficient, and R_0 is the characteristic impedance of the circuit. From (4.3), it can be seen that the minimum value of k that allows any bandwidth at all (a fractional bandwidth of greater than 1) is 0.67. When k=0.67, the minimum voltage loss through the transformer is roughly 0.5. This relationship places a well defined limit on the

broadband use of a monolithic transformer. Typical multi-turn monolithic transformers have coupling coefficients on the order of 0.8, which will result in a fractional bandwidth of 2 (octave bandwidth). Tuning can reduce the loss through the structure, but the fundamental limit on bandwidth remains.

The coupling factor of a monolithic transformer is highly dependent on the line width to gap ratio. In fact, if one ignores second order effects, (capacitance, short line effects and loss), the coupling factor of a complete transformer structure depends only on the line width and spacing, the substrate height, and the number of turns. Figure 4.12 is a plot of the coupling factor versus number of turns for a rectangular transformer designed as shown in Figure 4.1b. This graph was derived by fitting a simple mutual inductance model to the GEMCAP model (with capacitive and resistive elements removed from the model). From

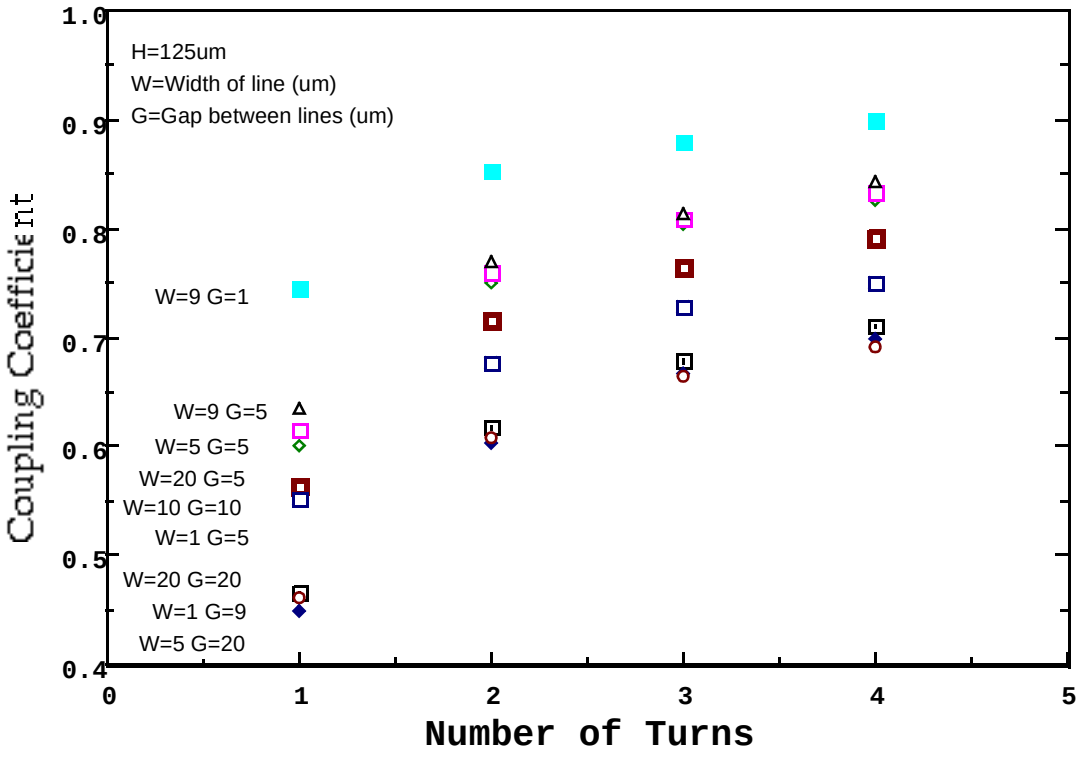

Figure 4.12. Coupling factor for transformers with various winding pitches, versus number of turns.

this graph, it can be seen that little improvement in coupling factor is made by increasing the transformer size beyond 3 turns. It is also apparent that the gap between conductors should be made as small as practically possible. The graph also suggests that for a given pitch, wide lines yield the largest coupling factor. If the lines in a transformer are widened, while the gap dimension is maintained, both the self and the mutual inductance decrease (although the self inductance decreases slightly faster). The resulting transformer will have less self inductance and therefore higher (poorer) low frequency cutoff frequency. Wide lines may be necessary to reduce resistive losses, or provide sufficient DC current capacity. Although a narrow gap increases the mutual coupling, it also increases the interwinding capacitance. As the transformers are usually operated below their self resonant frequency, the extra capacitance associated with the tight coupling is less important. In fact, capacitance is sometimes intentionally added to resonate out the self inductance. As will be seen from (4.4), the added capacitance will tend to reduce bandwidth.

Low impedance transformers can be made by adding windings in parallel, such as in the example shown in Figure 4.2a. The mutual coupling versus winding spacing and number of windings is exactly the same as the series connected case, and the same graph can be used.

A simple model can be useful in suggesting how to optimise a transformer design for wide bandwidth. The model of a simple 1 to 1 transformer with unity coupling coefficient is shown in Figure 4.13. This model is derived from the model in Figure 2.2 by adding stray capacitance, and assuming k=1. The inductance is simply the self inductance of either winding, and the capacitance represents the stray winding capacitance. The low frequency limit is determined by the frequency where the inductive reactance of the mutual inductance equals the system impedance. The high frequency operational limit (if k=1) is determined by the frequency where the capacitive reactance of the stray capacitance equals the system impedance. The fractional bandwidth is the upper frequency divided by the lower frequency. Equation (4.4) shows approximately the expected bandwidth.

$$\text{Bandwidth} \propto \frac{1}{R_0^2}\frac{L}{C} \tag{4.4}$$

where $R_0=R_{in}=R_{out}$ is the characteristic impedance of the system (assumed to be real), L is the self inductance, and C is the stray capacitance. As might be expected, the impedance of the system can be lowered to decrease the loaded Q, and increase bandwidth. The main cost associated with driving a lower impedance load is increased loss, as conductor loss is always dominant in monolithic transformers.

The stray capacitance of a transformer is difficult to calculate from the transformer's dimensions. Tables of inductor models supplied by GaAs foundries give the parallel parasitic capacitance and inductance of inductors with a fixed line width to gap ratio [31]. These tables indicate that the stray capacitance of inductors in the form of Figure 4.1b increases (with the number of turns of the inductor) more slowly than the inductance. This would suggest that, ignoring distributed effects, a larger transformer (i.e. an inductor with more turns) would have a wider bandwidth. The reason that capacitive effects increase relatively slowly is because most capacitance is between adjacent turns; end to end capacitance will actually decrease as the ends become farther apart.

Transformers with parallel windings, such as in Figure 4.2b will tend to have less bandwidth than the series wound transformers because inductance decreases as the number of parallel turns is increased, but capacitance increases. Hence, the L/C ratio, and therefore the bandwidth will decrease as the number of turns increases.

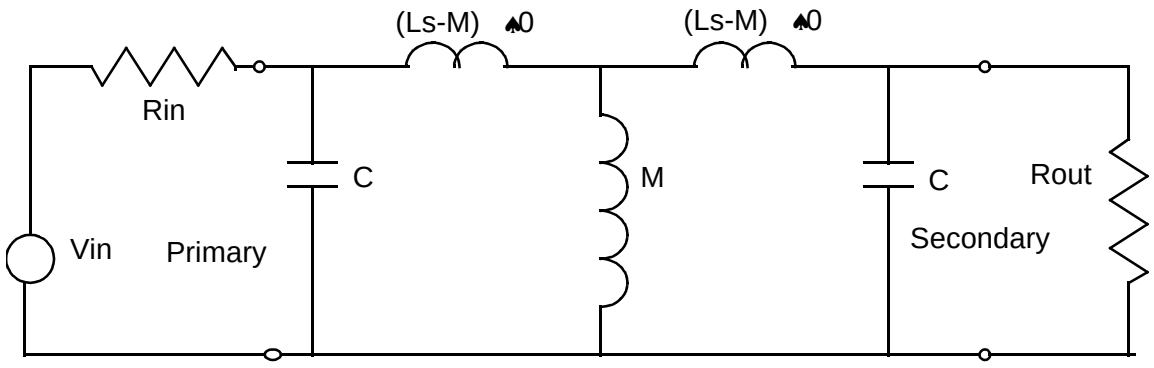

Figure 4.13. Elementary transformer model for bandwidth calculation.

The other factor that will tend to limit upper frequency response is the length of either winding. If either winding approaches a quarter wavelength in length, the simple rules of thumb described above can not be employed. Although GEMCAP can still be used if a sufficient number of elements are included in the model, more traditional transmission line analysis tends to be more convenient.

4.5.2. Transformer Design

The complexity of the model of a transformer makes the use of look-up tables or nomograms for an exact design unwieldy. Instead, this section outlines a procedure that can be used to determine the approximate size and configuration of a transformer for a given application. The dimensions of the transformer can be entered into the GEMCAP program so that a circuit model can be generated. The physical dimensions in the GEMCAP model can be altered if the electrical characteristics of the first guess are not appropriate.

There are several guidelines that should be kept in mind when laying out monolithic transformers. Adjacent conductors should belong to different windings. If adjacent conductors belong to the same winding, then the mutual inductance between these adjacent conductors is being converted into the self inductance of that winding, lowering the coupling coefficient of the transformer. If step-up or step-down transformers are to be made, it may be beneficial to employ parallel turns on low impedance winding to lower loss and increase coupling. A more balanced transformer design results when the capacitance between either end of the primary winding is split evenly between the two ends of the secondary winding.

Steps that can be employed to design a monolithic transformer are outlined below.

1) The inductance of each winding must be determined. The inductance is determined largely by the circuit configuration. If the transformer is itself matching a capacitive source or load, as is the case in FET amplifier designs, the inductance will be determined by the impedance of the device connecting to it. Usually, the inductance tunes out the capacitance exactly, making the combination parallel resonant at centre frequency. If the transformer is to have a non-unity turns ratio, the inductance ratio must equal the impedance ratio.

If the transformer is operating into real impedances, then the designer must consider tuning in order to reduce reflections and improve coupling. In examples given here, over a 3 dB improvement in S_{21} (in a 50 ohm system) can be achieved through tuning. Tuning improves insertion loss for any transformer that does not have perfect coupling and has resistive losses. The amount of tuning that yields a transformer with minimum loss at a given frequency, or the transformer size that yields optimum insertion loss when tuned is not easy to calculate. In fact, even if it could be calculated for an ideal system, the capacitive parasitics would perturb the calculation sufficiently such that re-tuning would be required. For the losses usually encountered in monolithic transformers, selecting a winding self inductance with an inductive reactance roughly equal to the system impedance yields good results. The capacitor required to tune this circuit will also have a reactance of roughly the system impedance. The effect of tuning the two turn BNR transformer discussed in section 4.3 is illustrated in Figure 4.14. Identical capacitors were placed in parallel with the primary and secondary of the transformer, and its frequency response in a 50 ohm system was simulated. Both inverting and non-inverting transformers are shown. The plots, from right to left are for transformers tuned with 0 pf, .5 pF, 1 pF, 1.5 pF, and 2 pF capacitors. Notice that there is a frequency at which the S_{21} is optimum. Also notice that higher values of capacitance make the two configurations look more similar. At higher frequencies, series tuning capacitors are more effective.

Using the transformer without any tuning capacitors will yield the broadest design, but very high mismatch losses are seen. The cause of this is the low self inductance of the windings. This is the principal dilemma in monolithic transformer design. Self inductance must be kept low to reduce losses, save space, and to avoid distributed effects. In designs such as this, the self inductance of each winding of a transformer to be used untuned should be greater than the characteristic impedance of the system at the lowest frequency of operation.

2) Determine the maximum DC and AC current that will flow the windings. Using information about the characteristics of the metallisation used, determine the minimum permissible transformer winding width.

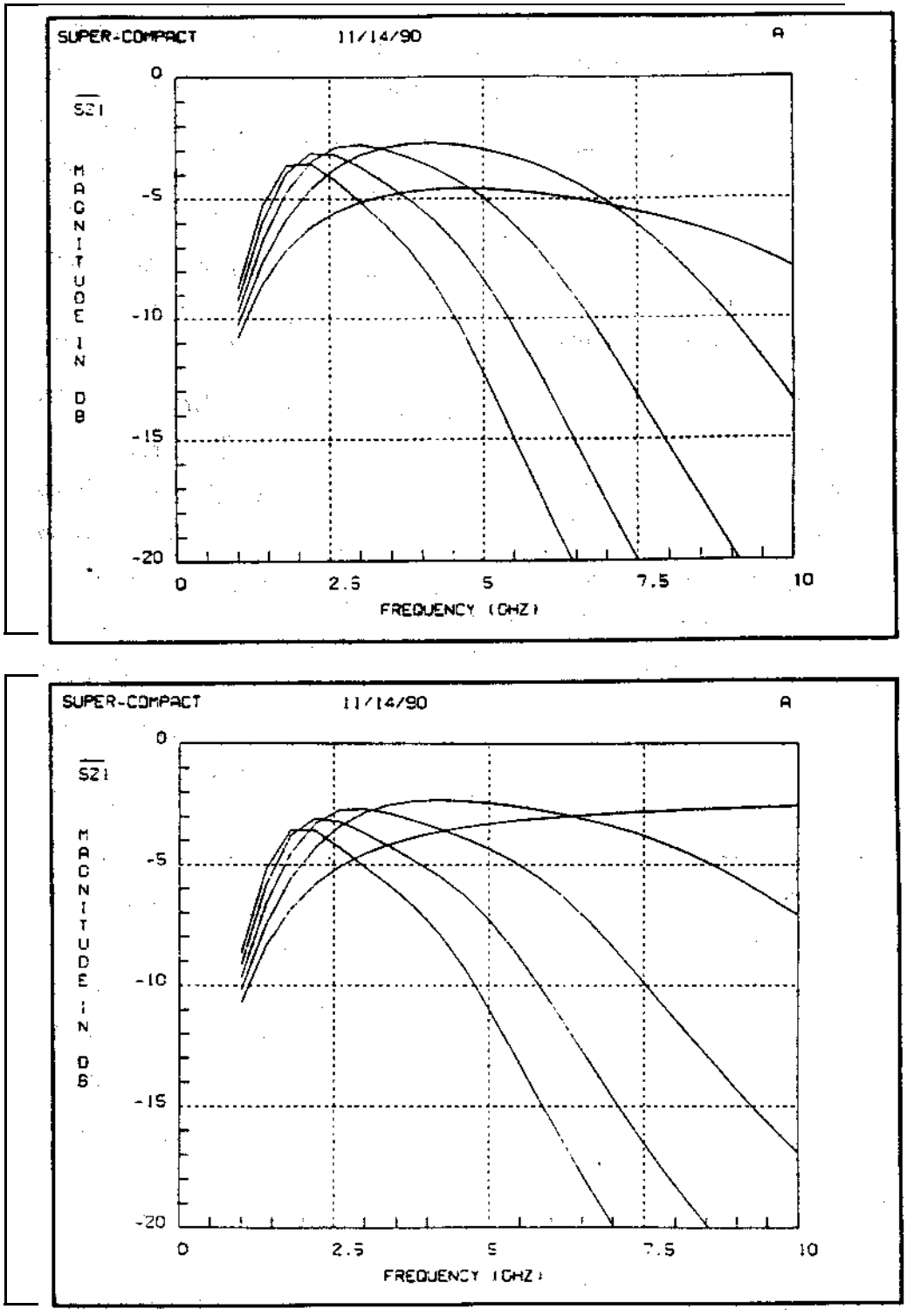

Figure 4.14. Magnitude of S_{21} of a tuned two turn transformer tuned with 0, .5 pF, 1 pF, 1.5 pF, and 2 pF parallel capacitors, right to left. The upper transformer is operating in the non-inverting mode, and the lower transformer is operating in the inverting mode.

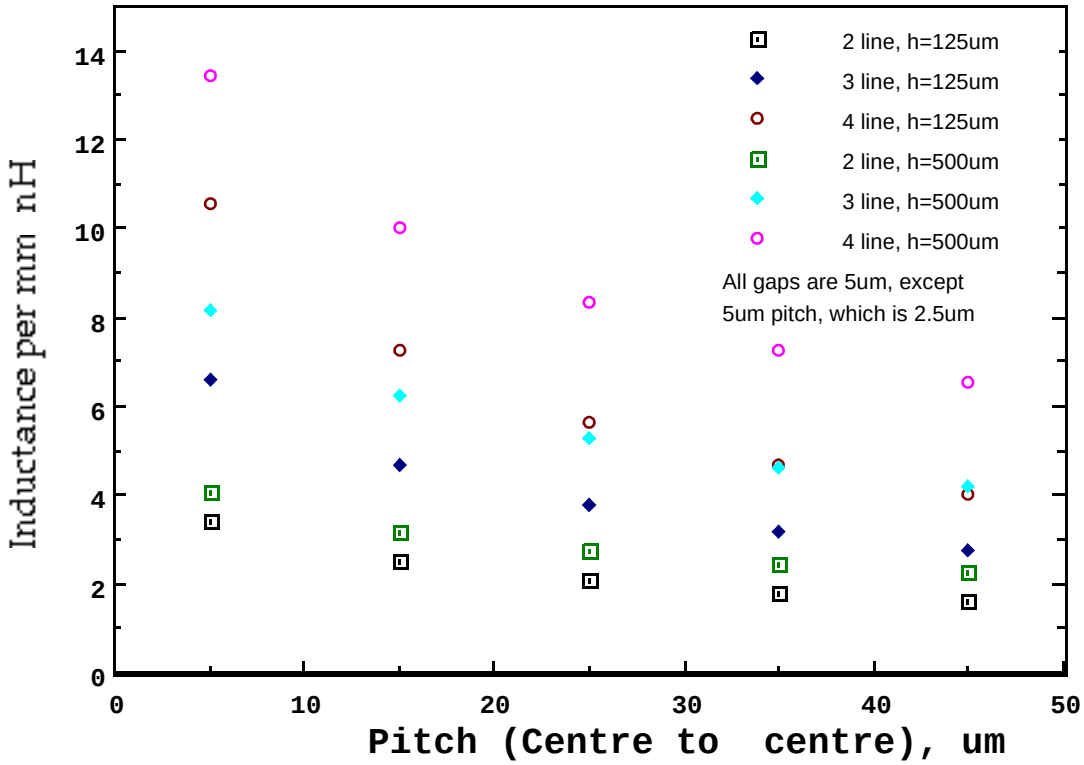

Figure 4.15. Inductance per mm for the elementary transformer shown in Figure 4.16 for various substrate heights.

3) The physical dimensions of a transformer to achieve the desired inductance can be estimated with the graph in Figure 4.15. This graph gives the self inductance per unit length (at low frequencies) for linear transformers consisting of 2, 3 and 4 conductors, with various line pitches (centre to centre distance of lines). An illustration of the linear transformer used in these calculations (with 3 conductors) is shown in Figure 4.16. Note that this transformer can not be physically laid out in the form shown. Instead, it is assumed that the characteristics of the transformer will not change significantly when bent around to form a spiral transformer of the form shown in Figure 4.1. These graphs are approximate as the inductance will also depend on line width and length. In particular, transformers in which the length of each side is less than the substrate height will have less inductance than predicted from Figure 4.15. The short line effect can be accounted for by using Figure 4.17. This graph gives the reduction in inductance given the ratio of the substrate height to line length.

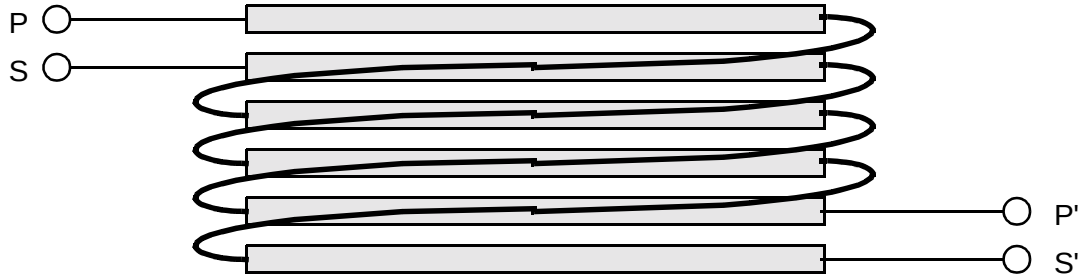

Figure 4.16. Elementary linear transformer used as a basis for Figure 4.15 and Figure 4.17. Note that this transformer is not physically realizable, as the right to left return paths are assumed not to couple to the rest of the transformer.

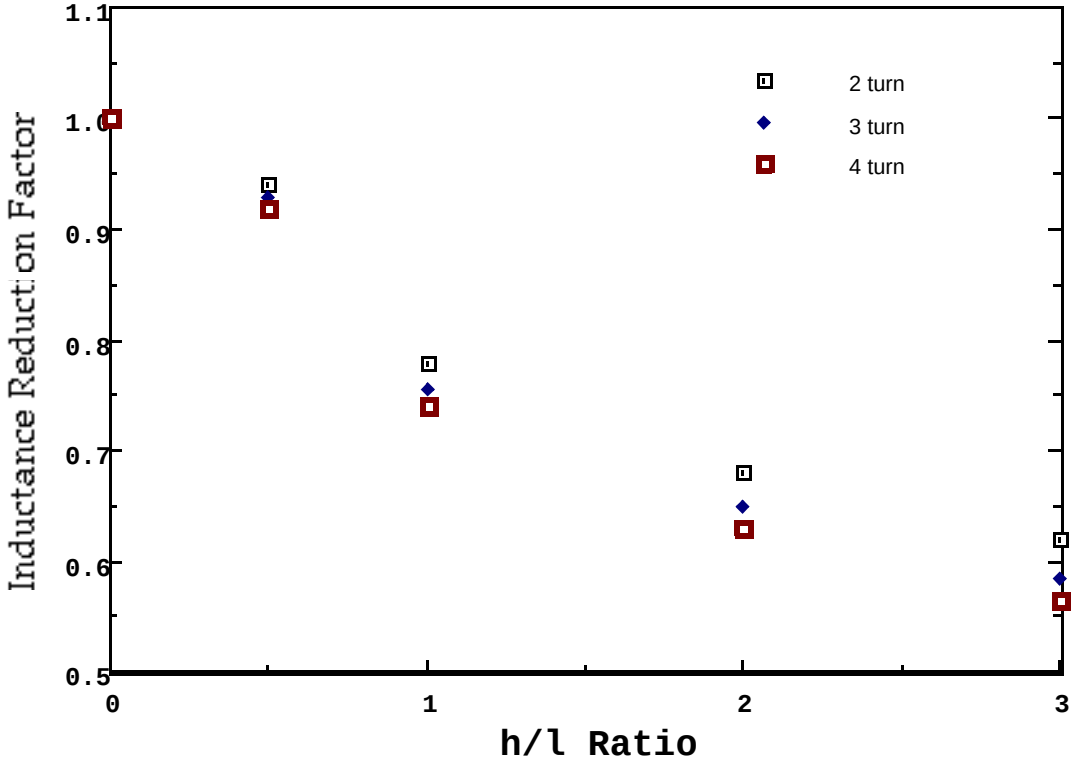

Figure 4.17. Inductance reduction factor for inductors and transformers made with short lines.

To use this graph, one first calculates the pitch required. Generally, the minimum spacing between lines, as specified by the process design rules, is suggested, and the line width calculated in step 2 is used. Next, the number of turns and substrate height are determined. Generally, a 3 or 4 turn transformer is preferred over a 2 turn transformer, as the former has better coupling coefficient. Using the above information, one can determine the overall transformer length required by referring to Figures 4.15 and 4.17. The actual rectangular layout should be sketched out, to insure that it is physically realizable. The hole in the middle of the transformer should be at least 5 line widths wide. If it is not, then there will be significant negative mutual inductance between opposite sides of the transformer.

Transformers with non-unity turns ratios can also be designed with this graph. First, the designer must determine a basic layout that will give the required ratio. Suggested layouts are shown in Figure 4.2. If a winding is made of a single conductor, (normally of several turns), then Figure 4.15 can be used directly. To calculate the inductance of a winding made of parallel conductors, such as shown in Figure 4.1c, then the inductance of a single path is calculated. The added parallel windings will reduce the inductance slightly (roughly 20%).

The use of this graph is best illustrated with an example. Assume that a transformer with self inductance of 6 nH is required, and that a minimum line width of 10 um is required to carry DC current. If a 5 um gap is employed, the pitch of the windings is 15 um. From the graph, a 3 turn transformer made with such a pitch, on a 500 um substrate, has an inductance of 6.5 nH per mm. Therefore, a transformer length of 920 um is required. The length of each side will be roughly 250 um, which is less than the substrate height, so a correction factor from Figure 4.17 must be applied. Dividing 920 um by 70% yields a length of approximately 1300 um, or 325 um per side. Figure 4.18 illustrates one possible implementation such a transformer. Note that the length calculated by Figure 4.15 represents the length of the centre conductor in the 6 conductor bundle. Although the outer and inner conductors are larger and smaller, respectively, the average length is correct. This transformer was entered into GEMCAP and modelled. The self inductance was 6.2 nH, which is very close to the desired value of 6 nH.

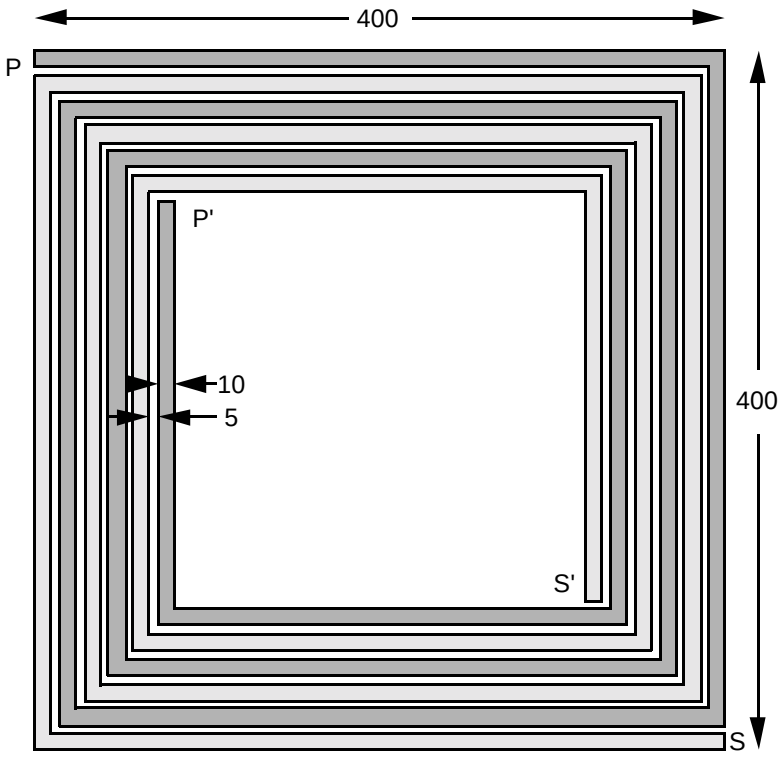

Figure 4.18. A 3 turn transformer designed with the transformer design technique.

4) The resistance of the windings can be used to determine approximately the dissipative loss of the transformer. The approximate portion of the power that enters a winding that is not dissipated by that winding's series resistance is given by (4.5).

$$P_{\text{loss}} = \frac{R_0}{R_0 + R_s} \tag{4.5}$$

R_s is the series resistance of the winding and R_0 is the characteristic impedance of the circuit driving the transformer and the load. This equation assumes a good match and assumes that $R_s << R_0$. Note that this must be applied to both the primary and the secondary windings of the transformer. By applying (4.5), one can determine the maximum winding resistances that will yield a given loss. One can determine the DC resistance of the windings by multi-

plying the sheet resistivity of the metal by the number of squares that make up the winding. If the resistance exceeds the number calculated with (4.5), then a wider metal width should be selected, and the inductance re-calculated in step 3. In the example cited above, the DC resistance (for 1 um thick gold conductors) was 8.4 ohms, which causes a loss of 0.8 dB in the primary winding and 0.8 dB in the secondary winding, for a total of 1.6 dB total. The simulated tuned loss (with lossless series inductor and shunt capacitor tuning) was 1.59 dB.

5) The transformer length should be less than .25 wavelengths long at the maximum operating frequency.

4.6. Transmission Line Transformers

Transformers in use at frequencies above 1 MHz typically fall into one of two categories: conventional transformers that rely strictly on the flux linkage between windings for power transfer, and transmission line transformers that transfer energy through a transmission line mechanism. In designing the former transformer, one minimizes parasitic capacitance between the primary and secondary. Transformers of the later design use “parasitic” capacitances to form transmission lines. This form of transformer could be further classified into devices with a length of less than a quarter wavelength, and those with a length roughly equal to, or greater than a quarter wavelength. The latter are usually referred to as couplers rather than transformers, and will not be discussed. Electrically short transmission line transformers, when formed on a low-loss ferrite core, can have losses as low as .02 dB in the 3-30 MHz frequency range [34]. Transmission line transformers can only be fabricated in certain discrete ratios, but clever design can yield many useful configurations. In order to illustrate the difference between the transformers, the operation of an isolation transformer will be described.

The purpose of an isolation transformer is to allow the transfer of energy between two circuits that may be at different potentials. A conventional transformer can accomplish this (with isolation down to DC) because the primary and secondary circuits are not electrically connected; the magnetic flux linkages provide the energy transfer. A transmission line of sufficient length can provide isolation between its ends because of the self inductance of the line, although this isolation does not extend down to DC. Transmission lines of quarter wavelength length (the wavelength of the transmission line in its surrounding medium must be considered) are frequently used in baluns as they behave like a quarter wavelength shorted stub, which has a high impedance. The impedance between the ends of a transmission line can also be increased by wrapping it around a magnetic material, as shown in Figure 4.19. The characteristics of the transmission line, as far as the “differential” signals travelling on it are concerned, do not change, as the currents on each conductor of the line are equal, and the magnetic fields produced exactly cancel outside the line. “Common mode” signals imposed from the output of the circuit to a common ground will be blocked

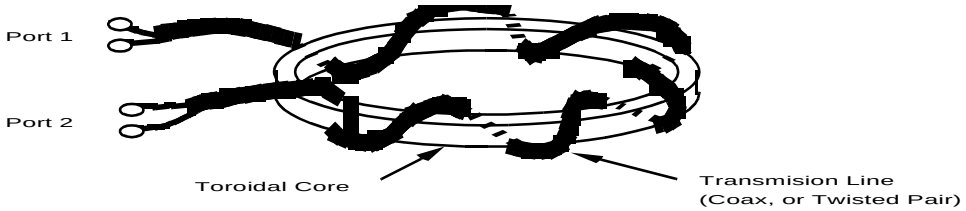

Figure 4.19. Pictorial view of basic transmission line transformer made by wrapping a twisted pair or coaxial cable around a ferrite toroid.

from the input of the circuit because of the extra inductance. A transmission line transformer can not usually provide DC isolation between circuits but can provide RF isolation.

The most common type of transmission line transformer uses a twisted pair transmission line wrapped on a toroidal ferrite or powdered iron core. For broadband operation, the transmission line length is less than a quarter wavelength. The loss of such a transformer is determined by the loss of the transmission line, and this can be made extremely low if the correct characteristic impedance is maintained. In Figure 4.20 this isolation transformer is illustrated in both a conventional and a transmission line form. Although these two transformers, in the inverting configuration, yield the same schematic, this is true only in the simplest cases. The transformer shown in Figure 4.20 forms the basis for transmission line transformers, including the Ruthroff designs [6].

This transmission line transformer can easily be converted into a balun by adding a third (often smaller) winding. This winding induces half of the output voltage into the transmission line to make an exact balance. The current in this winding is determined by the inductance of the transmission line, and can be made small. This balun is illustrated in schematic form in Figure 4.21.

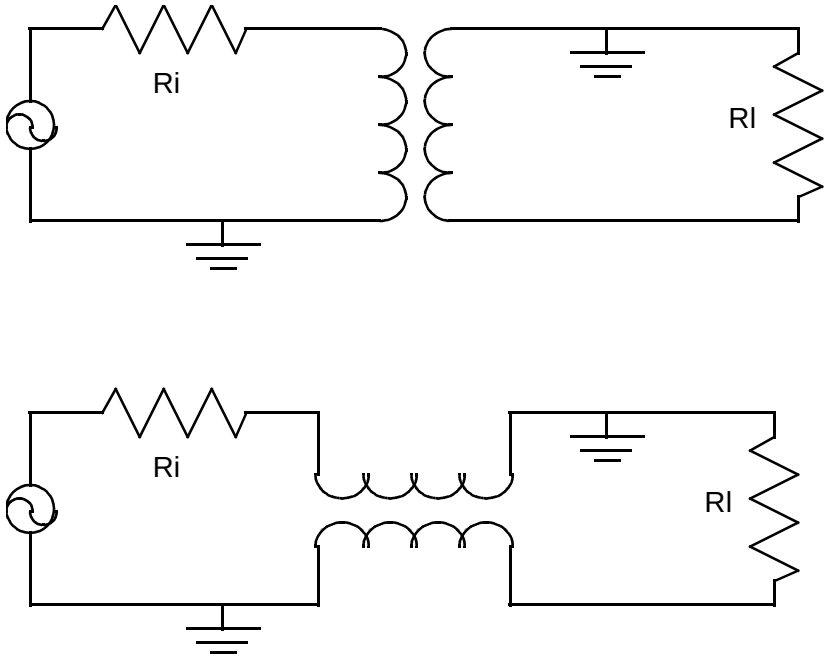

Figure 4.20. Comparison between “Conventional” transformer (top) and transmission line transformer (bottom).

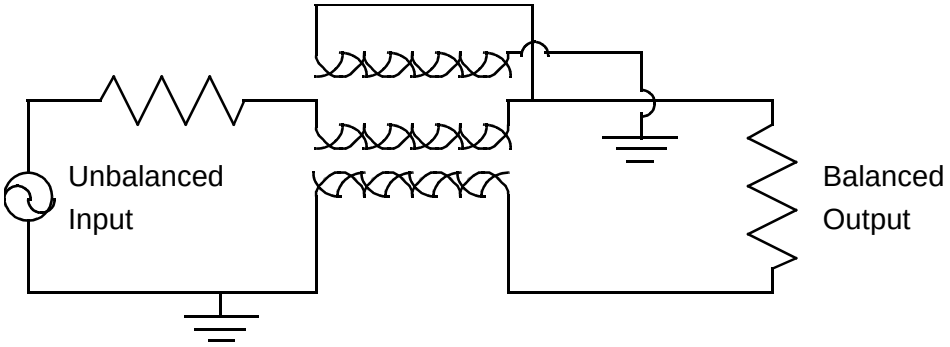

Figure 4.21. Trifilar transmission line balun. Note that the upper winding can be smaller than the other two windings.

At this point, it is interesting to compare monolithic transformers with toroidal transformers wound on a ferrite core, and explain the differences. The magnetic core is the key to the toroidal transformer performance. If the two (or more) windings are isolated from each other on the core, then a conventional transformer results. The core increases the coupling

factor by confining the magnetic fields, and also increases the self inductance of the windings. All of this is done without adding any capacitance. If twisted pair is used for the two windings, coupling between windings is increased, and interwinding capacitance is added. The result is a transmission line transformer. Since the required self inductance can be achieved with less wire, losses can also be kept very low.

Transmission line transformers are possible only because the end to end inductance of the transmission line can be increased (by using a ferrite core, for example) without modifying the properties of the transmission line. Transmission line transformers can not be made conventional monolithic circuits because it is difficult to make a shielded transmission line. Since magnetic material for the confinement of the magnetic field is not available, the transmission line must be wound very tightly to achieve sufficient longitudinal inductance. This tightness increases the undesired capacitive and inductive coupling between windings, and between the opposite ends of windings.

4.7. Baluns

A balun is a device that splits a single signal into two signals of equal amplitude and opposite phase. Since a balun is a reciprocal device, it can also combine two out-of-phase signals into one signal, with equal weighting on both input signals. At low frequencies, this function is commonly performed with great precision by a transformer. Transmission line transformers make especially good baluns at RF frequencies up to 1 GHz.

There are no standard techniques for fabricating a balun on a monolithic circuit at microwave frequencies. Circuits that split a signal into two, and route one signal through a high pass network and the other signal through a low pass network have been used [35]. These "High-pass low-pass" structures offer two signals, lagging and leading the input by 90 degrees. They suffer from an inherently low bandwidth, and fairly high loss. Baluns that use sections of slot line and coplanar waveguide in conjunction with microstrip have been proposed [36]. They look promising at frequencies above 20 GHz, but their use below this frequency is precluded by their size. Active baluns using GaAs FETs may be the most compact solution at low microwave frequencies. They can be configured to have gain, and their bandwidth can extend down to DC [37]. The principal disadvantage of the active balun is that they consume DC power, and they may add unwanted distortion to the incoming signal. Baluns that employ tuned coupled line sections work on the same principals as the monolithic baluns described here, but take more space. "Rat-Race" and hybrid ring structures can also be used over fairly narrow frequencies, but they are distributed, and take an enormous amount of area.

Monolithic transformers such as the ones discussed in Chapter 4.3 are not exceptionally well suited for use as baluns unless a great deal of care is exercised. This section deals with the requirements for a good balun.

4.7.1. Balun Models

Baluns are often made with transformers that have three windings, and are known as trifilar transformers. They can be represented by either of the equivalent circuits shown in

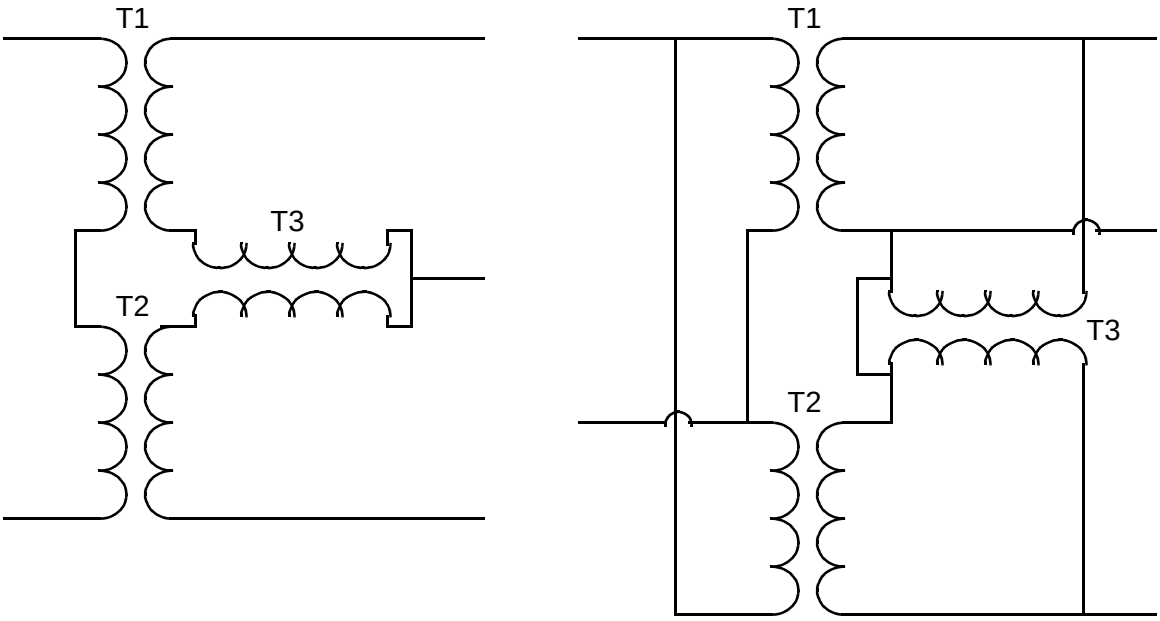

Figure 4.22. Two possible models for a balun. The model on the right can be simplified if the balun is indeed balanced because the mutual inductance of T3 becomes zero, and the self inductance can be incorporated into T1 and T2.

Figure 4.22. These schematics are based on the models in Chapter 2.2. The model shown in Figure 4.22b affords extra simplicity as a model of a balun. If one assumes that the characteristics of the two balanced windings are identical, (which is true for an ideal balun), then transformers T1 and T2 have identical characteristics, and the mutual coupling of transformer T3 is zero, and can be eliminated from the circuit. Thus, a perfectly balanced balun transformer can be represented by the equivalent circuit shown in Figure 4.5. This model is useful for circuit design, because it implies that two halves of a push-pull circuit can be analysed singly, and then placed in parallel. When a similar analysis is done to the model shown in Figure 4.22a, it becomes apparent that similar simplifications can not be made to it. Therefore, a transformer balun can not be modelled as two transformers with their primary windings in series.

4.7.2. Baluns Fabricated from Transformer Pairs

The model in the previous paragraph suggests a possible implementation of a balun. Two separate but identical transformers connected as shown in Figure 4.5 should yield a perfect balun. Intuitively, it would appear that a transformer with perfectly symmetrical windings should have equal performance in both configurations. If there was no interwinding capacitance, this would be true. Unfortunately, the transformer's interwinding capacitance causes an unbalanced output signal as described in Chapter 4.3.

A two transformer balun using the two turn transformers described in section 4.3 has been modelled. Since the transformers are in parallel, the optimum impedance of each of the balanced output arms is twice the impedance of the input circuit. The frequency response of this balun in a system with 50 ohms on the input, and 100 ohms on both outputs is shown in Figure 4.23a. The broken line represents the inverting output, and the solid line represent the non-inverting output. If the transformer is tuned with a shunt capacitor on each of the three terminals, to give the lowest loss at 5 GHz, the frequency response shown in Figure 4.23b is found. From these graphs, it is obvious that the outputs are balanced at low frequencies, but become progressively less balanced at high frequencies. Adding capacitive tuning improves the balance and insertion loss at low frequencies, at the expense of making the bandwidth narrower.

4.7.3. Centre Tapped Baluns

The more conventional way of making a balun at lower frequencies is to use a centre-tapped transformer. Monolithic transformers can be centre-tapped at any position along any winding, but the transformer in Figure 4.1c can be used to position the tap exactly in the centre. Transformers of this nature have been simulated, and measured, and their characteristics are very similar to two discrete transformers. A 1:1 (overall turns ratio) centre tapped transformer with layout shown in Figure 4.24 was simulated with GEMCAP. Figure 4.25a shows the frequency response of both outputs of the transformer. Each of the two outputs was loaded with a 50 ohm impedance, and the input was driven with a 100 ohm source. The performance of the transformer with tuning capacitors on all 3 ports is shown on Figure 4.25b.

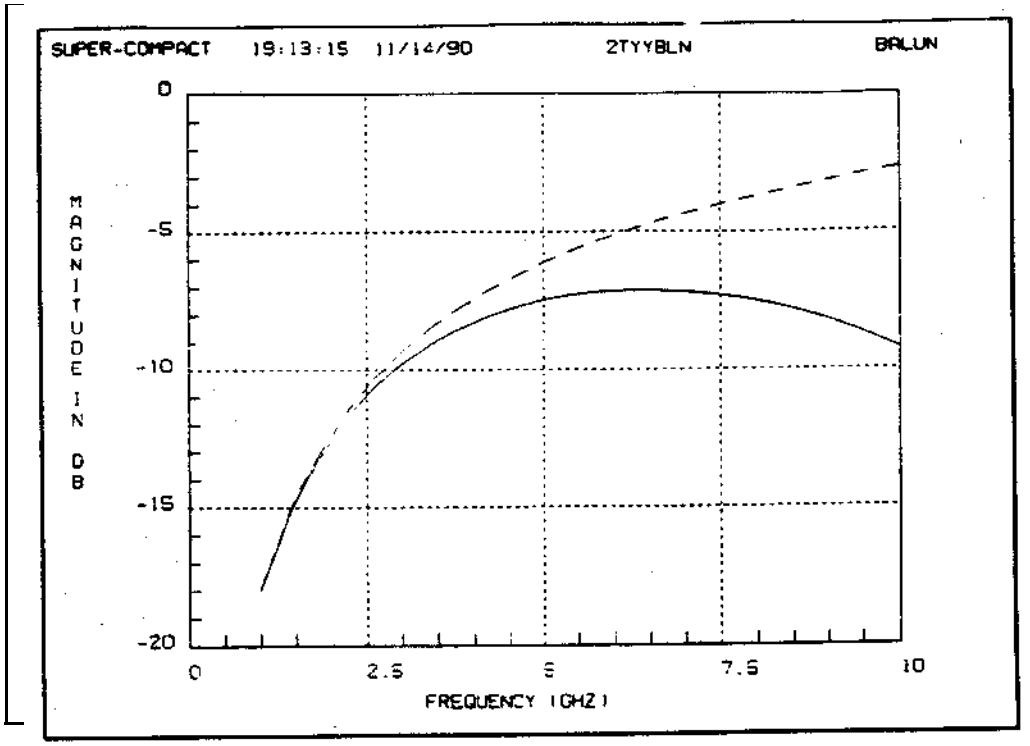

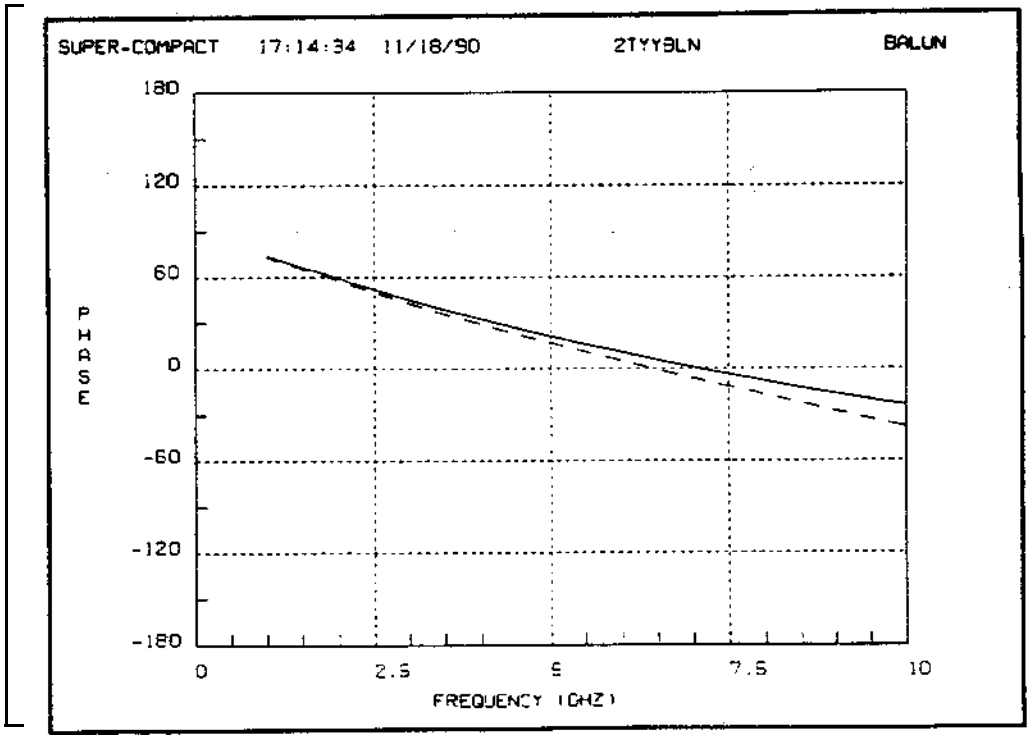

Figure 4.23a. Magnitude and phase of S_{21} of a basic balun made from two transformers. The solid line is the non-inverting port response, and the broken line is the inverting port response. 180 degrees has been added to the phase of the inverting configuration.

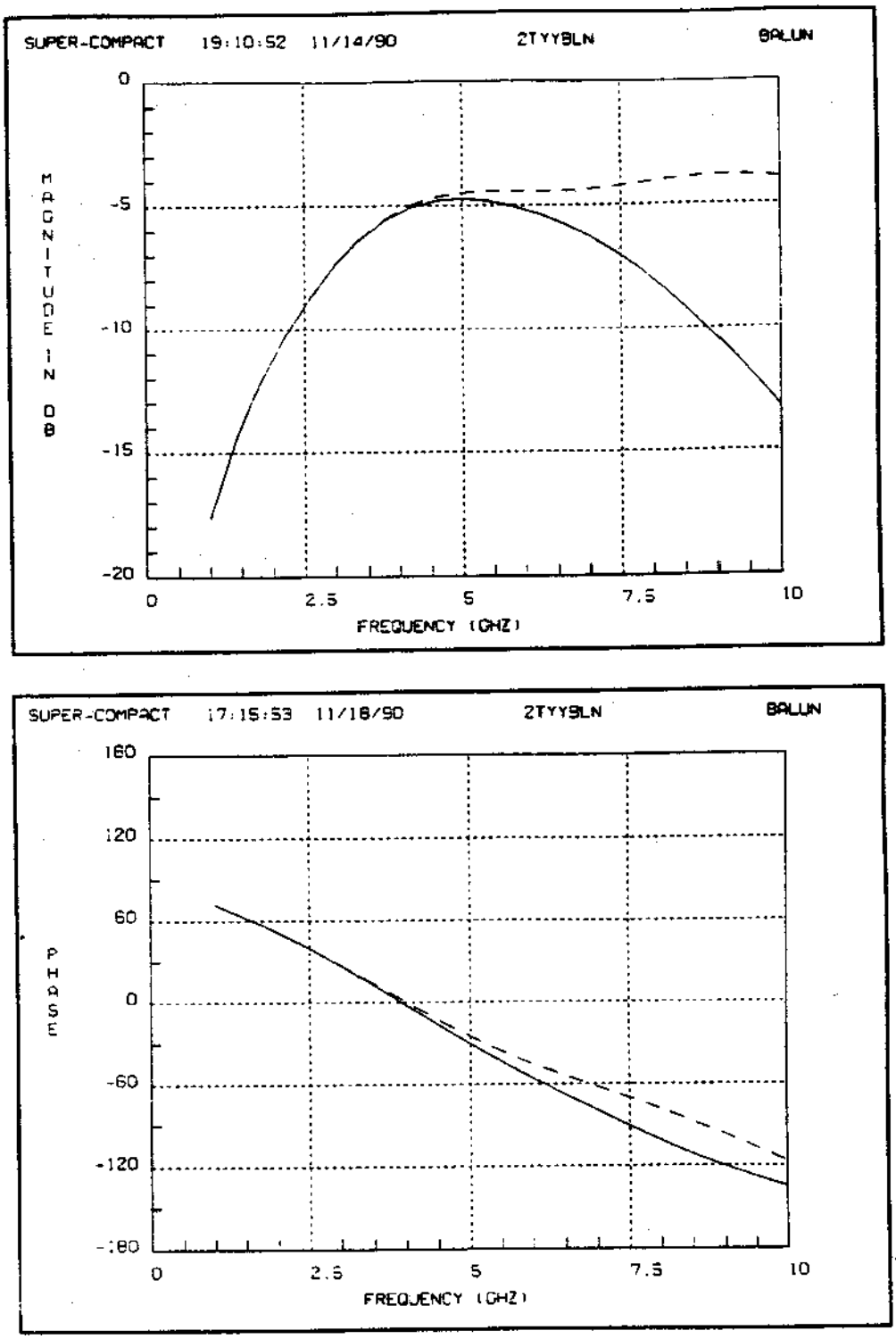

Figure 4.23b. Magnitude and phase of S_{21} of a basic balun made from two transformers with parallel tuning applied to both ports. The solid line is the non-inverting port response, and the broken line is the inverting port response.180 degrees has been added to the phase of the inverting configuration.

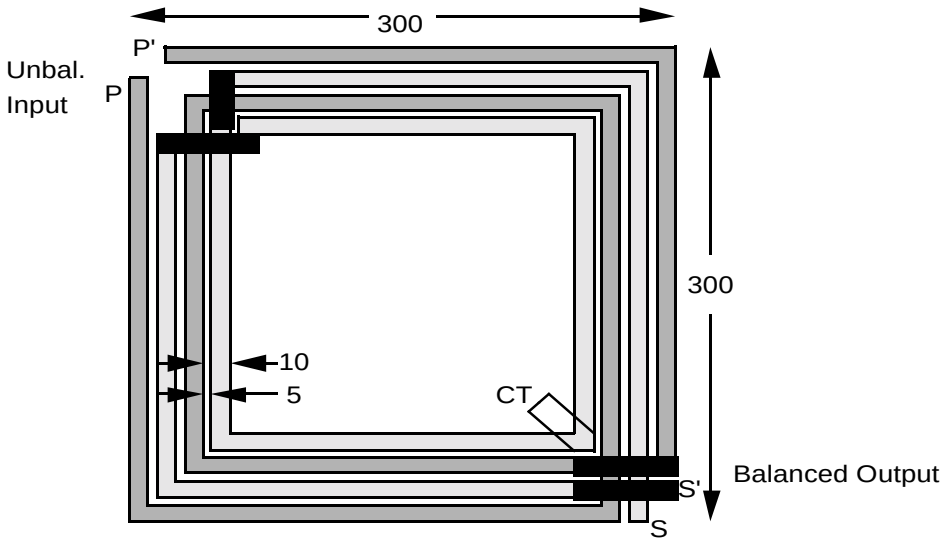

Figure 4.24. Layout of a centre tapped balun. The black bars are air-bridges.

The frequency response of this balun is quite flat but its loss (over 5 dB tuned) is larger than other baluns. The large loss is not intrinsic to this type of transformer; it comes about because each secondary winding has only 1 turn. The next design to be discussed is very similar to this design, but it has 1.5 turns on each half of the secondary winding.

4.7.4. Trifilar Baluns

The first implementation of a trifilar monolithic spiral balun was published by Boulouard and Le Rouzic [38]. The transformer consists basically of three parallel microstrip lines wrapped into a spiral, forming 1 or 1.5 turns. The middle line is excited, and the outer two lines are connected to yield two out of phase signals. Although they refer to their design as a “Ruthroff” design, the fact that there is little increase in inductance along the length of the windings would suggest that it is simply a trifilar transformer. In fact, this design is simply a centre tapped transformer with an overall 1:2 turns ratio. The measured (from [38]) and GEMCAP modelled s-parameters of one half of the 1 turn “Triformer” (with the remaining port open-circuited) is shown in Figure 4.26. Notice that the loss is on the order of 5 dB.

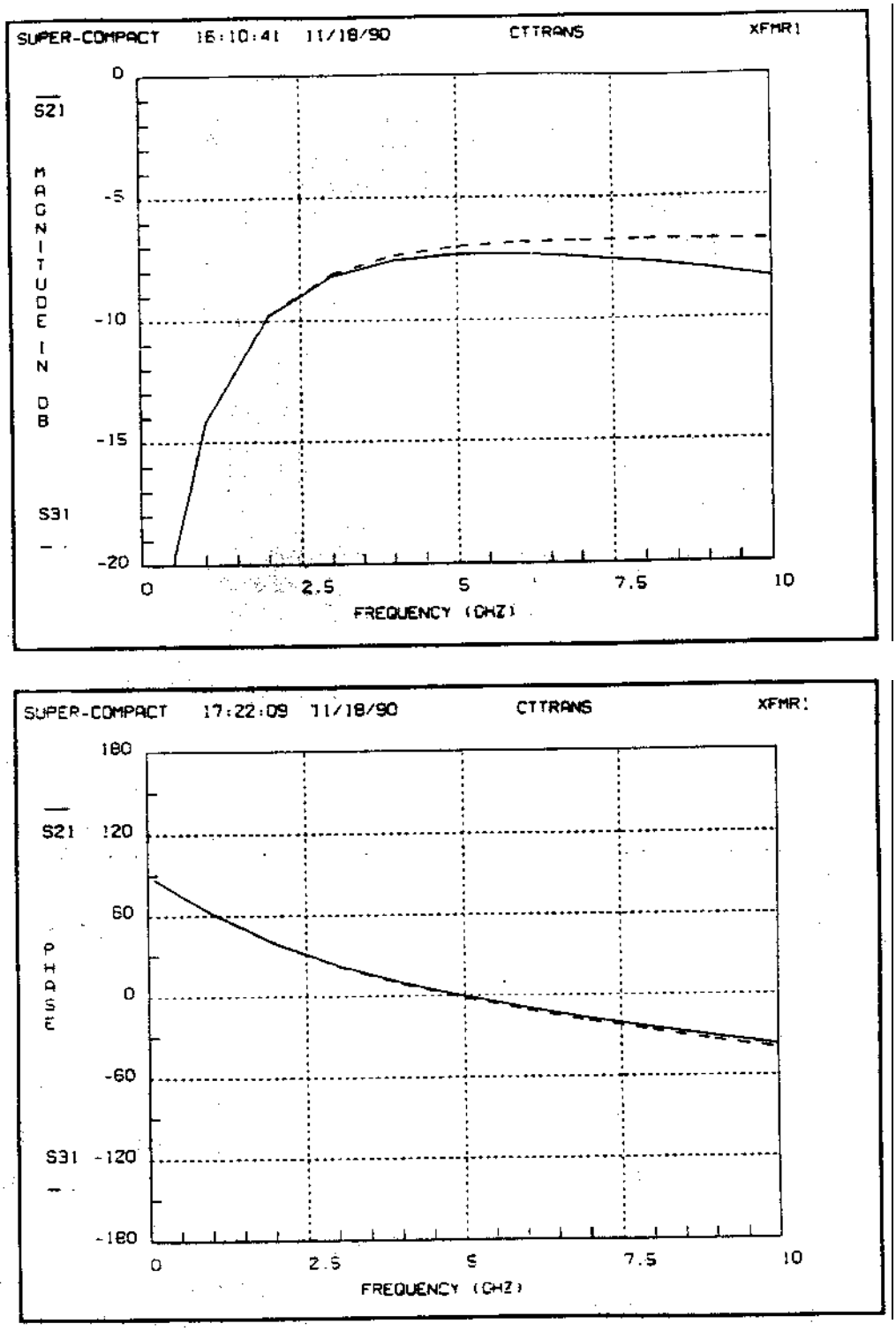

Figure 4.25a. Magnitude and phase of S_{21} of a centre tapped transformer with an overall turns ratio of 1:1. The solid line is the non-inverting port response, and the broken line is the inverting port response. 180 degrees has been added to the phase of the inverting configuration.

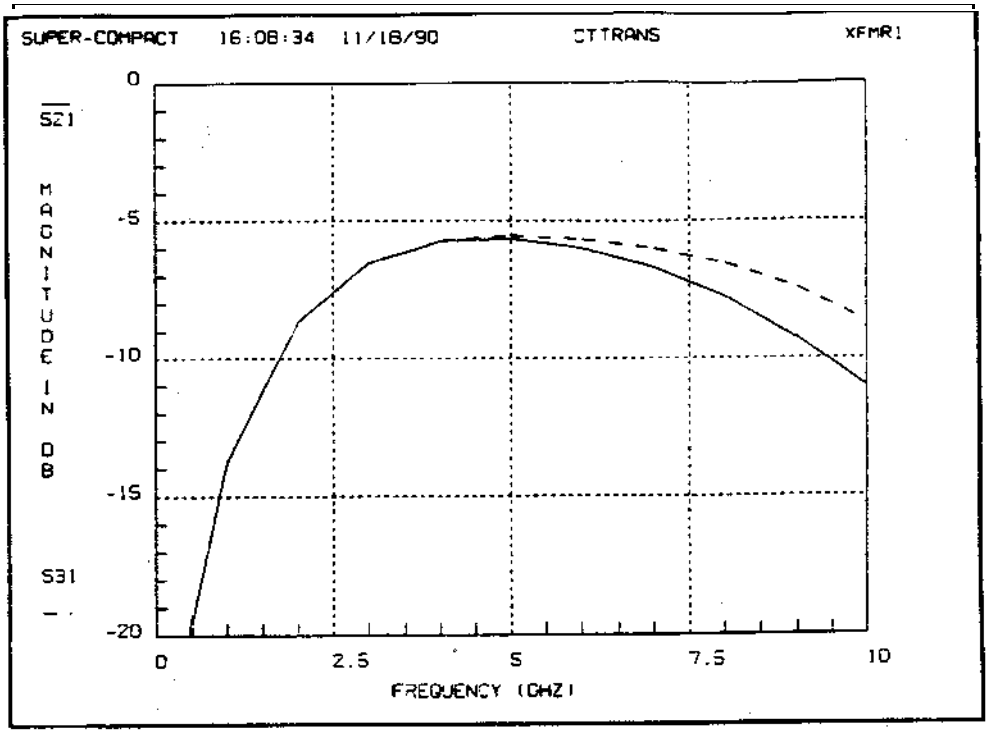

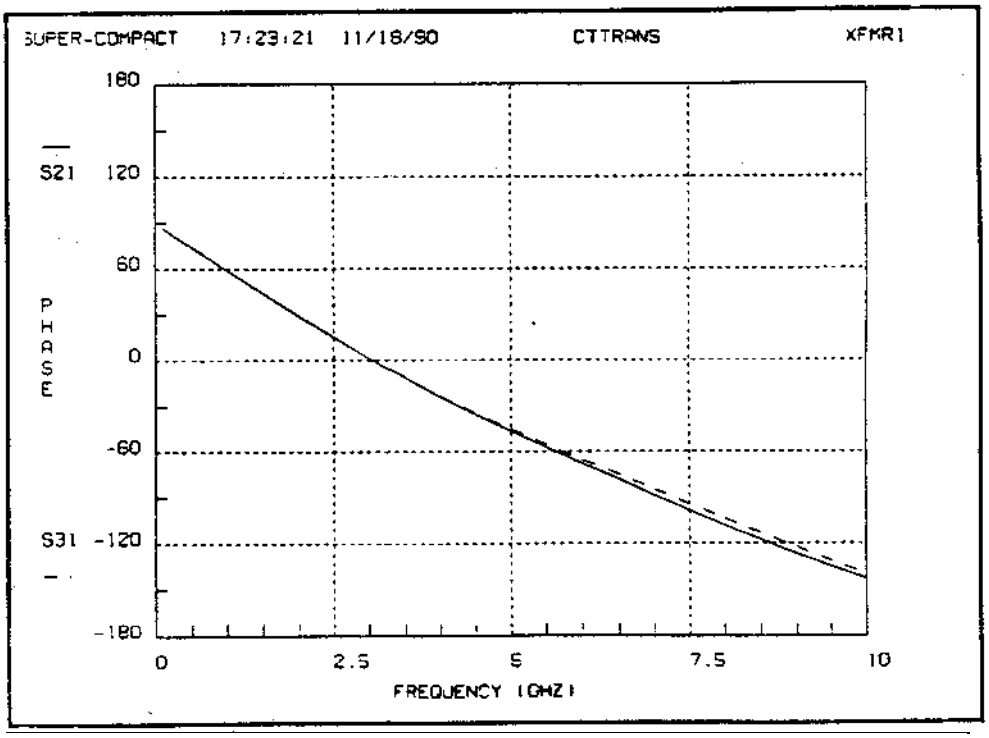

Figure 4.25b. Magnitude and phase of S_{21} of a centre tapped transformer with an overall turns ratio of 1:1, tuned for peak response at 5 GHz. The solid line is the non-inverting port response, and the broken line is the inverting port response. 180 degrees has been added to the phase of the inverting configuration.

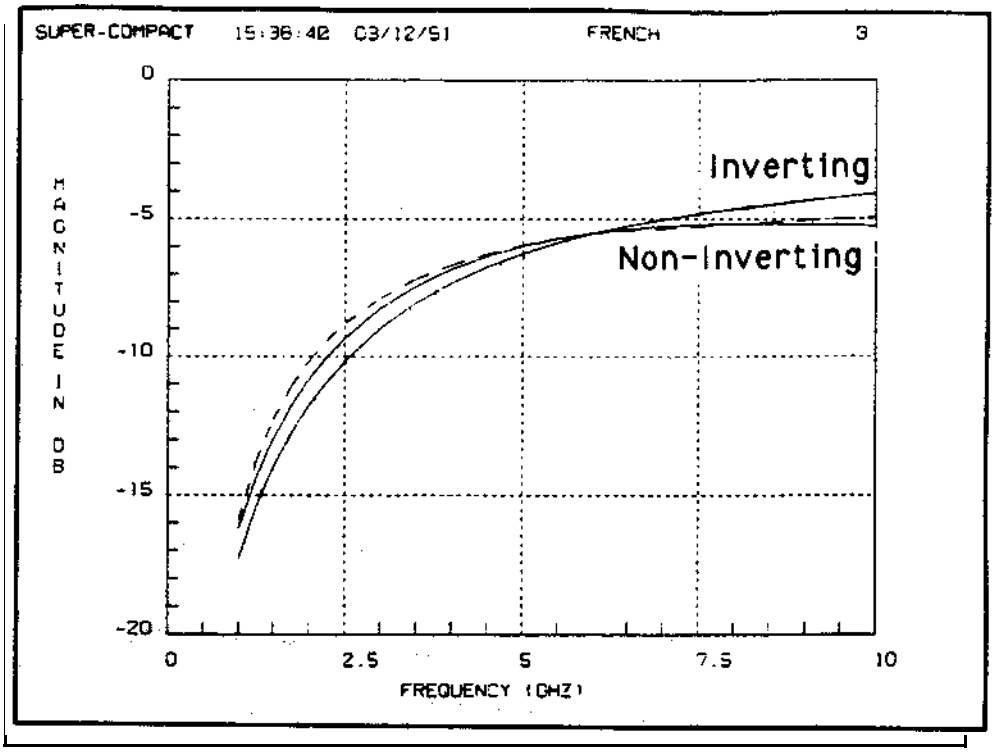

Figure 4.26. Measured (broken line, from [38]) and computed (solid line) S_{21} of a trifilar transformer. Note that the measured response of only the non-inverting port is available.

This loss does not include the power transmitted to the other output, since the other output is open-circuited. The phase difference between the two outputs is within 3 degrees between 1 GHz and 9 GHz, but the amplitude imbalance between the two outputs reaches 2 dB at 9 GHz.

In order to compare the performance of the trifilar balun with the other baluns in this section, a trifilar balun of dimensions similar to the other devices was simulated. The layout of this balun is shown in Figure 4.27. To achieve good coupling, a 2:3 turns ratio was employed. (A 2 turn primary was used to make the comparison with the other transformers fair. If a standard trifilar spiral was used, secondary lines would lie next to each other, “wasting” mutual inductance. This design ensures that all mutual coupling from adjacent lines contributes to S_{21} or S_{31}.) The overall impedance ratio for this transformer is 1:2.25, so ideally it should be tested an a system with 50 ohms on the primary, and 56.25 ohms on

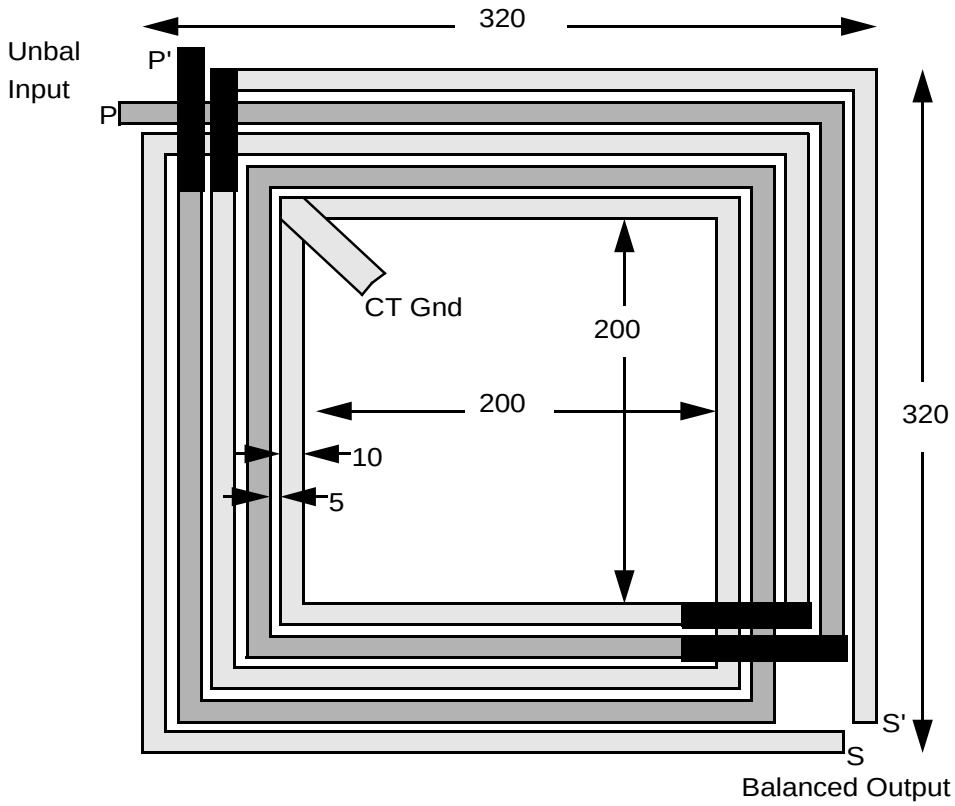

Figure 4.27. Layout of the trifilar transformer. Dimensions are in microns.

each secondary. The transformer was simulated in a system with 50 ohms on all ports as the extra loss is small. The frequency response is shown in Figure 4.28a. The frequency response of the transformer with shunt tuning capacitors on all 3 ports (adjusted for peak coupling at 5 GHz) is shown in Figure 4.28b. This response is similar to the other centre tapped transformer but the loss was slightly lower.

4.7.5. The Symmetrical Balun

As was discussed in section 4.3, the main reason that an otherwise perfectly symmetrical balun behaves asymmetrically is because it is driven from an asymmetric source so that the interwinding capacitances are excited differently. If the source could be made to look symmetrical, then there would be no imbalance. If a transformer is made with both primary and

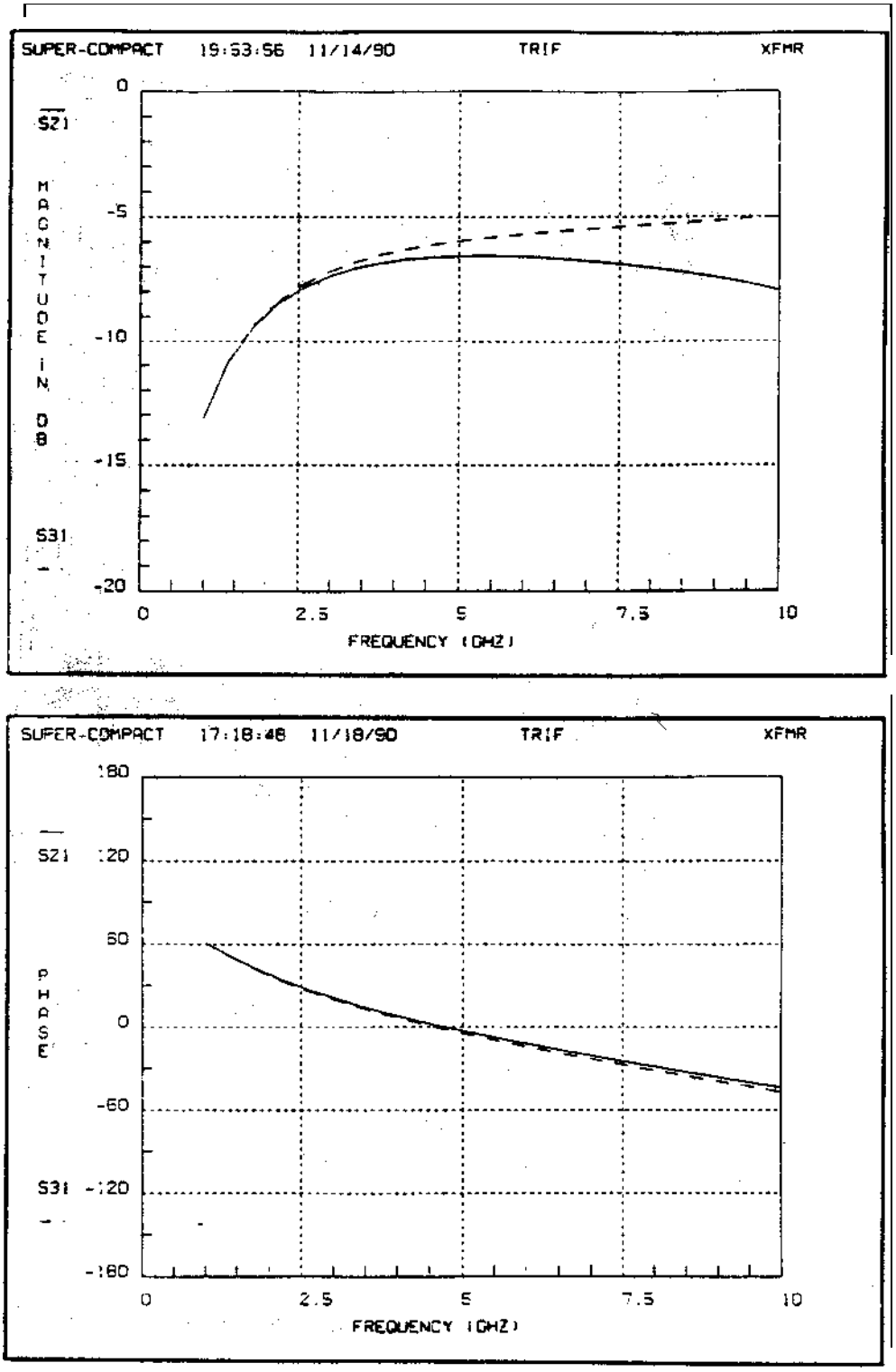

Figure 4.28a. Magnitude and phase of S_{21} of a trifilar transformer with an overall turns ratio of 1:2.25. The solid line is the non-inverting port response, and the broken line is the inverting port response. 180 degrees has been added to the phase of the inverting configuration.

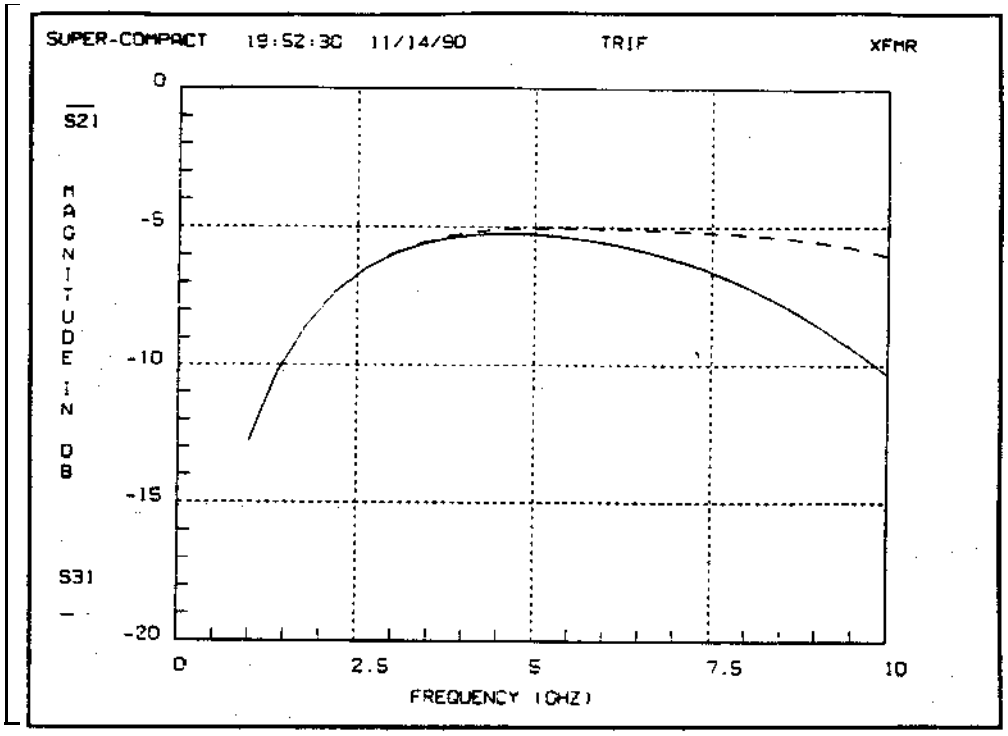

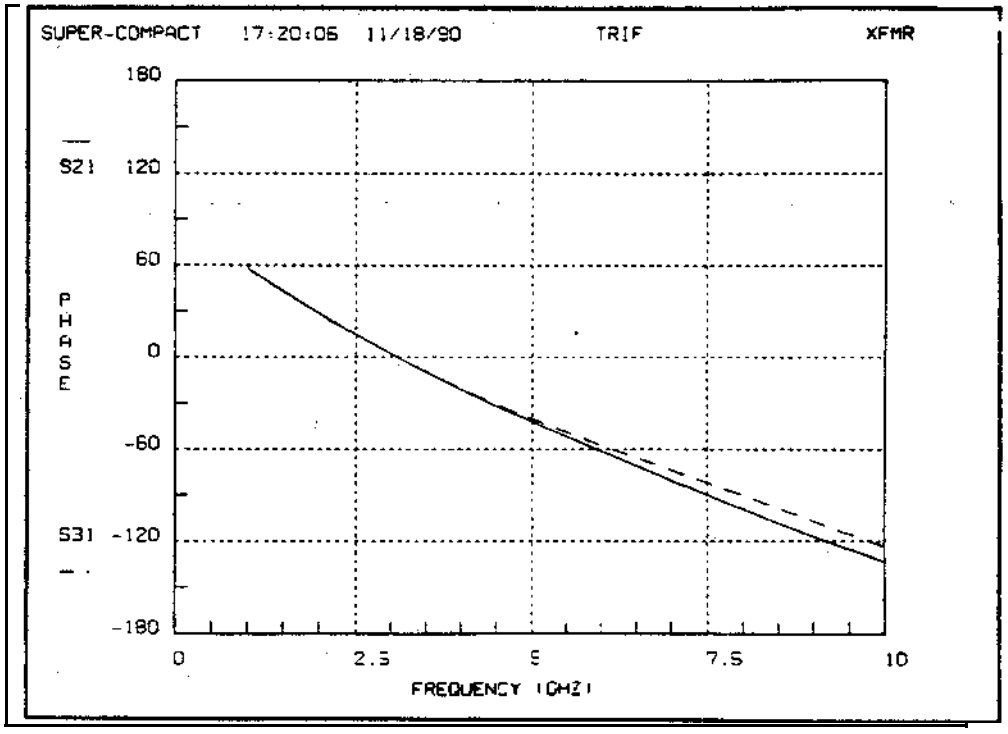

Figure 4.28b. Magnitude and phase of S_{21} of a trifilar transformer with an overall turns ratio of 1:2.25 when tuned for peak response at 5 GHz. The solid line is the non-inverting port response, and the broken line is the inverting port response. 180 degrees has been added to the phase of the inverting configuration.

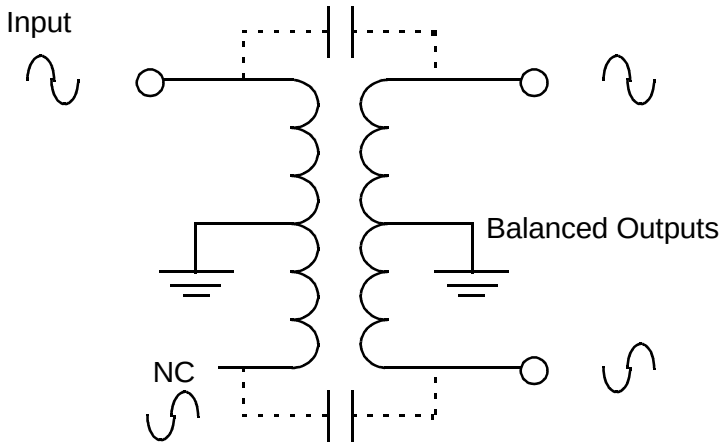

Figure 4.29. Schematic of the symmetrical transformer balun. The unconnected primary "Dummy" winding improves balance.

secondary centre-tapped, then one half of the primary could be driven, while the other half is left to float, as shown in Figure 4.29. The floating terminal of this transformer will have a signal induced on it 180 degrees out of phase from the incoming signal. The voltage between the two outer primary terminals is balanced with respect to ground. As long as the transformer is symmetrical, the interwinding capacitances will be driven symmetrically, and the two outputs will be balanced. The circuit is still not perfectly balanced, as the currents flowing in each half of the primary are not the same. As long as each half of the primary inductively couples equally to both halves of the secondary, the effect is small.

Such a transformer has been laid out, simulated and tested [39]. The layout of the transformer is shown in Figure 4.30. The transformer was tested with coplanar waveguide probes. Due to space limitations, the unused port was left unterminated. Although the coupling was quite low, the balance was better than other monolithic baluns. Since only half of the primary winding is used, the overall turns ratio of the transformer is 1:2. The simulated frequency response of the transformer when the primary is driven with a 50 ohm source, and each secondary is loaded with 100 ohms is shown in Figure 4.31a. Figure 4.31b shows the frequency response of the transformer when it has been tuned for maximum coupling at 5 GHz with shunt capacitors on all three ports. The bandwidth of this transformer is

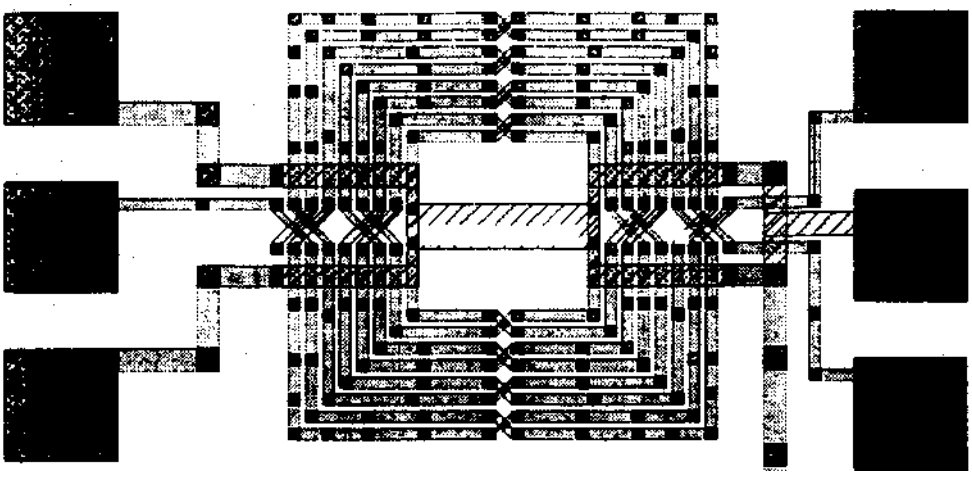

Figure 4.30. Layout of the symmetrical balun.

slightly larger than the other designs. The insertion loss is comparable to other designs. The ultimate balance of this transformer is not quite as good as the other transformers. A short length of transmission line on one of the ports improves the phase response. If this line was coupled to the rest of the transformer, improved amplitude response might result. Beyond 10 GHz, all of the transformers exhibit drastic degradation in balance, as seen in Figure 4.8.

Note that all simulations were performed under the same processing and electrical constraints. The lines were 10 um wide, and the spaces were 5um wide. The metal was assumed to be 1 um thick with a sheet resistivity of .02 ohms per square (gold). The substrate material was GaAs, 500 um thick. The input ports were terminated with 50 ohms, and the output ports were terminated according to the turns ratio. By comparing the frequency response of the different configurations, one can see a slight advantage to using the balanced design. The main disadvantage of using the balanced design is that the range of turns ratio is limited. The requirement for an extra, unused winding also makes the transformer larger than more conventional designs.

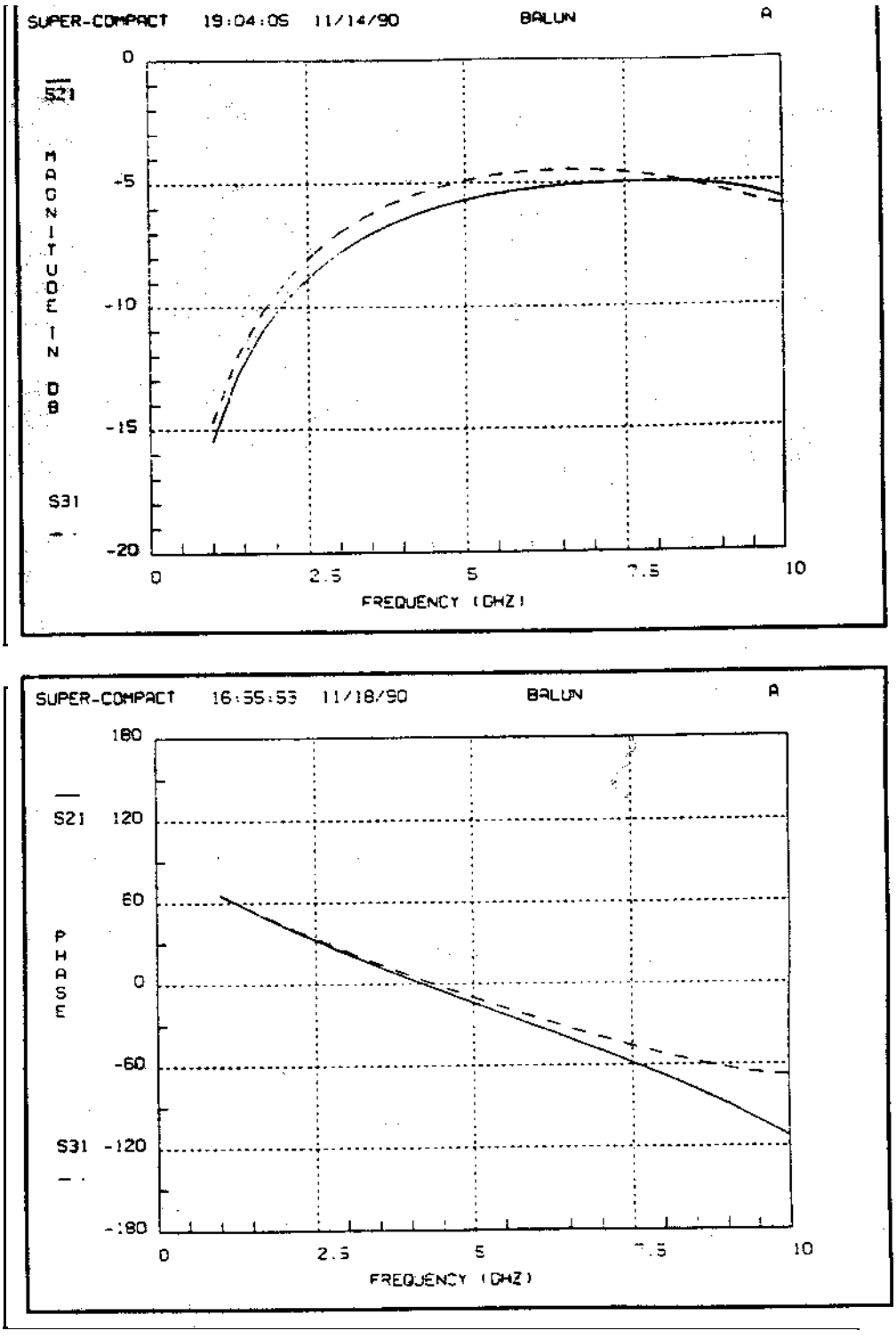

Figure 4.31a. Magnitude and phase of S_{21} of a symmetrical balun. The solid line is the non-inverting port response, and the broken line is the inverting port response. 180 degrees has been added to the phase of the inverting configuration.

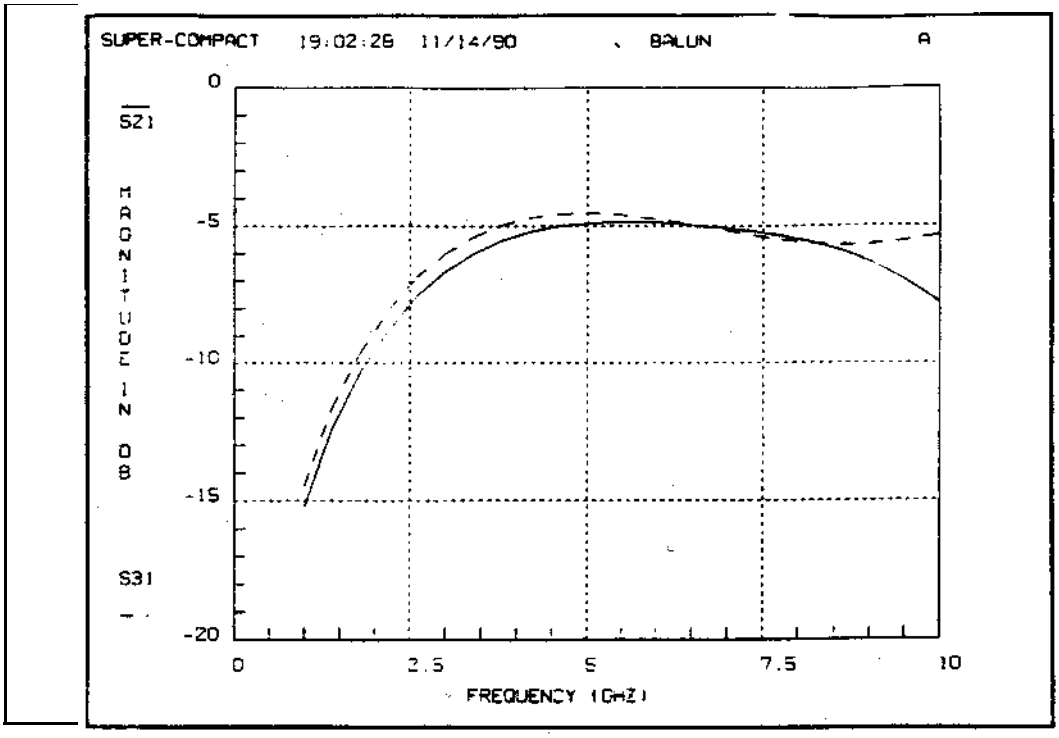

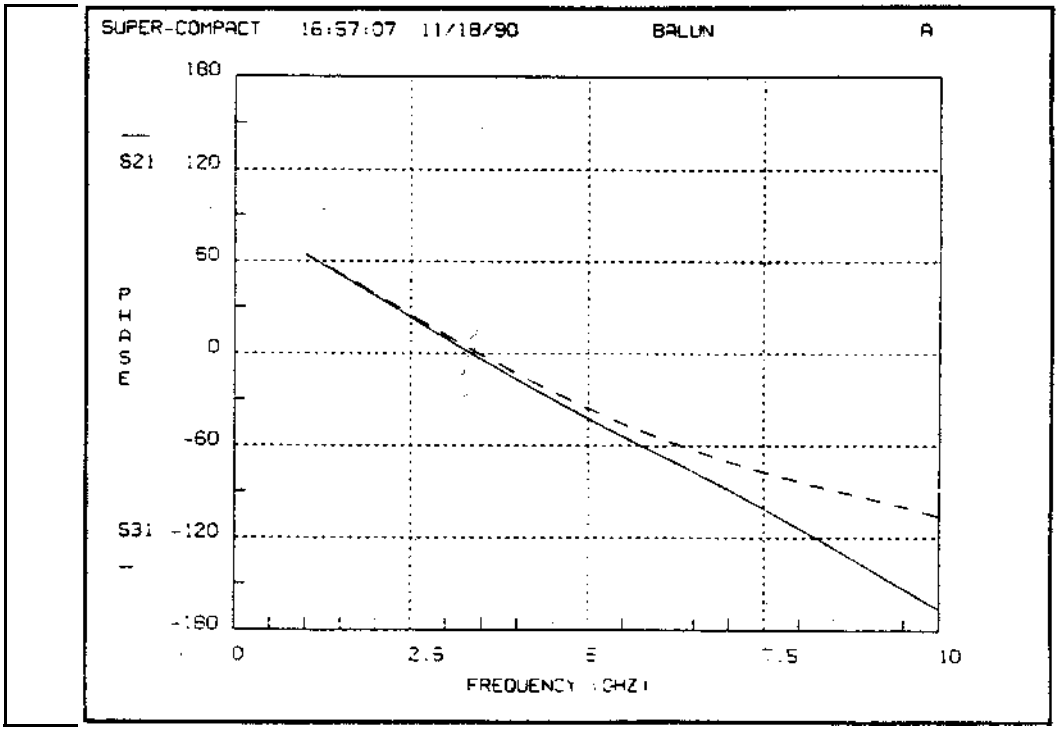

Figure 4.31b.Magnitude and phase of S_{21} of a symmetrical balun tuned for 5 GHz. The solid line is the non-inverting port response, and the broken line is the inverting port response. 180 degrees has been added to the phase of the inverting configuration.

4.8. Conclusions

From examination of the different transformers, one can conclude that there is little fundamental difference between the various designs. All designs are capable of operating over a narrow band of frequencies. Wider band performance can be achieved with the symmetrical design, but only at the expense of balance. The loss can be reduced by employing thicker metal or wider lines, and through improved matching techniques.

Higher frequencies will necessitate smaller transformers. Ideally, one could simply scale down the size of the transformer to allow operation at arbitrarily high frequencies, subject only to lithographic constraints. Unfortunately, the skin effect causes losses to increase as well. The ultimate useful frequency of operation of these baluns with gold metallisation in a 50 ohm environment is on the order of 20 GHz. Beyond that frequency, conventional distributed structures will be more useful.

CHAPTER 5
CONCLUSIONS AND RECOMMENDATIONS

The major goal in performing this research was to gain an understanding of monolithic transformers, and to determine their suitability for use in MMICs. To achieve this goal, a technique for analysing monolithic coupled structures was developed, and tested with measurements from various devices. The technique was then used for evaluating various hypothetical structures. As a by-product of this exercise, a number of microstrip structures could be analysed.

5.1. CAD Program Design

The analysis technique used two different techniques for the calculation of the inductance matrix; closed form equations, and the inversion of a unity ε capacitance matrix (the ICM technique). The two techniques gave different results, especially when short conductors were considered. The closed form equations, which, in their simplest form can be derived without approximation from the Biot-Savart law, predict that shorter lines have less inductance per unit length than long lines. The ICM technique predicts constant per unit length inductance, and agrees with the closed form equations for long lines. Although experiments to verify these equations directly on simple structures gave mixed results, the closed form equations were consistently more accurate for inductors and transformers whose dimensions were on the order of the substrate thickness.

The resulting program (GEMCAP) was verified with measured and published results. Even though the devices examined were modelled strictly with simple lumped elements, excellent agreement was seen into the microwave region. An important conclusion of this work is that compact MMIC designs do not need especially elaborate distributed models, but all forms of stray coupling must be accounted for.

GEMCAP was optimized to analyse spiral transformer and inductor structures, and can analyze some devices more efficiently than any other program. The mutual coupling between two adjacent inductors can be analysed at 200 frequency points in less than 3 min-

utes. The only other programs capable of performing such operations are full wave electromagnetic simulators that require orders of magnitude more time to perform a similar task. GEMCAP has been used to design transformers consisting of up to 9 turns for use at UHF frequencies. A useful s-parameter model of such a transformer can be determined in the space of 10 to 15 minutes. GEMCAP's flexibility allows it to analyze other structures commonly found on MMIC devices. It has been very useful for analysing stray coupling between coupled line structures and surrounding ground planes.

5.2. GEMCAP Accuracy

An important criterion for the selection of a modelling technique is its accuracy. Unfortunately, the accuracy that can be obtained depends on what structures are being analysed. The source of inaccuracies can be broken down into three categories: inaccuracy due to inherent limitations of the computer algorithms, inaccuracy because of second order effects not taken into account in the model (the models ability to deal with the real world), and inaccuracy because of conscious simplifications made by the user of the program. These categories are elaborated on below.

The actual capacitance and inductance calculations are fundamentally very accurate. For filamentary conductors, the closed form equation is exact. The accuracy of the method of moments technique is better than 1% [19]. The calculation of the loss is empirically based, and has a theoretical accuracy of 10%, although actual loss has been as much as 50% higher than this theory.

The application of these techniques leads to larger errors, however. For example, the analysis of inductance of conductors with finite cross-sectional area has more error associated with it. How much more depends on the aspect ratio of the conductors. The capacitance algorithm assumes infinitely thin conductors, and metal with finite thickness will have more capacitance associated with it. The loss of real metal with grain bounders and surface roughness is higher than that of pure metal.

Finally, the application of any algorithm is subject to the intelligence of the designer using it. The effect of coupling between adjacent components, ground inductance, and end effects will add inaccuracy to any simulation.

These variables would make the exact specification of any accuracy subject to so many conditions that the user would find the specification useless. From the analysis and measurement of several components, one can estimate the accuracy of the program for certain common applications. The program has been able to calculate the inductance of monolithic inductors reliably to within 10%. The loss of these inductors increases with frequency more

rapidly than the program predicts, and actual loss at the inductor's resonant frequency can be a factor of 2 higher than predictions. The resonant frequency can be predicted with less than 10% error. The coupling between inductors depends on the setup of the test, and little measured data is available, but accuracy to within 3 dB should be possible.

Many of the same estimates apply to transformers. A transformer's coupling can be predicted to within ± .5 dB up to the frequency of the first resonance. Beyond that frequency, poorer agreement is seen, although much of the error may be due to measurement inaccuracies.

The program has no lower frequency limit of operation. The upper frequency limit will be determined primarily by the frequency at which the loss calculations become inaccurate. For typical monolithic integrated circuits, an upper limit of 20 GHz is recommended. Beyond this frequency, surface roughness, radiation, and other non-idealities need to be taken into account. (Even below 20 GHz, loss predictions are usually optimistic.) After losses, the next most significant source of error is the discontinuity. At 6 GHz, the discontinuities on typical MMIC inductors and transformers are insignificant, especially if corners are bevelled, but their effect becomes important at higher frequencies. Depending on the structure, discontinuities will start to become significant between 15 GHz and 20 GHz. If SuperCompact or Touchstone is used with GEMCAP, then the simulator's discontinuity models can be used to improve accuracy. At frequencies above 20 GHz, spiral components are usually rejected in favour of traditional transmission lines. For typical MMIC devices, dispersive effects can be ignored. For .5 mm thick substrates, dispersion will become significant only above 30 GHz.

More measurements need to be done to quantify the program's accuracy. Several devices have already been fabricated with aid from this program, and the results have been satisfactory.

5.3. Monolithic Transformers and Baluns

Many sizes and topologies of monolithic transformers were analysed. All transformers had surprisingly similar characteristics. All limitations of monolithic transformers stem from the low inductance and low coupling factor attainable on a monolithic device. This low inductance makes the trade-off between the length of the windings and loss severe. Inductance (and therefore coupling coefficient and bandwidth) can only be increased by increasing the length of the windings, and this increases loss. Transformers typically had a loss of 1 dB or more in a 50 ohm system when tuned, and bandwidths of less than one octave. The loss problem can be overcome with thicker metal, but ultimately the skin effect will limit the gains that can be made.

Despite their shortcomings, monolithic transformers can be useful in narrow band (less than an octave) circuits. Monolithic transformers can be used as a compact, high coupling alternative to the coupled line. As a coupling device, a transformer can take the place of two tuning inductors and a coupling capacitor. The loss through the transformer would be comparable to conventional circuitry, but the transformer will have a space advantage.

A design procedure that allows the designer to accurately synthesize a transformer with certain self inductances has been demonstrated. It can be used to provide a “first cut” transformer design accurate to within 20%. GEMCAP can then be used refine the transformer and to develop an exact model.

Transformers can be connected as baluns, or special centre tapped transformers can be designed. In either case, the baluns have similar characteristics to the transformers that they are made from. Baluns with a output balance of better than .5 dB and 5 degrees have been demonstrated. As there are presently no satisfactory compact passive balun designs available, the spiral transformer balun could become a commonly used circuit element. The techniques presented in this thesis are ideal for exploiting these new elements.

REFERENCES

[1] S. Jamison *et al.*, "Inductively Coupled Push-Pull Amplifiers for Low Cost Monolithic Microwave ICs," in *Proc. IEEE GaAs IC Symposium.* Oct 1982, pp. 91-93

[2] L. Weimer, R. Jansen, I. Robertson, J. Swift, "Computer Simulations and Experimental Investigation of Square Spiral Transformers for MMIC Applications," *IEE Colloquium on CAD of Microwave Circuits.* Digest 99, Nov. 1985, pp. 2/1-2/5.

[3] R. Jansen, "LINMIC: A CAD Package for the Layout-Oriented Design of Single- and Multi-Layer MICs/MMICs up to mm-Wave Frequencies," *Microwave Journal*, Feb. 1986, pp. 151-161.

[4] J. Culp, L. Almsted, S. Jamison, A. Podell, "Integration is Paramount in Gallium Arsenide Receiver Design," *Microwave System News*, April 1983, pp. 91-98.

[5] D. Furguson *et al*, "Transformer Coupled High Density Circuit Techniques for MMIC," in *Proc. IEEE MTT-S Monolithics Symposium* (San Fransisco), May 1984, pp. 34-36.

[6] C. Ruthroff, "Some Broad-Band Transformers," *Proc. of the IRE,* vol. 47, pp. 1337-1342, Aug. 1959.

[7] E. Frlan, S. Meszaros, M. Cuhaci, J. Wight, "Computer Aided Design of Square Spiral Transformers and Inductors," in *Proc. IEEE MTT-S* (Long Beach, CA), June 1989, pp. 661-664.

[8] G. Howard, J.Dai, Y. Chow, M. Stubbs, "The Power Transfer Mechanism of MMIC Spiral Transformers and Adjacent Spiral Inductors," in *Proc. IEEE MTT-S* (Long Beach, CA), June 1989, pp. 1251-1254.

[9] SuperCompact (A linear microwave design tool), Compact Software Inc. Patterson, N.J., 1988.

[10] Touchstone (A linear microwave design tool), EEsof. Inc. Westlake Village, CA. 1989.

[11] Scamper (A linear/non-linear electronics design tool), BNR, Ottawa, Ontario. 1990.

[12] R. Pucel, "Design Considerations for Monolithic Microwave Circuits," *IEEE Trans. Microwave Theory and Techniques*, vol. MTT-29 no. 6, pp. 513-534, June 1981.

[13] P. Shepherd, "Analysis of Square Spiral Inductors for use in MMICs," *IEEE Trans. Microwave Theory and Techniques*, vol. MTT-34 no. 4, pp. 467-472, Apr. 1986.

[14] W. Weeks, “Calculation of Coefficients of Capacitance of Multiconductor Transmission Lines in the Presence of a Dielectric Interface,” *IEEE Trans. Microwave Theory and Techniques*, vol. MTT-18 no. 1, pp. 35-43, Jan. 1970.

[15] M. Maury Jr.,“Microwave Coaxial Connector Technology: A Continuing Evolution,” *Microwave Journal 1990 State of the Art Reference*, Sept. 1990, pp. 39-59.

[16] T. Edwards, Foundations for Microstrip Circuit Design. New York: Wiley, 1981.

[17] W. Hayt, Engineering Electromagnetics. New York: McGraw Hill 1974.

[18] J. Smith, “The Even- and Odd-Mode Capacitance parameters for Coupled Lines in Suspended Substrate,” *IEEE Trans. Microwave Theory and Techniques*, vol. MTT-19 no. 5, pp. 424-431, May. 1971.

[19] D. Kammler, “Calculation of Characteristic Admittances and Coupling Coefficients for Strip Transmission Lines,” *IEEE Trans. Microwave Theory and Techniques*, vol. MTT-16 no. 11, pp. 925-937, Nov. 1968.

[20] T. Bryant, J. Weiss, “Parameters of Microstrip Transmission Lines and Coupled Pairs of Microstrip Lines,” *IEEE Trans. Microwave Theory and Techniques*, vol. MTT-16 no.12, pp. 1021-1027, Dec. 1968.

[21] B. Syrett, “CAPCOE,” An unpublished program written in Fortran. Carleton University.

[22] A. Gopinath, P. Silvester, “Calculation of Inductance of Finite-Length Strips and its variation with Frequency,” *IEEE Trans. Microwave Theory and Techniques*, vol. MTT-21 no. 6, pp. 380-386, June. 1973.

[23] F. Grover, *Inductance Calculations* . Princeton, NJ: Van Nostrand, reprinted by Dover, 1946, 1962.

[24] H. Greenhouse, “Design of Planar Rectangular Microwave Inductors,” *IEEE Trans. Parts, Hybrids and Packaging*, vol. PHP-10 no. 2, pp. 101-109, June. 1974.

[25] D. Krafcsik, D. Dawson, “A Closed-Form Expression for the Distributed Nature of the Spiral Inductor,” in *Proc. IEEE MTT-S* (Baltimore), May 1986, pp. 87-92.

[26] A. Gray, *Absolute Measurements in Electricity and Magnetism Vol II Part I*. MacMillan & Co. Ltd, 1893. pp. 302-303. Or, pp. 484-485 in the 1921 edition.

[27] E. Rosa, “On the Geometrical Mean Distance of Rectangular Areas and the Calculation of Self Inductance,” National Bureau of Standards Bulletin 3,5 1907.

[28] G. Matthaei *et al*, “The Nature of the Charges, Currents, and Fields in and About Conductors Having Cross-Sectional Dimensions of the Order of a Skin Depth,” *IEEE*

Trans. Microwave Theory and Techniques, vol. MTT-38 no. 8, pp. 1031-1035, Aug. 1990.

[29] R. Pucel *et al*, "Losses in Microstrip," *IEEE Trans. Microwave Theory and Techniques*, vol. MTT-16 no. 4, pp. 342-350, Apr. 1968.

[30] E. Pettenpaul *et al*, "Cad Models of Lumped Elements on GaAs up to 18 GHz," *IEEE Trans. Microwave Theory and Techniques*, vol. MTT-36 no. 2, pp.294-304, Feb. 1988.

[31] TriQuint 1A GaAs foundry design manual. TriQuint Semiconductor Inc., Beaverton, OR. 1986.

[32] Harris G-30 GaAs foundry design manual. Harris Microwave Semiconductor, Milpitas, CA. 1988.

[33] M. Kumar, *et al*, "Monolithic GaAs Interdigital Couplers" *IEEE Trans. Microwave Theory and Techniques*, vol. MTT-31 no. 1, pp.29-32, Jan. 1983.

[34] J. Sevik, *Transmission Line Transformers*. ARRL Press: New Haven, Conn. 1987.

[35] T. Ton *et al*, "An X-Band Monolithic Double-Double-Balanced Mixer for High Dynamic Range Receiver Applications", in *Proc. IEEE MTT-S* (Dallas), May 1990, pp. 197-200.

[36] G. Lewis, I. Bahl, A. Geissberger, "GaAs MMIC Slotline/CPW IF Upconverter,"*Proc. IEEE MTT-S Monolithic Circuits Symposium* (New York), May 1988, pp. 51-54.

[37] T. Tokumitsu, S. Hara, T. Takenaka, M. Aikawa, "Divider and Combiner Line-Unified FET's as Basic Circuit Function Modules-Part 1,"*IEEE Trans. Microwave Theory and Techniques*, vol. MTT-38 no. 9, pp. 1210-1217, Sept. 1990.

[38] A. Boulouard, M. Le Rouzic," Analysis of Rectangular Spiral Transformer for MMIC Applications,"*IEEE Trans. Microwave Theory and Techniques*, vol. MTT-37 no. 8, pp. 257-260, Aug. 1989.

[39] G. Rabjohn, "Balanced Planar Transformer," Canadian Patent 1278051, Dec.18, 1990.

APPENDIX A
DERIVATION OF GROVER'S FORMULA

Grover's formula [23] gives the mutual inductance of two equal length, parallel, filamentary conductors. It forms the basis for most of the inductance calculations in the GEMCAP program, and most other monolithic inductor calculations. The formula can be derived by determining the magnetic field around a length of conductor carrying a DC current, and then integrating the field to find the flux linking a second conductor.

The Biot-Savart law gives the magnetic field at any point, P caused by a (fictitious) current element of length dL carrying a current of I amperes (refer to Figure A.1):

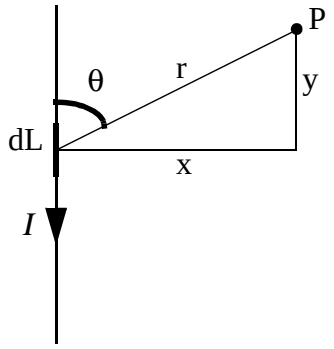

Figure A.1. Definition of variables in Biot-Savart law.

$$d\mathbf{B} = \frac{\mu I d\mathbf{L} \times \hat{\mathbf{a}}_r}{4\pi r^2} \tag{A.4}$$

Where the point is located at a distance of r from the current element dL, and $\mathbf{a}_r$ is the unit vector pointing from the element to the point.

The vector cross-product can be simplified to yield:

$$d\mathbf{B} = \frac{\mu I dl \sin\theta}{4\pi r^2}\hat{\mathbf{a}}_r \tag{A.5}$$

Where θ is defined in Figure A.1. This can be used to calculate the field produced as a result of current flowing in a finite length of filamentary conductor. The conductor, of length l is situated on the y axis, and y_0 is a point on this conductor. The point at which the field is to be monitored will be point (x,y). The axial symmetry of this procedure makes it unnecessary to consider the z axis.

From Figure A.1, r and θ can be defined.

$$\sin\theta = \frac{x}{r} \tag{A.6}$$

and

$$r^2 = (y_0 - y)^2 + x^2 \tag{A.7}$$

(3) and (4) can be inserted into (2) to get:

$$d\mathbf{B} = \frac{I\mu x dL}{4\pi((y_0 - y)^2 + x^2)^{1.5}} \tag{A.8}$$

To find the total field at point (x,y), one must integrate over the length of the filamentary conductor, l.

$$\mathbf{B} = \frac{I\mu}{4\pi}\int^{l} \frac{x dy_0}{((y_0 - y)^2 + x^2)^{1.5}} \tag{A.9}$$

$$\mathbf{B} = \frac{I\mu}{4\pi}\left(\frac{y_0 - y}{x\sqrt{y_0 - 2yy_0 + y^2 + x^2}}\right)\Bigg|_0^{l} \tag{A.10}$$

$$\mathbf{B} = \frac{I\mu}{4\pi}\left(\frac{l - y}{x\sqrt{(l - y)^2 + x^2}} + \frac{y}{x\sqrt{x^2 + y^2}}\right) \tag{A.11}$$

This expression gives the **B** field at any point, (*x*,*y*) as a result of a current, *I* flowing in a conductor of length *l*.

In order to calculate the mutual inductance, one must calculate the flux (Φ) linking another wire placed next to the wire analysed above. As flux linkage is calculated through a surface (S), a return path (that defines the boundary of the surface) must be defined. If the return path is taken at infinity, it is necessary to integrate over a rectangular area of dimensions *l* by infinity (see Figure A.2).

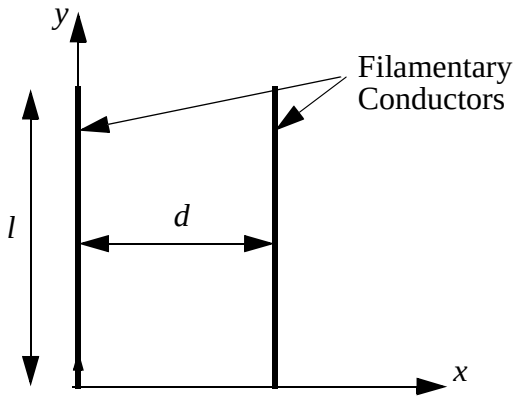

Figure A.2. Configuration for the calculation of mutual inductance between 2 filaments.

$$\Phi = \int \mathbf{B} \bullet d\mathbf{S} \tag{A.12}$$

$$\Phi = \int_{d}^{\infty}\int_{0}^{l} \frac{I\mu}{4\pi}\left(\frac{l-y}{x\sqrt{(l-y)^2+x^2}} + \frac{y}{x\sqrt{x^2+y^2}}\right)dy\,dx \tag{A.13}$$

$$\Phi = \int_{d}^{\infty} \frac{I\mu}{2\pi}\left(\frac{\sqrt{l^2+x^2}}{x} - 1\right)dx \tag{A.14}$$

$$\Phi = \frac{I\mu l}{2\pi}\left(\ln\left(\frac{l}{d}+\sqrt{1+\frac{l^2}{d^2}}\right)-\sqrt{1+\frac{d^2}{l^2}}+\frac{d}{l}\right) \tag{A.15}$$

The inductance can be easily calculated by applying equation A.16.

$$L = \frac{\Phi}{I} \tag{A.16}$$

$$\mu = 4\pi\times 10^{-7} \tag{A.17}$$

$$L = 2l\times 10^{-7}\left(\ln\left(\frac{l}{d}+\sqrt{1+\frac{l^2}{d^2}}\right)-\sqrt{1+\frac{d^2}{l^2}}+\frac{d}{l}\right) \tag{A.18}$$

$$L = 2l\left(\ln\left(\frac{l}{d}+\sqrt{1+\frac{l^2}{d^2}}\right)-\sqrt{1+\frac{d^2}{l^2}}+\frac{d}{l}\right)(\text{cm,nH}) \tag{A.19}$$

Notice that there were no approximations employed in the derivation of this equation, although the fact that an infinite return path was assumed implies that there will generally be approximations in its employment.

APPENDIX B

EXACT FORMULA FOR GMD

The exact formula for the GMD between two rectangles is listed below [27].

$$
\begin{aligned}
\ln(\mathrm{GMD}) \;=\; \{ & \left[(p+b+b')^2\left(\beta^2-\frac{1}{6}(p+b+b')^2\right)-\frac{1}{6}\beta^4\right]\ln((p+b+b')^2+\beta^2) \\
& -\left[(p+b')^2\left(\beta^2-\frac{1}{6}(p+b')^2\right)-\frac{1}{6}\beta^4\right]\ln((p+b')^2+\beta^2) \\
& -\left[(p+b)^2\left(\beta^2-\frac{1}{6}(p+b)^2\right)-\frac{1}{6}\beta^4\right]\ln((p+b)^2+\beta^2) \\
& +\left[p^2\left(\beta^2-\frac{1}{6}p^2\right)-\frac{1}{6}\beta^4\right]\ln(p^2+\beta^2) \\
& -\left[(p+b+b')^2\left(\alpha^2-\frac{1}{6}(p+b+b')^2\right)-\frac{1}{6}\alpha^4\right]\ln((p+b+b')^2+\alpha^2) \\
& +\left[(p+b')^2\left(\alpha^2-\frac{1}{6}(p+b')^2\right)-\frac{1}{6}\alpha^4\right]\ln((p+b')^2+\alpha^2) \\
& +\left[(p+b)^2\left(\alpha^2-\frac{1}{6}(p+b)^2\right)-\frac{1}{6}\alpha^4\right]\ln((p+b)^2+\alpha^2) \\
& -\left[p^2\left(\alpha^2-\frac{1}{6}p^2\right)-\frac{1}{6}\alpha^4\right]\ln(p^2+\alpha^2) \\
& +\frac{4}{3}\beta(p+b+b')\left((p+b+b')^2\operatorname{atan}\left(\frac{\beta}{p+b+b'}\right)+\beta^2\operatorname{atan}\left(\frac{p+b+b'}{\beta}\right)\right) \\
& -\frac{4}{3}\beta(p+b')\left((p+b')^2\operatorname{atan}\left(\frac{\beta}{p+b'}\right)+\beta^2\operatorname{atan}\left(\frac{p+b'}{\beta}\right)\right) \\
& -\frac{4}{3}\beta(p+b)\left((p+b)^2\operatorname{atan}\left(\frac{\beta}{p+b}\right)+\beta^2\operatorname{atan}\left(\frac{p+b}{\beta}\right)\right) \\
& +\frac{4}{3}\beta p\left(p^2\operatorname{atan}\left(\frac{\beta}{p}\right)+\beta^2\operatorname{atan}\left(\frac{p}{\beta}\right)\right) \\
& -\frac{4}{3}\alpha(p+b+b')\left((p+b+b')^2\operatorname{atan}\left(\frac{\alpha}{p+b+b'}\right)+\alpha^2\operatorname{atan}\left(\frac{p+b+b'}{\alpha}\right)\right) \\
& +\frac{4}{3}\alpha(p+b')\left((p+b')^2\operatorname{atan}\left(\frac{\alpha}{p+b'}\right)+\alpha^2\operatorname{atan}\left(\frac{p+b'}{\alpha}\right)\right) \\
& +\frac{4}{3}\alpha(p+b)\left((p+b)^2\operatorname{atan}\left(\frac{\alpha}{p+b}\right)+\alpha^2\operatorname{atan}\left(\frac{p+b}{\alpha}\right)\right) \\
& -\frac{4}{3}\alpha p\left(p^2\operatorname{atan}\left(\frac{\alpha}{p}\right)+\alpha^2\operatorname{atan}\left(\frac{p}{\alpha}\right)\right) \\
& -\frac{1}{2}(\beta^2-\alpha^2)((p+b+b')^2-(p+b')^2-(p+b)^2+p^2)-\frac{22}{3}aa'bb'\}/4aa'bb'
\end{aligned}
$$

where the two rectangles are symmetrically placed with dimensions a by b and a' by b', and are separated by a distance of p, with the dimensions of facing edges of the rectangles being the a and a' dimensions, and:

$$\beta \;=\; \frac{1}{2}(a+a') \text{ and } \alpha \;=\; \frac{1}{2}(a-a')$$

APPENDIX C
INSTRUCTIONS FOR THE OPERATION OF GEMCAP

C.1 Introduction.

This section describes the operation of the GEMCAP (General Microstrip Coupling Analysis Program) program. The program accepts as input physical descriptions of microstrip coupled line structures, and produces files that can be analysed by SuperCompact, Scamper, and Touchstone.

This appendix describes the format of the input lines, the format of the profile file, and basic operation of the program.

C.2 Input Syntax

There are 7 statements that can be used in addition to the regular simulator elements. They are listed below:

XSUB	εr	height(um)		
XCON	thickness(um)	ohms/square		
WID	width1	width2	width3...	(um)
GAP	gap1	gap2	gap3....	(um)
NUM	number			
NUMM	number1	number2		
SEG	node1	node2	length(um)	
SEG	node1 node2	length (um)	node3 node4	length (um)...

These statements can be used to describe conductors in 2 different manners. The possible configurations are shown in figure C.1 and C.2.

XSUB εr h This defines the substrate εr and height (in microns). This must appear at least once before the first NUM statement, and can be used over and over again to redefine the parameters.

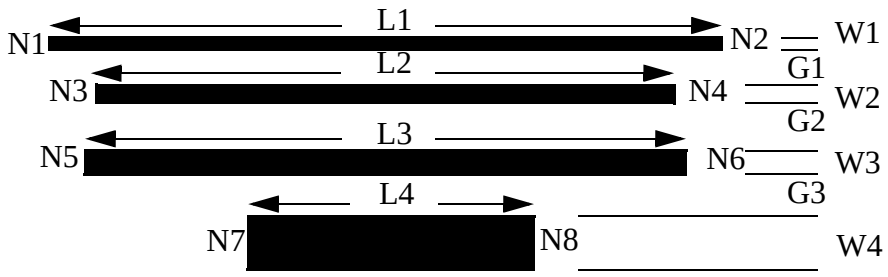


```
WID W1 W2 W3 W4
GAP G1 G2 G3
NUM 4
SEG N1 N2 L1
SEG N3 N4 L2
SEG N5 N6 L3
SEG N7 N8 L4
```

Figure C.1. Basic coupled line configuration for GEMCAP.

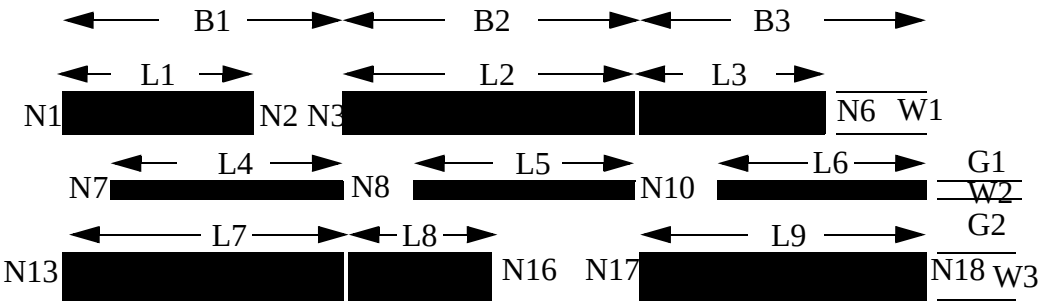


```
WID W1 W2 W3
GAP G1 G2
LEN B1 B2 B3
NUMM 3 3
SEG N1 N2 -L1 N3 N4 L2 N5 N6 -L3
SEG N7 N8 L4 N9 N10 L5 N11 N12 L6
SEG N13 N14 L7 N15 N16 -L8 N17 N18 L9
```

Figure C.2. Lines configured for analysis with end coupling.

XCON t r This defines the conductor thickness (in microns) and the conductor DC sheet resistivity. Again, it must appear at least once.

WID w1 w2 ... This statement defines the widths of the conductors in order. If there are 6 conductors, then this line must have at least 6 entries. All entries are in microns. This line must appear once and may be repeated.

GAP g1 g2 ... This statement defines the gaps between the conductors in order. If there are 6 conductors, then this line must have at least 5 entries. All entries are in microns. This line must appear once, and may be repeated.

LEN b1, b2, ... When end coupling is simulated, using the format in Figure A.2, the program assumes all segments, regardless of their length, fit into one of a regular array of areas. The number of areas in the array is defined in the NUMM statement, and the size of each area is defined by the LEN (the length) and WID statements. The LEN statement is required only if there are blocks that use the NUMM command. There must be m entries in the LEN statement. The lengths are in microns.

NUMM n m. This statement defines the number of parallel conductors (n) and end coupled conductors (m) in an array of end coupled lines. If this line is used, then the input is assumed to be in the form of Figure A.2.

NUM n This line defines the number of conductors in a group of coupled lines. It must be less than or equal to the number of entries in the WID statement. If this line is used, then the input is assumed to be in the form of Figure A.1.

SEG n1 n2 l This line defines one segment in a group of coupled lines. It will typically follow a NUM statement. Note that there must be a block of n (n defined in the NUM statement) SEG statements without any other lines in between. The node numbers must be numbers, not letters. (even in Scamper. Also note that in scamper 01 is not the same as 1, so do not use any leading zeros) The lengths are specified in microns. If not all lengths in a block are equal, then the program assumes that the segments are entered relative to each other.

SEG n1 n2 l1 n3 n4 l2 ... This line defines end coupled segments in a group of coupled lines. It will typically follow a NUMM statement. Note that there must be a block of n (n defined in the NUM statement) SEG statements without any other lines in between, and there must be m pairs of nodes and lengths in every segment line. The node numbers must be numbers, not letters. (even in Scamper. Also note that in scamper 01 is not the same as 1, so do not use any leading zeros) The lengths are specified in microns. If the lengths are positive, then the segments are assumed to be in the right side of the area defined by the LEN statement. If the lengths are negative, then they are assumed to be in the left side of the area defined in the length statement. If the length specified in the SEG line is the same as the length specified in the LEN statement, then the sign of the length is immaterial.

All GEMCAP statements must start on the far left side of the page. (Indentation is not allowed) Exponential notation may be used.

C.3 GEMCAP Profile

There is a profile that specifies some of the options that GEMCAP uses. This file, called TRANSF PROFILE must exist on the A disk.

A typical file is shown below.

8	NUMBER OF SUBSTRIPS IN CAPACITOR CALCULATION	4 TO 10
600	FIRST NODE NUMBER TO BE USED	100 TO 900
Y	INCLUDE EFFECT OF BACK METALIZATION	Y OR N
Y	USE GMD CALCULATION FOR CLOSE CONDUCTORS	Y OR N
N	DISPERSIVE LOSS CALCULATION	Y OR N
Y	INDUCTANCE CALCULATION NEXT ADJACENT?	Y OR N
Y	USE “PI” STRUCTURE FOR CAP TO GROUND?	Y OR N
Y	USE “PI” STRUCTURE FOR MUTUAL CAP?	Y OR N
Y	USE STATIC INDUCTANCE CALCULATION	Y OR N

The lines must be left in the same order. Only the number or letter in the far left is read, the rest is comment.

First line: This line specifies the number of strips used in an individual capacitance calculation. It must lie between 4 and 10 and be even. 6 or 8 is recommended. The higher this number is, the more accurate, and slower the capacitance calculation is.

Second line: GEMCAP needs to add nodes to the network, and they should not correspond to any node that the user has used. GEMCAP will start at this number and work up. So, if it is set to 600, the user must not use any nodes greater than number 599.

Third Line: This line determines whether the ground plane image is considered when using the closed form equations.

Fourth Line: If you are using closed form inductance calculations, you can increase the accuracy of mutual inductance calculations (by using the GMD calculation in Appendix B) when the conductors are close by specifying Y here.

Fifth line: This line specifies whether DC resistance is to be used in the loss calculations (specify N) or if skin effect is to be included (specify Y).

Sixth Line: This line turns the end coupling option on and off. If N is specified, both input formats are still valid, but end to end mutual inductance is ignored.

Seventh line: You have the choice of using a Π (Three element) or Γ (Two element) model for each segment for the capacitance to ground. Π (Specify Y) is more accurate, but results in a larger output file. If you cascade a large number of segments, then specifying N here will save space, with little loss in accuracy.

Eighth Line: As above for the mutual capacitance.

Ninth Line: Inductance can be calculated with closed form formulae or by inverting a unity ε capacitance matrix (ICM Technique). Specifying Y here invokes the ICM calculation. Note that if ICM is specified here, lines 3 and 4 are ignored.

C.4 Running GEMCAP

1: Type MACOM to link the correct disks.

2: Type PREPVS to link the IMSL disk and the correct TXTLIBs.

3: Prepare an input file (file type INP) according to the format shown in section A.2. The examples in the text will also be useful guides.

4: To run the program, you need a file called “TRANSF PROFILE” on your A disk. Copy this from “H” disk and modify as necessary.

5: Type GORD31 fn, where fn is the name of the input file. When it asks, tell it what kind of file it is (Compact, Scamper or Touchstone).

6: It should tell you that you have no errors in your file, and then processing begins. When it is done, it will create a “Human readable” file for the simulator that you requested. There are 4 other files left on the disk. These files contain the input and output data for the inductance and capacitance calculation routines, and can be edited.